The Pennsylvania State University

The Graduate School

Department of Energy and Mineral Engineering

PHOTOINDUCED ACTIVATION OF CO_2 ON TiO_2 SURFACES: QUANTUM CHEMICAL MODELING OF GROUND AND EXCITED STATES, AND IN SITU EPR STUDIES

A Dissertation in

Energy and Geo-Environmental Engineering

by

Venkata Pradeep Indrakanti

Submitted in Partial Fulfillment
of the Requirements
for the Degree of

Doctor of Philosophy

May 2009

The dissertation of Venkata Pradeep Indrakanti was reviewed and approved* by the following:

Harold H. Schobert
Professor of Fuel Science
Dissertation Advisor
Co-Chair of Committee

James D. Kubicki
Associate Professor of Geosciences
Co-Chair of Committee

Kwadwo Osseo-Asare
Distinguished Professor of Metallurgy and Energy and Geo-Environmental Engineering

Chunshan Song
Professor of Fuel Science and Chemical Engineering
Director, EMS Energy Institute
Associate Director, Penn State Institutes of Energy and Environment

Adri C.T. van Duin
Associate Professor of Mechanical and Nuclear Engineering

Yaw Yeboah
Professor of Energy and Mineral Engineering
Head of the Department of Energy and Mineral Engineering

*Signatures are on file in the Graduate School

ABSTRACT

The conversion of CO_2 using light energy (CO_2 photoreduction) has the potential to produce useful fuels or valuable chemicals while decreasing CO_2 emissions from the use of fossil fuels. This thesis describes computational and experimental studies on the initial steps of photoinduced CO_2 activation on TiO_2 surfaces necessary to develop a mechanistic understanding of CO_2 photoreduction. Initially, the state of the art in the field is reviewed, and the performance of CO_2 photoreduction catalysts is compared to that of solar hydrogen production catalysts.

To design efficient CO_2 photoreduction catalysts, we need to understand the intermediates and energetics of various reactions involved in the photoreduction of CO_2 in greater detail. As a first step in this process, the ground states of CO_2 chemisorbed on small clusters from various anatase surface planes were modeled (Chapter 2). We find favorable agreement for the existence of three different CO_2-surface complexes on small TiO_2 clusters ($Ti_2O_9H_{10}$) extracted from the (010), (001) and (101) anatase surface planes.

Secondly, identifying the mechanism and the active sites involved in the formation of negatively charged CO_2 species on TiO_2 surfaces represents a significant advance in our understanding of CO_2 photoreduction. Both post-Hartree-Fock calculations on small model surface clusters as well as density-functional theory (DFT) calculations on larger clusters indicate that conduction band electrons in irradiated, stoichiometric TiO_2 surfaces may not be transferred to CO_2. On the other hand, oxygen vacancies may act as the active sites for CO_2 photoreduction (Chapter 3).

The role of oxygen vacancies in promoting the light-induced conversion of CO_2 (CO_2 photoreduction) on TiO_2 surfaces is discussed Chapter 4 of this thesis. Two different side-on bonded bent-CO_2 (bridging Ti-$CO_2^{\delta\bullet-}$-Ti species) were formed on the reduced rutile (110) and anatase (010), (001) surfaces. Consistent with CO_2 adsorption on other n-type metal oxides such as ZrO_2, the bent-CO_2 species do not gain further charge from the TiO_2 surface under illumination and are likely photodesorbed as neutral species. Additionally, although the formation of species such as CO and HCHO is thermodynamically possible, we find that the energy needed to regenerate the oxygen vacancy on TiO_2 surfaces is greater than that available through band-gap illumination. Therefore, CO_2 reactions with water on irradiated anatase TiO_2 surfaces are likely to be stoichiometric.

The role of lanthanide doping of TiO_2 in influencing electron-hole recombination was investigated using EPR (electron paramagnetic resonance) spectroscopy. In situ pulsed-EPR experiments on calcined TiO_2 samples provide evidence for surface electron and hole-centers on TiO_2 (Chapter 5). However, contrary to expectations, no additional paramagnetic centers created due to lanthanide doping of TiO_2 could be detected in the EPR experiments. Additionally, irradiating TiO_2 in the presence of CO_2 did not create paramagnetic signals corresponding to the $CO_2^{\bullet\delta-}$ radical anion.

TABLE OF CONTENTS

LIST OF FIGURES

LIST OF TABLES

PREFACE

This thesis comprises a series of four papers either published or in-submittal in journals. In chronological order, these papers are:

1. Indrakanti, V. P.; Kubicki, J. D.; Schobert, H. H., Quantum chemical modeling of ground states of CO2 chemisorbed on anatase (001), (101), and (010) TiO2 surfaces. Energy & Fuels 2008, 22, (4), 2611-2618. (Chapter 2)
2. Indrakanti, V. P.; Kubicki, J. D.; Schobert, H., Photoinduced activation of CO2 on Ti-based heterogeneous catalysts: Current state, chemical physics-based insights and outlook, accepted for publication in Energy and Environmental Science, 2009. (Chapter 1)
3. Indrakanti, V. P.; Schobert, H.; Kubicki, J. D., Quantum mechanical modeling of CO2 interactions with irradiated stoichiometric and oxygen-deficient anatase TiO2 surfaces: Implications for the photocatalytic reduction of CO2, to be submitted to Energy & Fuels. (Chapter 3)
4. Indrakanti, V. P.; Schobert, H.; Kubicki, J. D., A density functional theory study of CO2 adsorption on oxygen vacancies on rutile (110) and anatase (010), (001) surfaces: Implications for spectroscopic studies and photoreduction of CO2 on irradiated TiO2., to be submitted to Energy & Fuels. (Chapter 4)

Chapters 1, 2, 3 and 4 of this thesis are in part, verbatim reproductions of the text of the above journal chapters. In all cases, first-authorship establishes my principal role in developing and executing the analyses. Therefore, any reference to “we” indicates me, and not the co-authors of these journal publications.

ACKNOWLEDGEMENTS

"Knowledge is in the end based on acknowledgement."

- Ludwig Wittgenstein

I deeply thank Dr. Harold Schobert and Dr. James Kubicki for their inputs and mentorship during my PhD. This thesis could not have been possible without their encouragement and support. I express my gratitude to Dr. Mercedes Maroto-Valer, for her guidance and her confidence in my ability to successfully complete this rollercoaster ride. I also thank my committee members, Dr. Kwadwo Osseo-Asare, Dr. Chunshan Song, Dr. Adri van Duin and a former committee member Dr. Yaw Yeboah for their feedback and interest in my work. I also thank Dr. Sarma Pisupati for supporting me as a Teaching Assistant for three semesters. The assistance of Dr. David Doetschman and his research group towards conducting EPR experiments at Binghamton University is greatly appreciated. Likewise, I also thank Dr. Gianluca Li Puma for photoreactor access at the University of Nottingham. Discussions with Dr. Alexander Mitin also helped shape this work.

Financial support from the Center for Environmental Chemistry and Geochemistry (CECG), the Earth and Environmental Systems Institute (EESI), the Graduate School, and the Materials Research Institute (MRI) helped conduct the research in this thesis. A number of people at Penn State, including the late David Clifford, Parvana Gafarova, Dania Fonseca, Ron Wasco, and the staff at the EMS Energy Institute and the EME department provided me timely help and advice. I also thank all my colleagues and friends, especially Brandie, Denis, George, Goutham, Meredith, Marielle, Nari, Prabhat, and Prasanna for enriching my academic life during the course of our hikes, games, and discussions.

Finally, I thank my parents for their belief in my abilities and their unconditional support. I am greatly appreciative of everything they have done for me.

Chapter 1

Photoinduced activation of CO_2 on Ti-based heterogeneous catalysts: Current State, Chemical Physics-based Insights and Outlook

1.1 Abstract

This chapter is a review of current knowledge of the chemical physics of carbon dioxide (CO_2) conversion to fuels using light energy and water (CO_2 photoreduction) on titania (TiO_2)-based catalysts and Ti-species in porous materials. Fairly comprehensive literature reviews of CO_2 photoreduction are available already. However, this chapter is focused on CO_2 photoreduction on Ti-based catalysts, and incorporates fundamental aspects of CO_2 photoreduction, knowledge from surface science studies of TiO_2 and the surface chemistry of CO_2. Firstly, the current state of development of this field is briefly reviewed, followed by a description of and insights from surface state and surface site approaches. Using examples such as metal-doping of TiO_2, dye-sensitization, oxygen vacancies in TiO_2 and isolated-Ti centers in microporous/mesoporous materials, the utility of these approaches to understand photoinduced reactions involved in CO_2 activation is examined. Finally, challenges and prospects for further development of this field are presented. Enhanced understanding of the CO_2:TiO_2 system, with a combination of computational and experimental studies is required to develop catalysts exhibiting higher activity towards CO_2 photoreduction.

1.2 Introduction

"Chemistry began by saying it would change the baser metals into gold.
By not doing that it has done much greater things."

- Ralph Waldo Emerson

1.2.1 CO_2 Utilization

There is a growing need to mitigate CO_2 emissions. Some of the strategies to mitigate CO_2 emissions are energy conservation, carbon capture and storage and using CO_2 as a raw material in chemical processes as well as in enhanced oil recovery (EOR) (CO_2 utilization). Catalytic reactions involving CO_2 and producing value-added products are reviewed by Xu and Moulijn[1]. More recent reviews by Song[2], Sakakura et al.[3] and Aresta and Dibenedetto[4] detail additional opportunities to use CO_2 as a feedstock. Reactions involving CO_2 typically require energy input and/or a high energy substrate. As pointed out by Song[2], processes involving CO_2 could be endergonic (or endothermic) and can still be feasible, provided the products are valuable enough. Moreover, as carbon legislation becomes imminent, a price for CO_2 (either as a carbon tax, or as a CO_2 offset in a cap-and-trade system) would benefit processes having a positive net CO_2 balance.

What is the potential for utilizing CO_2 by the use of various renewable energy technologies? Current global industrial consumption of CO_2 (approximately 115 mega (metric) tonnes (Mt)/year[5]) is insignificant compared to anthropogenic CO_2 emissions (~26 gigatonnes (Gt) of CO_2/year). However, we note that U.S. CO_2 consumption for enhanced oil recovery as well as chemical synthesis (~40 Mt/year[6]) is similar in scale to other projected means of U.S. greenhouse gas (GHG) reduction (data from a McKinsey

report[7]), such as using solar PV electricity, wind energy and cellulosic biofuels, as shown in Figure 1. With the caveat that most processes utilizing CO_2 would need reducing power and/or a source of energy that is not reflected in the dotted lines shown in Figure **1-1** , we note that comparatively larger amounts of GHG mitigation could be possible if CO_2 is converted into fuels. This conversion leads to a reduction in CO_2 emissions only if the underlying energy infrastructure is not based on primary fossil fuels[5].

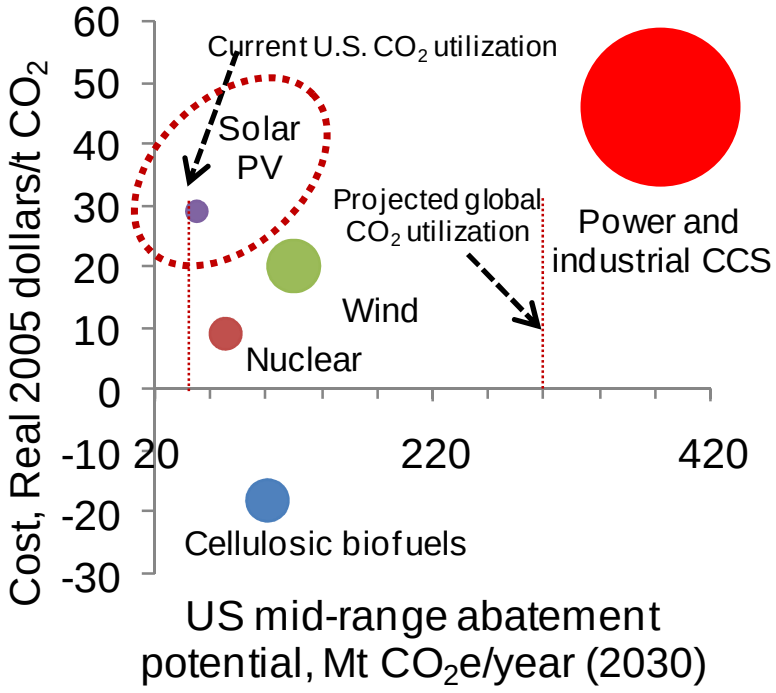

Figure **1-1**: Comparison of the greenhouse gas (GHG) abatement potential (in megatonnes of CO_2 equivalents ($MtCO_2e$)/year) for selected technology options. Aresta and Dibenedetto[8] project that globally, direct solar conversion of CO_2 to fuels would mitigate 300-700 Mt CO_2/year. This is comparable in scale to U.S. GHG mitigation via carbon capture and storage (CCS)

For example: the quantity of U.S. CO_2 emissions mitigated by solar PV technologies (50 Mt CO_2e/year by 2030) represents approximately 50% of the CO_2 currently utilized by the global chemical industry. The data shown in Figure 1 for solar photovoltaic (PV) technologies could be considered as representing the upper limits for converting light energy to electricity. Solar fuel production could be thought of as involving solar PV electricity production, followed by generation of hydrogen or reduction of CO_2 using the electrical energy. If we assume (simplistically) that the efficiency of conversion dictates the potential size of the market, using 10% efficiency for this solar-electricity-chemicals conversion results in a 5 Mt CO_2/year potential for the abatement of greenhouse gas emissions using solar photoreduction (of CO_2 or water). Given reasonable economies of scale, and conversion efficiencies, the costs of producing fuels from sunlight and CO_2 could be offset by CO_2 emission credits (under a carbon cap-and-trade framework) and the sale of the hydrocarbons produced. On the other hand, Aresta and Dibenedetto[8] point that global CO_2 utilization to make chemicals and fuels could reach 300-700 Mt CO_2/year globally in the near- to long-term. Therefore, the potential for the indirect utilization of CO_2 by using renewable electricity/hydrogen would be less than the direct solar conversion of CO_2 and water to chemicals or fuels.

Although CO_2 utilization may not make an impact on directly reducing emissions, it may provide a means to limit the use of fossil fuels and thereby contribute indirectly. As noted by Aresta and Dibenedetto[9], a life cycle analysis (LCA) approach should be used to determine whether a given process indeed decreases fossil fuel use and the carbon intensity.

1.2.2 CO_2 photoreduction

CO_2 photoreduction refers to the conversion of CO_2 to reduced C_1 and C_2 compounds using light-induced reactions. Since CO_2 does not absorb either visible or UV radiation in the wavelengths 200-900 nm, this process requires suitable photosensitizers. Both metal complexes and semiconductors have been utilized to absorb visible/UV radiation and transfer this energy to CO_2[10]. Additionally, various Ti species in silicate-based micro/mesoporous materials are also active towards CO_2 photoreduction. These include isolated, tetrahedral Ti species substituting framework-Si in mesoporous silicates[11, 12], TiO^{2+} species prepared via ion-exchange in microporous aluminosilicates[13], isolated[14, 15] and bimetallic[16] Zr^{4+}- and Ti^{4+}-containing species grafted onto the pore surface of mesoporous materials.

Whereas the semiconductor-mediated reduction of CO_2 involves the generation of electron-hole pairs and their subsequent transfer to CO_2 and a reductant respectively, the metal complexes undergo local charge transfer transitions leading to electron transfer to CO_2. Analogously, the isolated and bimetallic Ti-centers in micro/mesoporous silicates also undergo local ligand-to-metal charge transfer (LMCT) and metal-to-metal charge transfer (MMCT) transitions respectively. Although the metal complex photocatalysts exhibit comparatively higher yields and turnovers towards CO_2 photoreduction, a sacrificial electron donor (typically an amine) is required to regenerate the photocatalyst. On the other hand, a semiconductor that has its conduction and valence bands placed suitably to transfer electrons to CO_2 and oxidize inexpensive reductants, such as water, can be designed. Among various semiconductors, TiO_2 is widely used in many

photoinduced processes because of its comparatively low cost, low toxicity[17] and its ability to resist photocorrosion[18]. TiO_2 is a wide-band gap semiconductor (E_g ~3.2 eV) and occurs as three polymorphs: anatase, rutile and brookite. Among these, anatase is obtained via "soft" chemical syntheses, and transforms upon heating (to temperatures greater than 700-800 K) to the rutile phase. Surface science aspects of TiO_2 have been described in detail by Diebold[19]. Anatase is the more photocatalytically active form of TiO_2, though not for all applications. Anatase also has a larger band gap compared to rutile. However, surface science studies of anatase single crystals have only begun in the past eight years[20-28], whereas the rutile surfaces have been studied more extensively[29-33].

A semiconductor photocatalyst mediating CO_2 reduction and water oxidation needs to absorb light energy, generate electron hole pairs, spatially separate them, transfer them to redox active species across the interface and minimize electron hole recombination. This requires the semiconductor to have its conduction band electrons at higher energy compared to the CO_2 reduction potential while the holes in the valence band need to be able to oxidize water to O_2. A single semiconductor does not usually satisfy these requirements. Moreover, current CO_2 photoreduction catalysts do not perform as effectively as current solar hydrogen generation catalysts. Therefore, to develop better Ti-based CO_2 photoreduction catalysts, one needs to understand interactions between CO_2 on ground and excited state TiO_2 surfaces or Ti-based catalyst sites.

1.3 Current state of CO_2 photoreduction on TiO_2-based catalysts

Titania (TiO_2) based photocatalysts have been used to convert CO_2 to useful compounds, both in gas and aqueous phase photoreactions. The conversion of CO_2 and water to simple C products such as formic acid and formaldehyde using irradiated aqueous suspensions of titania was first demonstrated by Inoue et al.[34]. Researchers have also used homogeneous metal complexes in solution to reduce CO_2[35]. A summary of recent literature on CO_2 photoreduction involving isolated Ti-species as well as bulk TiO_2 materials is given in Table **1-1** and Table **1-2**.

Some recent developments in this field have been moves towards rational photocatalyst design, the use of highly active isolated Ti-species in mesoporous and microporous materials[11, 14, 15, 36-40], metal-doping of TiO_2, development of catalysts active at longer wavelengths than can be achieved with commercially available titania, and the elucidation of reaction mechanisms through in situ spectroscopic studies[14, 41]. A comparison of the CO_2 conversion rates from various studies is shown in Figure **1-2**. Although it would be more instructive to compare the conversion efficiencies and quantum yields of various TiO_2-based catalysts, often such data are not readily available. The data in Figure **1-2** illustrate typical rates of CO_2 photoreduction, and are dependent upon many variables such as metal doping, CO_2:H_2O ratios, dispersion of Ti, coordination of Ti species, light intensity, type of lamp used, etc., which are already discussed in detail in the literature (see for example, Usubharatana et al.[10],and references therein). In references b-c, f and g in Figure **1-2**, Anpo and coworkers used Ti-species in

microporous or mesoporous silicates as catalysts whereas the rest of the works cited used doped/undoped TiO_2.

Table **1-1**: Summary of results from recent literature on isolated Ti-species used as photocatalysts mediating CO_2 reduction.

Catalyst	Reaction system used	T, (K) and P, (Pa)	CO_2:H_2O mole ratio	Light source used	Notes	References
Pt impregnation of a) Ti-ion-exchanged zeolites and, b) framework-Si substituting Ti-MCM-48.	Gas-solid system. Flat-bottomed quartz cell connected to conventional vacuum system ($1x10^{-4}$ Pa), 88 ml	328 K, pCO_2 = 734 Pa	0.2	75 W high-pressure Hg lamp, $\lambda > 280$ nm	Pt addition increased selectivity towards CH_4 compared to CH_3OH, and quenched photoluminescence yields.	Anpo et al.[13], Yamashita et al.[37], Anpo et al.[11]
Fluorination of Ti-FSM-16	do	323 K	0.2	100 W high-pressure Hg lamp, $\lambda > 250$ nm	Fluorination (hydrophobicity) increased selectivity towards CH_3OH over CH_4.	Ikeue et al.[38]
Ti-containing porous silica thin film photocatalyst	do	323 K	0.2	100 W high-pressure Hg lamp, $\lambda > 250$ nm	Thin film photocatalyst exhibited high quantum yield (0.28%).	Ikeue et al.[39]
Framework-Si substituting Ti-MCM-41	Miniature infrared vacuum cell, 3.4 ml	298 K, P = 0.1 MPa	61.67	266 nm	CO, O_2 detected as products of single photon, two-electron transfer. H_2O confirmed as a stoichiometric electron donor.	Lin et al.[15]
Ti(IV)-Sn(II) bimetallic redox centers in MCM-41	Infrared vacuum cell	-	-	Third harmonic emission of a Nd:YAG laser, 355 nm	Ti^{3+} centers formed under 355 nm and visible light irradiation due to Sn(II) → Ti(IV) MMCT.	Lin and Frei[16]

Table **1-2**: Summary of recent literature on doped-TiO_2 used as photocatalyst mediating CO_2 reduction

Catalyst modification	Reaction system used	T, (K) and P, (Pa)	CO_2:H_2O	Light source	Notes	References
Cu(II) impregnation of JRC-TiO-4	Gas-solid system. Flat-bottomed quartz cell connected to conventional vacuum system ($1.33x10^{-4}$ Pa), 60 ml	275 K	0.33	75 W high-pressure Hg lamp, $\lambda > 290$ nm	Increased selectivity towards CH_3OH over CH_4 .	Yamashita et al.[42]
Cu(I) doping of TiO_2, sol-gel synthesis	Slurry photoreactor, 300 ml	~323 K, P = 0.1 MPa	-	8 W Hg lamp, UV-C, λ = 254 nm	Increased selectivity towards CH_3OH over CH_4 , Cu(I) active species.	Tseng et al.[43]
Cu(I) doping of TiO_2, sol-gel	Gas-solid continuous optical fiber photoreactor (OFPR), 120 optical fibers	348 K, pCO_2 = 0.1 MPa	50	λ = 365 nm	Cu_2O clusters influenced CH_3OH formation.	Wu et al.[44]
Nanoscale Ag-coated TiO_2 particles embedded in Nafion membrane	High-pressure optical cell, stacked catalyst films. 2 ml H_2O added after irradiation	pCO_2 = 13.7 MPa	-	990 W Xe arc source, water filter.	Small TiO_2 nanoparticles (4-6 nm) embedded in ionomer. CH_3OH main product after Ag-coating of TiO_2. Catalyst films could be reused and were chemically stable.	Pathak et al.[45]
Dye ($[Ru(Bpy)_3]^{2+}$, perylene diimide based)-sensitized, Pt-promoted, thin and thick film-TiO_2 photocatalysts	Glass chamber connected to a vacuum line	298 K, pCO_2 = 0.09 MPa	34.5	75 W visible daylight lamp, 150 W UV A lamp	Pt-impregnation resulted in higher CH_4 yields under UV irradiation compared to sol-gel synthesized Pt/TiO_2. Organic sensitizers decreased catalytic activity under UV light and resulted in CH_4 evolution under visible light irradiation.	Ozcan et al.[46]
TiO_2-coated Pyrex glass pellets, H_2, H_2O as reductants	Packed bed, circulated photocatalytic reactor	316 K	1, H_2:CO_2 = 90	4 near-UV lamps, λ = 365 nm	CH_4, CO and C_2H_6 formed as reaction products.	Lo et al.[47]

Table 1-2 continued

Catalyst modification	Reaction system used	T, (K) and P, (Pa)	CO_2:H_2O	Light source	Notes	References
Cu, Fe substitution in TiO_2-SiO_2, sol-gel synthesis	Same as above, 216 fibers	348 K	-	150 W high-pressure Hg lamp, λ = 320-500 nm, concentrated sunlight, λ = 500-800 nm,	Fe substitution resulted in full visible light absorption. Cu-Fe/TiO_2 favors C_2H_2 formation, Cu-Fe/TiO_2-SiO_2 favoredCH_4 formation (quantum yield: 0.0235%).	Nguyen et al.[48, 49]
Ruthenium dye (N3)-sensitized Cu-Fe/TiO_2 catalysts	Same as above, 216 ml	348 K	-	same as above, I^{solar} = 20 mW/cm^2, I^{lamp} = 225 mW/cm^2	Dye sensitization resulted in higher CH_4 yields under concentrated sunlight due to stronger absorption bands in the visible spectrum. N3 dye stable after 6 h-photoreactions.	Nguyen et al.[50]
Mixed phase TiO_2 nanocomposite prepared by $TiCl_4$ hydrolysis in the presence of anatase powder	Annular glass reactor, isopropanol hole scavenger, 1280 ml	293 - 298 K	-	450 W, medium-pressure Hg lamp, UV-visible irradiation	Anatase-rutile nanocomposite exhibited higher CH_4 evolution rates compared to Degussa P-25 TiO_2 and pure anatase catalysts. Effective charge separation between anatase and rutile phases postulated to explain the higher photoactivity.	Li et al.[51]

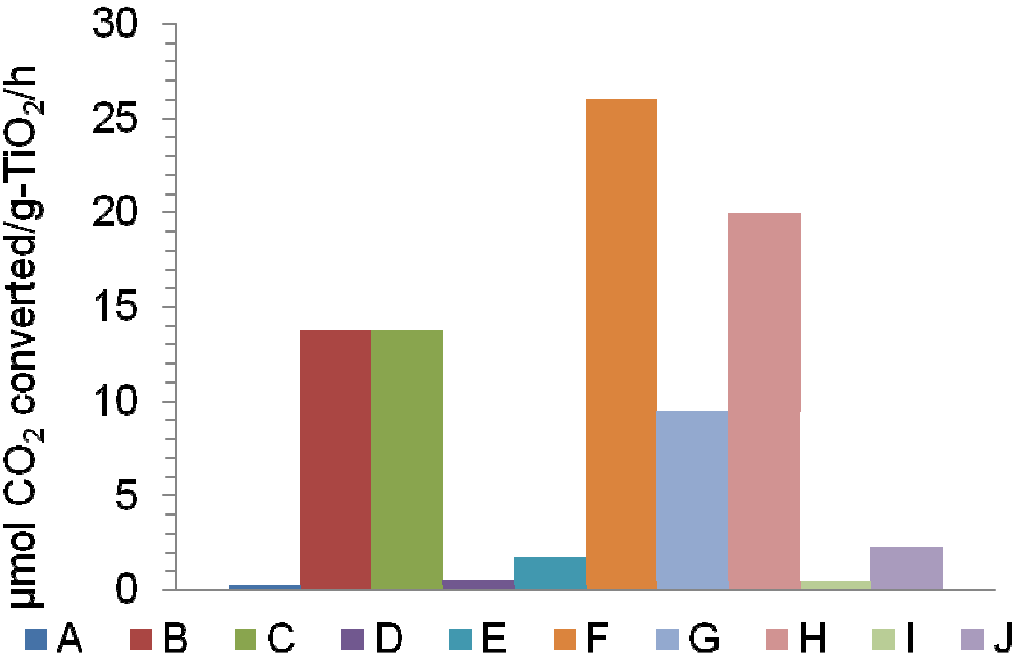

Figure **1-2**: The highest specific rates of CO_2 photoreduction (µmol CO_2 converted/g TiO_2/h) obtained using various doped and undoped Ti-based catalysts in selected recent articles. (A): Yamashita et al., (1994)[52], (B): Anpo et al.[13], (C): Yamashita et al.[37], (D): Kaneco et al.[53], (E): Kaneco et al.[54], (F): Ikeue et al.[38], (G): Ikeue et al.[39], (H): Tseng et al.[43], (I): Wu et al.[44], (J): Nguyen et al.[6, 55]

1.4 Comparisons of CO_2 photoreduction rates to solar H_2 generation

Although CO_2 photoreduction has been studied since the 1970s, to the authors' knowledge, there are no studies on its performance versus alternative approaches. Comparing the rates of CO_2 photoreduction with other photosynthetic processes, such as solar hydrogen generation, presents another means to assess the viability of CO_2 photoreduction to limit GHG emissions. To better understand the current state of CO_2

photoreduction using Ti-based catalysts, we converted the specific weights in Figure **1-2** to units of micromoles CO_2 converted/hour, using the catalyst weights, and titania weight percentages. These data were used to determine the ratio of CO_2 converted by photoreactions to the amount of CO_2 emitted during lamp operation (all references in Figure **1-4** used UV lamps) These data indicate that current Ti-based photoinduced CO_2 conversion processes emit more CO_2 than that converted. As a caveat, we note that only minimal efforts were likely made to improve the light absorption in the references cited in Figure **1-4**. This might be one reason why the overall efficiency (kg CO_2 converted/kg CO_2 emitted by lamp) is low. However, significant improvements, both in the specific rate of CO_2 reduction (as indicated by the arrow in Figure **1-4**) as well as the quantum yield of the photoreaction, are needed to make this process economically feasible.

There are two conceptual routes to producing renewable C-containing fuels using solar energy. The first, the topic of this review, is the direct photoreduction of CO_2 using water as a reductant, whereas the second route involves the photolysis of water to generate hydrogen and further reaction of this hydrogen with carbon dioxide, forming C_1-C_2 fuels. Both the efficiency of the conversion of solar energy to useful chemical energy as well as the rates of photoreduction of hydrogen/reduced C_1-C_2 compounds are pertinent parameters that determine economic feasibility of such processes. Assuming that the efficiency of solar energy conversion is almost the same in the two routes, the choice between direct and indirect hydrogenation of CO_2 is determined by the rates of photoreduction.

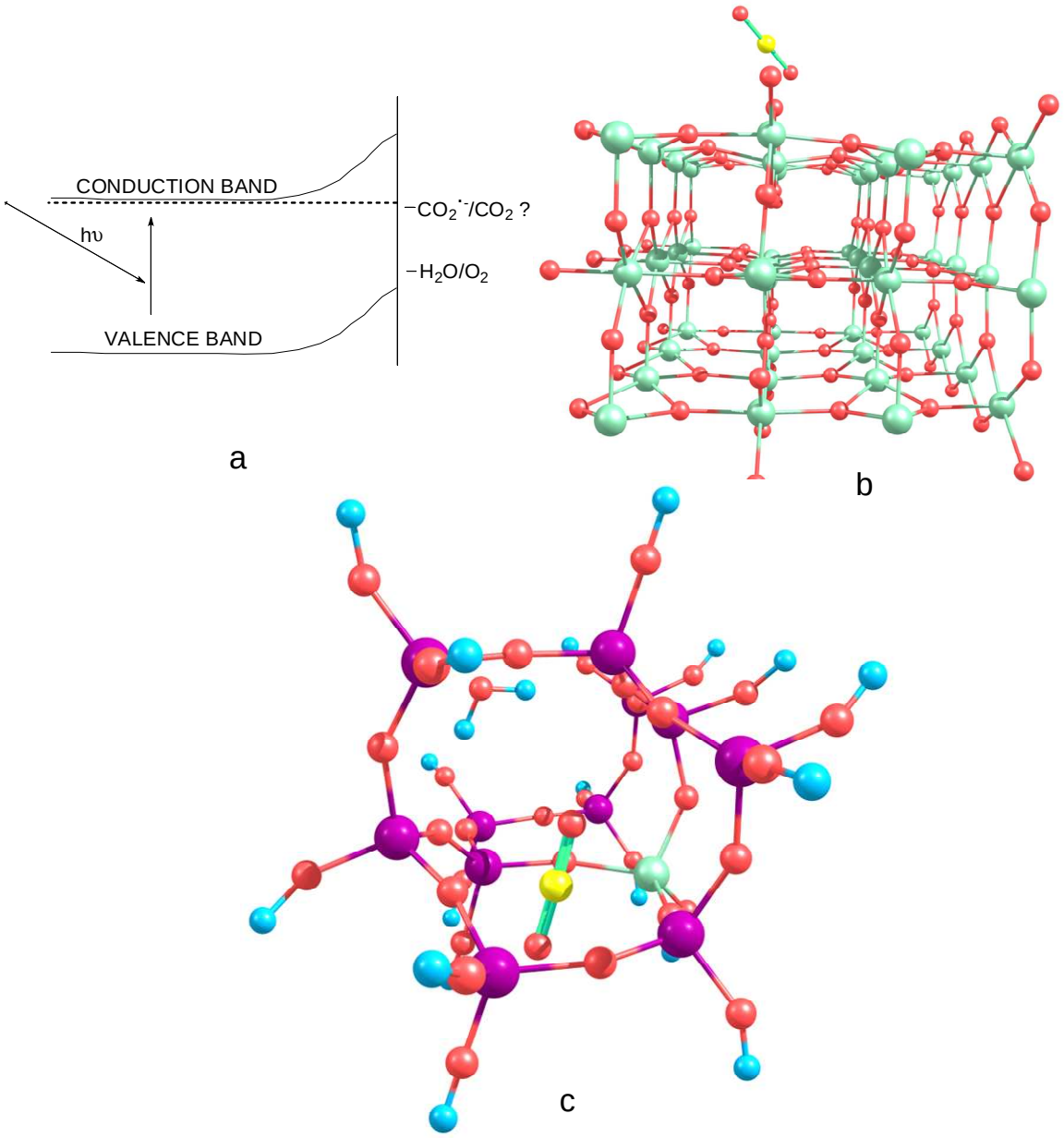

Figure **1-3**: Scope of the aspects of CO_2 photoreduction discussed in this review: (a): Surface state models indicating the location of the $CO_2^{\bullet-}/CO_2$ energy levels in comparison with the conduction and valence bands of TiO_2, Surface site models of CO_2 on Ti-based catalysts, (b): CO_2 adsorption on doped/undoped TiO_2 surfaces, (c): CO_2 interacting with isolated model Ti sites in meso/microporous materials such as titanosilicates

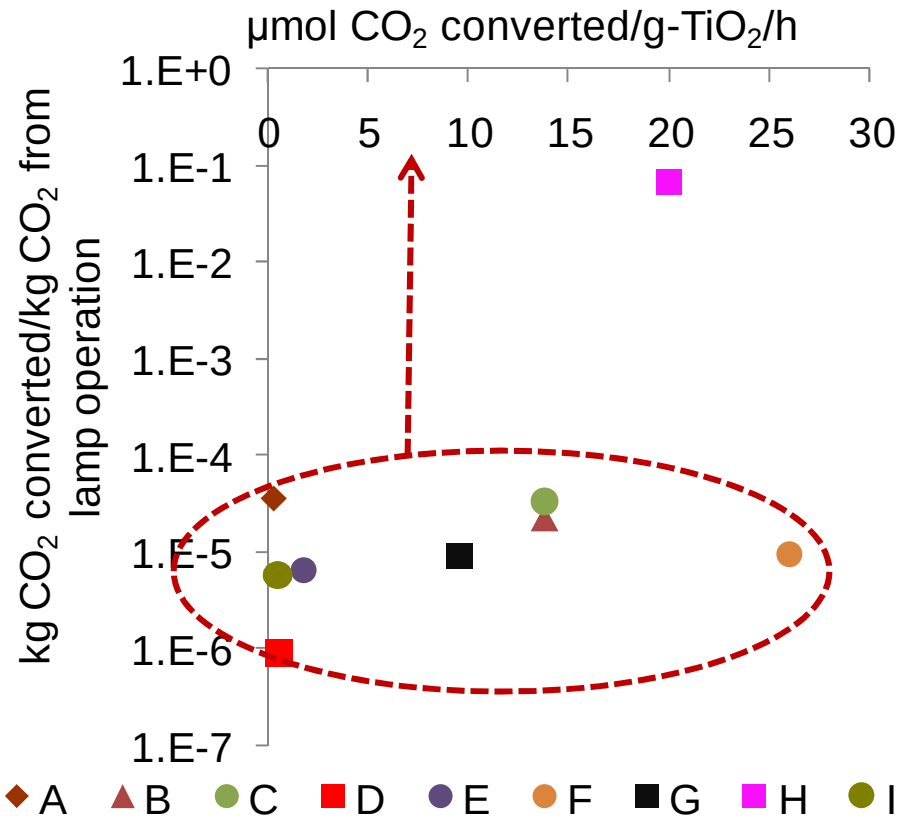

Figure 1-4: Amount of CO_2 converted to reduced-C species per unit of CO_2 evolved from lamp operation (assuming coal-fired power generation), from recent literature data on CO_2 photoreduction using Ti-based catalysts.[1] Current Ti-based photoinduced CO_2 conversion processes emit more CO_2 than they convert. References same as those in Figure 1-2.

On the other hand, typical rates of CO_2 photoreduction in aqueous systems containing suspended metal oxides (TiO_2, $BaTiO_3$ etc.) are much lower, approximately 1 μmol/h C_1/C_2 product/h under UV radiation[36]. Using copper-doped TiO_2 and by conducting the photoreduction under a pH bias, Tseng and Wu[56] obtained a slightly higher methanol formation rate of 12 μmol/h. In gas-solid systems, using isolated Ti-sites

[1] A lamp power of 150 W was assumed in Wu et al.(2005). All references except Tseng et al.(2002) used lamp wattages ≥75 W.

in micro/mesoporous materials, Anpo and co-workers[11-13] obtained CH_4/CH_3OH formation rates of approximately 0.05 μmol/h. Although the intensity of the light used in these various studies is not the same, the above numbers indicate that current CO_2 photoreduction catalysts do not perform well in comparison with solar-hydrogen generating catalysts, both in terms of product formation rates, and the wavelengths of light needed to sustain reaction. This is because both water oxidation as well as fuels formation from CO_2 are multi-electron transfer reactions. Whereas oxygen evolution via water oxidation is the major limiting factor in solar hydrogen production, both CO_2 photoreduction as well as water oxidation have to occur simultaneously in a photoreactor using water as the reductant. In this connection, we also note that a recent design for a 100 T/year pilot plant producing methanol[57] from CO_2 involves solar photolysis of water to produce H_2 and subsequent hydrogenation of CO_2 using a heterogeneous catalyst and not the direct photoreduction of CO_2. Additionally, Zeman and Keith propose producing carbon-neutral hydrocarbons from atmospheric CO_2 and renewable hydrogen[58].

Although the kinetics of CO_2 photoreduction are two-three orders of magnitude slower than hydrogen photoreduction, one advantage of the direct photoreduction of CO_2 compared to hydrogen evolution is the lower energy needed per electron transferred to convert CO_2 to CH_4 or CH_3OH, Additionally, the use of carbon-based solar-derived fuels likely does not need significant investments in infrastructure, unlike solar hydrogen generation and further reactions with CO_2. The thermodynamics of CO_2 photoreduction are discussed in the following section.

1.5 Thermodynamics and initial steps of CO_2 activation and further conversion

"Activation" refers to the transformation of a relatively inert species (such as CO_2, CH_4) to more reactive forms using some form of energy input and/or an *activating agent*. The activating agent may or may not be regenerated after the process. Because of its significance in steam reforming and methanol production processes, CO_2 activation on the surfaces of metals such as Pt, Fe, Ni etc. has been studied in detail, both through in situ experiments on well defined surfaces[59] as well as by computational modeling (see for example, Wang et al.[60], and references therein). Metals belonging to the platinum-group are however either expensive or will be in limited supply in the future. Nevertheless, metals play an important role in industrial catalytic processes where CO_2 is either a reactant or a product. For example: Ni-based supported catalysts are used in CO_2 reforming/steam reforming of methane. The similarities between homogeneous metal complexes of CO_2 and heterogeneous metal-CO_2 surface species have been noted by Gibson in a review[61]. As an example, a study by Wovchko and Yates demonstrated the activation of CO_2 by a metal complex ($Rh^I(CO)_2$) immobilized on an alumina support[41]. Similar studies would lead to the rational design of photocatalysts mediating CO_2 reduction. The surface chemistry of CO_2 on metals and oxide surfaces was reviewed by Freund and Roberts[62].

CO_2 is one of the most stable compounds of carbon. Gaseous CO_2 is linear and does not have a dipole moment. However, the oxygen atoms each have a lone pair of electrons and can donate these electrons to surface Lewis acid centers. The carbon atom could also gain electrons from Lewis base centers such as oxide ions, forming carbonate-

like species. Additionally, the (C-O) π electrons can also participate in reactions with electron centers. Therefore, reactions of CO_2 involving Lewis acid and base centers and the π orbitals constitute the initial steps of its activation. The simplest reduction products that could be produced from CO_2 reduction are CO and $HCOO^-$. One, two, four, six and eight electron reduction potentials (vs.NHE) for CO_2 reduction and H_2O oxidation at pH 7 and 25°C assuming unit activities for all gaseous and aqueous species are given in Scheme **1.1**[63]

Reaction	E^0_{redox}, V vs. NHE	**1.1**
$2H^+ + 2e^- \longrightarrow H_2$	-0.41	
$H_2O \longrightarrow 1/2\,O_2 + 2H^+ + 2e^-$	-0.82	
$CO_2 + e^- \longrightarrow CO_2^{\bullet-}$	-1.90	
$CO_2 + H^+ + 2e^- \longrightarrow HCO_2^-$	-0.49	
$CO_2 + 2H^+ + 2e^- \longrightarrow CO + H_2O$	-0.53	
$CO_2 + 4H^+ + 4e^- \longrightarrow HCHO + H_2O$	-0.48	
$CO_2 + 6H^+ + 6e^- \longrightarrow CH_3OH + H_2O$	-0.38	
$CO_2 + 8H^+ + 8e^- \longrightarrow CH_4 + 2H_2O$	-0.24	

From Scheme **1.1**, it is clear that CO_2 photoreduction is not a single-step reaction. Additionally, single electron transfer to CO_2 is highly endergonic, because of the negative adiabatic electron affinity of CO_2[62]. CO_2 activation involves the formation of a negatively charged $CO_2^{\delta\bullet-}$ species[62, 64]. The first plausible step in CO_2 photoreduction on TiO_2 surfaces is therefore its activation to form a $CO_2^{\delta\bullet-}$ species. $CO_2^{\bullet-}{}_{(g)}$ is a 23 electron radical anion. It is significantly distorted from the linear $D_{\infty h}$ geometry due to the repulsion among the two lone electron pairs on the oxygen atoms and the unpaired electron on the carbon atom. Therefore, the lower the O-C-O bond angle, the higher the charge of the

$CO_2^{\delta\bullet-}$ moiety. $CO_2^{\delta\bullet-}$ can be detected via infra red spectroscopy[65] as well as electron paramagnetic resonance (EPR) spectroscopy[66].

The initial step in the photocatalytic reduction of CO_2 is the generation of electron-hole pairs upon absorption of photons of energy greater than or equal to the band gap of the photocatalyst. The time scale of this electron-hole recombination is two to three orders of magnitude faster than other electron transfer processes. Therefore, any process that inhibits electron-hole recombination would greatly increase the efficiency and improve the rates of CO_2 photoreduction. The kinetics of CO_2 photoreduction are also dependent upon many other factors such as incident light intensity, fraction of the incident light absorbed by the photocatalyst, the specific surface area of the photocatalyst absorbing the light, etc.. In this chapter, we examined four such factors: (a) the use of titania-supported noble metals, (b) the use of isolated Ti-tetrahedral centers in micro/mesoporous materials, (c) the use of dye-sensitized TiO_2 to shift the absorption spectrum to the visible region and (d) the role of oxygen vacancies in electron trapping and activating CO_2.

Charge transfer from excited TiO_2 surface to CO_2 is influenced by both bulk and local interactions. Two different approaches for understanding electron transfer to CO_2 are using surface sites and surface states[67]. A surface site is a collection of atoms on the surface that is reactive in some manner. It may be a coordinatively under-saturated metal atom, oxygen vacancy or a combination of various other surface features resulting in a orbital having unusual electron affinity. A surface state is a localized energy level at the surface. The location of the surface state with respect to the Fermi energy (E_F) of the

solid determines its occupation. The surface site and surface state approaches to CO_2 photoreduction on TiO_2 will be described in detail in the following sections.

1.6 Surface state description of CO_2 activation on TiO_2

The main questions addressed by a surface state approach are:

1. Is electron transfer from the TiO_2 conduction band to CO_2 feasible upon UV illumination?
2. How do surface states (created, for example: by metal doping) affect the reactivity towards CO_2 photoreduction?

A knowledge of surface state energy levels for the $CO_2/CO_2^{\bullet-}$ couple at the TiO_2 surface is required to determine the feasibility of electron transfer to CO_2 from the conduction band of TiO_2 A methodology to determine the energy levels (of the surface states) at the solid-gas interface has been proposed by Morrison[68]. Accordingly, for the case of a non-interacting redox couple on a solid surface, the location of the standard redox potential in the absolute vacuum scale (AVS) units with respect to the edges of the conduction and valence bands of the solid at the point-of-zero-charge (pzc) determines the potential for electron transfer. Because this chapter concerns the gas-solid photoreduction of CO_2, the relevant states in question are those at the TiO_2-CO_2 interface. However, it is helpful to compare the energy required to reduce CO_2 in gas-liquid systems to that in gas-solid systems. The location of the energy levels associated with the $CO_2/CO_2^{\bullet-}$ redox couple in various media (gaseous, aqueous solutions) are shown in comparison to the location of the conduction band edge of TiO_2 at pzc in Figure 5. The

standard reduction potential of the $CO_2/CO_2^{\bullet-}$ redox couple vs. the standard hydrogen electrode (SHE) is ~1.9 V[69]. On the absolute vacuum scale (AVS), this potential is 2.6 V, which corresponds to a redox state with an energy level at -2.6 eV. The main contributions to this energy are the electron affinity of CO_2 (-0.6 eV) and the solvation of $CO_2^{\bullet-}$ in water (-3.2 eV). The high free energy of solvation indicates that solvent reorganization energy will be significant. Therefore, a fluctuating energy level mechanism is needed to describe energy levels of CO_2 and $CO_2^{\bullet-}$. Nevertheless, without any specific interaction with the catalyst/electrode surface, it is clear from Figure **1-5** that the reduction of CO_2 on TiO_2 surfaces in aqueous solutions is unlikely because the energy level associated with the $CO_2/CO_2^{\bullet-}$ redox couple is higher in energy compared to the conduction band of TiO_2.

$$CO_{2(g)} + e^-_{(g)} \longrightarrow CO^{\bullet-}_{2(g)} \qquad \textbf{1.2}$$

$$\Delta G = -EA$$

$$CO^{\bullet-}_{2(g)} \xrightarrow{\text{Surface}} CO^{\bullet-}_{2(ad)}$$

$$\Delta G = \Delta G^0_{ad}$$

$$CO_{2(g)} + e^-_{(g)} \xrightarrow{\text{Surface}} CO^{\bullet-}_{2(ad)}$$

$$E^0_{vac,energy} = [\Delta G^0_{ad}(CO_2^{\bullet-}) - EA]/F$$

In Scheme **1.2**, EA is the adiabatic electron affinity of gaseous CO_2 (in kJ/mol) and $\Delta G_{ad}{}^0$ is the heat of chemisorption of $CO_2^{\bullet-}$ on the surface (in kJ/mol). F is the Faraday's constant (the charge of a mole of electrons). The overall free energy change of the reaction is $\Delta G^0 = [\Delta G_{ad}{}^0(CO_2^{\bullet-}) - EA]$. In the absolute vacuum scale (AVS), the energy level associated with such a conversion will be $E^0{}_{vac,energy} = \Delta G_{ad}{}^0/F$ (eV). In other

words, the effect of interactions of CO_2 with the surface is to decrease the energy required for CO_2 reduction.

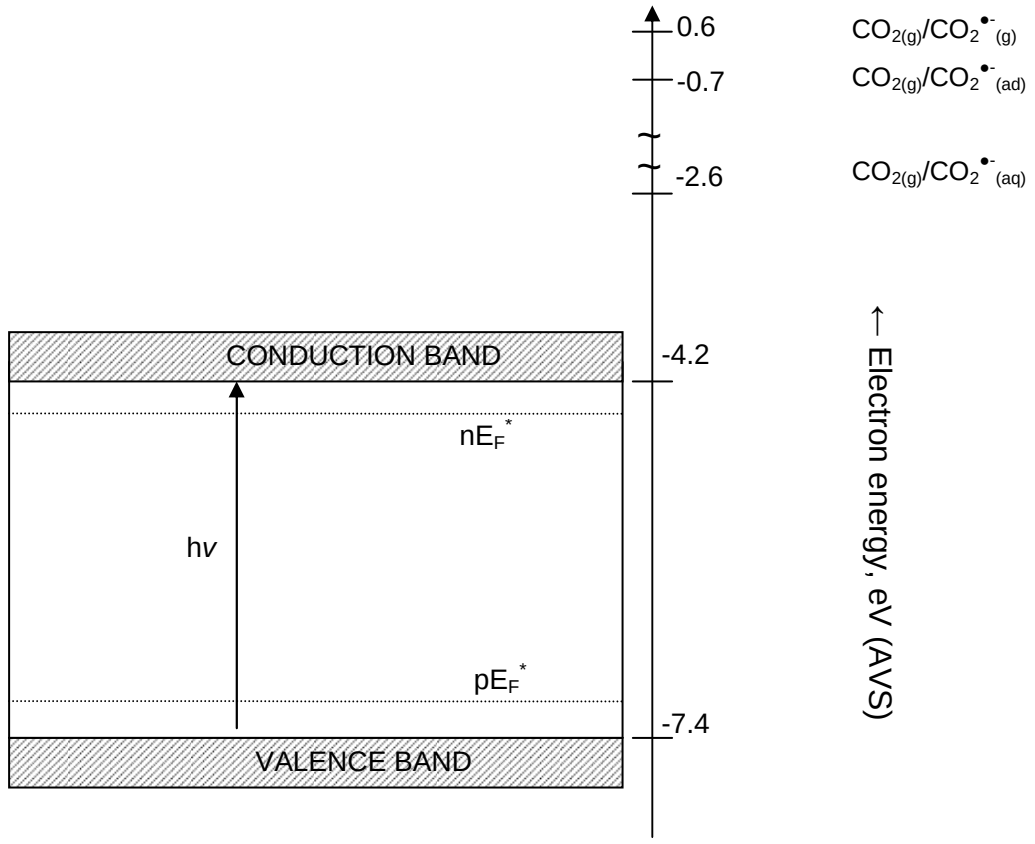

Figure 1-5: Location of the conduction band of TiO_2 (rutile) particles at the point-of-zero charge (pzc) with respect to the standard energy states associated with the $CO_2/CO_2^{\bullet-}$ couple. Photoinduced electron transfer from stoichiometric TiO_2 to CO_2 is not possible because the surface state is not lower than the Fermi energy (E_F) of the electrons in photoexcited TiO_2. The bands are shown at the flat band condition. The exact locations of the Fermi energy levels for electrons and holes (nE_F^* and pE_F^*) are not to scale.

Compared to the solid-liquid interface, measurement of band edges and surface states at the solid-gas interface is relatively more difficult. The exact location of the $CO_{2(surface)}^{\bullet-}/CO_{2(g)}$ surface state on TiO_2 is currently not known. One way to estimate this value

is using the an approach analogous to that used by Koppenol[69]. $CO_2^{\bullet-}$ adsorption on metal oxide surfaces can be conceptually thought of as the capture of an electron by CO_2 molecule in vacuum/gas-phase forming the anion radical, followed by its adsorption on the metal oxide surface. (In practice, CO_2 adsorbed on a hydrated/hydroxylated metal oxide surface captures a trapped electron either from the defect sites or trapping sites.)

Typical values for the heat of chemisorption of $CO_2^{\bullet-}$ on metal surfaces (Ni) are of the order of ~50 of kJ/mol[60]. If the heats of chemisorption $CO_2^{\bullet-}$ on TiO_2 surfaces were approximately 100 kJ/mol CO_2, the surface state associated with the $CO_2/CO_2^{\bullet-}$ couple will be lowered approximately 1.3 eV from its gas-phase value, resulting in values of $E_{energy,AVS}^{0}(CO_{2(g)}/\ CO_2^{\bullet-}{}_{(ad)})$ of -0.7 eV, which is much more negative than that in aqueous solution. This simplistic analysis is not fully accurate, because the heat of chemisorption (arising out of local interactions of $CO_2^{\bullet-}$ with the TiO_2 surface) is comparable to the gas-phase electron affinity of CO_2. Moreover, the electrostatic contribution (due to the Madelung potential of TiO_2) is ignored. To understand this further, one needs to study the exact bonding between $CO_2/CO_2^{\bullet-}$ couple and the surface. CO_2 is plausibly bonded to TiO_2 surface differently compared to $CO_2^{\bullet-}$. Therefore, the so called “Frank-Condon splitting” of surface state energy levels also needs to be taken into account, which requires some description of the interaction of $CO_2^{\bullet-}$ with the surface atoms. One example of this is a recent study by Bonapasta et al.[70] where the energy levels of neutral and electron-attached states of O_2 adsorbed on (100) anatase TiO_2 surface were calculated using a surface molecule description of adsorbates in combination with periodic density functional theory calculations.

Experimentally, such surface states may be identified by spectroscopic studies of CO_2 adsorbed on well-defined rutile TiO_2 surfaces. Using ultraviolet photoemission spectroscopy (UPS) and metastable impact electron spectroscopy (MIES), Krischok et al.[71] found that CO_2 interacted with rutile TiO_2 single crystals weakly, forming linearly adsorbed species. This is also supported by the results of an ab initio periodic study of CO_2 adsorption on rutile[72]. CO_2 therefore does not form a surface state upon linear adsorption (involving Lewis acid-base interactions) in the ground-electronic state (without irradiation). Irradiation with light of energy greater than the band gap creates electron-hole pairs in TiO_2, with the electrons populating the conduction band. Using the previous analysis, the energy of conduction band electrons in TiO_2 is likely to be lesser than that required for CO_2 reduction to $CO_2^{\bullet\delta-}$.

In conclusion, the above analysis indicates that the major factors controlling the surface state energy levels for $CO_2^{\bullet-}{}_{(ad)}$ are the electron affinity of CO_2 (in the gas phase) and the local interaction of $CO_2/CO_2^{\bullet-}$ redox couple with the TiO_2 surface. It is clear that a description of the energy levels of $CO_2/CO_2^{\bullet-}$ couple on TiO_2 surfaces requires a combination of local and collective approaches. Therefore, we describe the surface site model of CO_2 activation on TiO_2 in the next section.

1.7 Surface site description of CO_2 activation on TiO_2

In recent years, knowledge of surface photocatalytic processes has progressed from a surface state approach to a more detailed understanding of specific surface adsorbate structures that are involved in the charge transfer. Nowotny et al. [73] noted this,

using photooxidation of water as an example.. Compared to the understanding of the initial steps of H_2O oxidation on TiO_2 surface, not much is known about the initial steps of CO_2 activation during the photocatalytic reduction. As noted in the earlier section, to better understand the nature of this charge transfer, one also needs to understand local chemistry at surface sites where activated species are formed. CO_2 can be adsorbed as a carbonate and a linear species on TiO_2 surfaces. Various ground-state adsorbate configurations of CO_2 on TiO_2 surfaces have been studied[72, 74-76]. CO_2 acts as a net donor of electrons when it adsorbs with the oxygen end on Ti Lewis acid sites, and a net acceptor of electrons when the electrophilic C atom interacts with surface electron centers or Lewis basic sites (surface O atoms)[62]. A limiting case of the electrophilic interaction between the C atom of CO_2 and the surface oxygen atoms is the formation of surface carbonate and bicarbonate species. On the other hand, if CO_2 does not interact strongly with TiO_2 in the ground state, the LUMO of adsorbed CO_2 may not be lowered enough to ensure electron transfer from the TiO_2 surface. The primary questions addressed by a surface site approach are:

1. Upon illumination of the surface, how does electron transfer from the TiO_2 conduction band to CO_2 occur?
2. What specific sites and specific CO_2 configurations on the TiO_2 surface promote this electron transfer? Can these sites be engineered?

The mechanisms proposed for CO_2 photoreduction over TiO_2 or Ti-based catalysts assume that CO_2 gains electrons from the conduction band of TiO_2[10]. This indicates a strong interaction between CO_2 and the TiO_2 surface. Photoexcitation of TiO_2 produces electron-hole (Ti^{3+}-O^-) centers in TiO_2. In the next step, these Ti^{3+} centers are

proposed to interact with CO_2 forming $CO_2^{\delta\bullet-}$ species adsorbed on the surface. These carbon dioxide radical anions then undergo further reactions to form C radicals and CH_xO_y end products. Electron transfer from Ti^{3+} surface electron centers to CO_2 requires the presence of suitable unoccupied molecular orbitals on CO_2. Electronic interaction between the surface and CO_2 is necessary for CO_2 to gain electrons. Freund and Roberts[62] indicate that the lowest unoccupied molecular orbital (LUMO) of CO_2 decreases with the O-C-O bond angle. This variation of the LUMO of CO_2 with the O-C-O bond angle is shown in Figure 1-5.

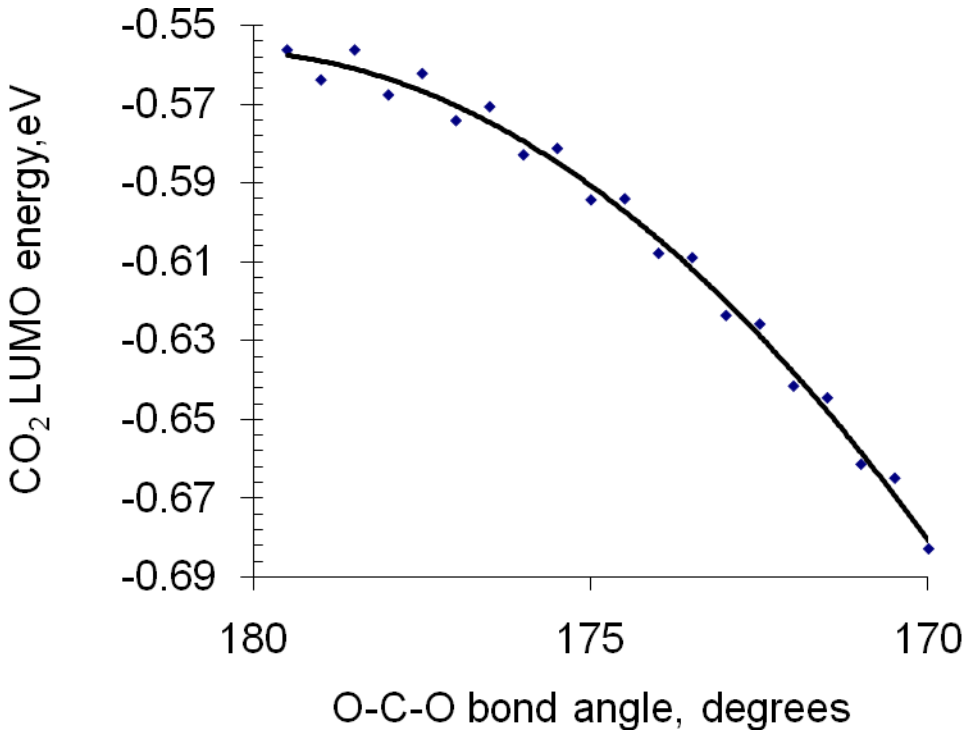

Figure **1-6**: The variation in the energy of the LUMO of gaseous CO_2 with the O-C-O bond angle, calculated using constrained quantum chemical calculations at the B3LYP/6-31+G(d) level of theory. Decreasing the O-C-O bond angle (via surface interactions) may facilitate charge transfer to CO_2 by lowering its LUMO

One role of the surface might be to interact with CO_2 reducing the bond angle. In the limiting case, this corresponds to the formation of carbonate-like species on the surface. This principle is not limited to CO_2 activation on irradiated metal oxides alone. Similar interactions of CO_2 with the electrocatalyst are supposed to decrease the overpotential for CO_2 reduction[77] during electrochemical reduction of CO_2.

Techniques such as Fourier transform infra red (FT-IR) spectroscopy have been used to study CO_2 adsorbed on surface electron centers (Ti^{3+}) created due to oxygen vacancies[74]. CO_2 adsorption on reduced TiO_2 surfaces generated IR signals corresponding to $CO_2^{\delta\bullet-}$ species.

In the following section, we will examine the use of these two (surface state, surface site) approaches to understand photoinduced reactivity of Ti-based catalysts towards CO_2

1.8 Utility of surface state and surface site approaches in understanding the elementary reactions involved in CO_2 photoreduction on Ti-based catalysts

1.8.1 Effects of alkali and transition metal doping on CO_2 photoreduction

Some approaches to make the thermodynamics of CO_2 reduction on TiO_2 more favorable are the use of promoters such as potassium (K) or through impregnation with noble metals. Alkali promotion of CO_2 activation on TiO_2 has been well studied[33]. The added alkali atom donates an electron to CO_2, forming $CO_2^{\bullet-}$ species. This reacts with the surface oxygen to form a surface carbonate species. Such promoters are stoichiometrically consumed upon charge transfer to CO_2 because they usually cannot be

regenerated (photo)catalytically in an environment containing water vapor and oxygen. On the other hand, the modification of TiO_2 surface with metals such as Pt, Rh etc. may affect both the thermodynamics as well as kinetics of CO_2 activation and further conversion.

In a study of photoinduced CO_2 dissociation on titania-supported noble metals, the activity towards CO_2 dissociation correlated with the work function of the polycrystalline metal for titania-supported Pt, Rh and Ir/TiO_2[76]. The following mechanism was proposed to account for photoinduced CO_2 activation on titania-supported noble metal catalysts: Chemisorption of CO_2 on polycrystalline metal islands results in a bent $CO_2^{\delta\bullet-}$ species formed by back donation between the metal d-orbitals and the (C-O) π^* orbitals. This electron transfer results in the "depopulation" of the metal surface state. Photogenerated electrons generated upon band gap illumination would be transferred from the conduction band of TiO_2 to the metal island (because the work function of these metals is higher than that of reduced TiO_2). Therefore, illumination of TiO_2-supported noble metal catalysts in a CO_2 atmosphere increased the intensity of signals corresponding to $CO_2^{\delta\bullet-}$ species. We note that such *activation* reactions require a concomitant oxidation reaction to be photocatalytic. Additionally, the study by Raskó[76] demonstrates that an understanding of both surface states as well as surface sites is needed to understand CO_2 activation on such TiO_2-supported metal photocatalysts. The case of Rh/TiO_2 is especially interesting, from a catalytic viewpoint if not from a practical perspective, rhodium being one of the most expensive metals in the world currently.

Recently, CO oxidation on gold clusters supported on TiO_2 has been studied extensively, both by experimental[78] and modeling[79, 80] studies. We note that CO oxidation also involves the formation of a $CO_2^{\delta\bullet-}$ intermediate. Therefore, a good CO oxidation catalyst may also promote CO_2 activation. Most studies have been performed on metallic clusters of gold on TiO_2. In these cases, density functional theory (DFT) calculations have shown that the binding strength of low-coordinated Au clusters with gaseous CO is a crucial parameter in the oxidation of CO[81]. Moreover, promotion effects may also contribute to the observed low temperature oxidation of CO to CO_2 in the presence of gaseous oxygen. In contrast, a Mars-van Krevelen mechanism was proposed by Chrétien and Metiu[82] to account for the activity of gold doped TiO_2, where the gold atom is positively charged and substitutes a five coordinate Ti atom on the rutile (110) surface.

In addition to activating CO_2, noble metal impregnation may also decrease the photogenerated electron-hole recombination rates, leading to higher product yields. Using femtosecond time resolved measurements of the intensity dependence of electron hole recombination in TiO_2 nanoclusters, Colombo et al.[83] found that more than half of the conduction band electrons underwent recombination within 20 picoseconds (ps). The remaining electrons were trapped at surface sites resulting in a longer lived species. Therefore, from an overall system perspective, the greatest gain in efficiency in CO_2 photoreduction may result by slowing down the rates of electron-hole recombination. Using surface photovoltage spectroscopy (SPS) measurements on Pd and Pd/RuO_2 doped TiO_2, Wang et al.[84] showed that the rates of CO_2 photoreduction to formate in aqueous solutions correlated with the surface photovoltage measured in air. Two pertinent conclusions could be drawn from their study. Firstly, surface modification of TiO_2 with

noble metals could lead to the formation of surface states, increasing the photogenerated electron-hole pair lifetimes. Secondly, the fact that photovoltages observed in air correlated with the yields in aqueous solutions indicates that electron-hole pair separation appears to be the primary control over the reactivity.

1.8.2 Visible light performance of dye-sensitized TiO_2 catalysts mediating CO_2 photoreduction

Another means to decrease electron-hole recombination rates and use higher wavelengths of the solar spectrum is the dye-sensitization of TiO_2. Closely related to this is the dye sensitized solar cell (DSSC), (see McConnell[85] and references therein for details about operation and comparisons). Briefly, the DSSC is a solar electric device where the light absorption and charge transport are physically separated. The organometallic dye attached to porous TiO_2 absorbs sunlight, and injects electrons into the conduction band of TiO_2, which flow through an external circuit, creating electricity. The oxidized dye is reduced by a mediator that in turn, is reduced at the metallic cathode of the solar cell. This concept has been applied to the photosensitization of TiO_2 anodes in photoelectrochemical (PEC) cells. A brief description of the operation of a dye-sensitized photoanode is provided by Bak et al.[86]. However, in the case of dye-sensitized TiO_2 used for photocatalytic CO_2 reduction applications[46, 50], it is less clear how the oxidized dye would be regenerated when the photoelectrochemical cell is short-circuited and no defined pathway for electron transport exists. Sacrificial photooxidation of the dye or other reagents probably occurs unless the oxidized state of dye has a surface state level ($Dye_{(surf)}^{+}/Dye_{(surf)}$) lower than that for water oxidation ($O_{2(surf)}/H_2O_{(surf)}$).

Nevertheless, Nguyen et al.[50] found substantial improvements in the photoactivity of (Cu,Fe)-TiO_2 photocatalysts towards CO_2 photoreduction in the presence of water and concentrated sunlight in an optical fiber photoreactor (OFPR). The higher activity was attributed to full visible light absorption, whereas TiO_2 only absorbs a fraction of the radiation above 400 nm. Only CH_4 was produced under sunlight, and the photocatalyst was reported to be stable for 6h. Whereas dye-sensitization of TiO_2 enables the use of visible light, we note that future studies should consider $^{13}CO_2$-isotope testing to ensure that the reduced C-products are due to CO_2 reduction, and not the sacrificial oxidation of the dye.

To summarize, both metal doping as well as dye-sensitization reduce the rates of electron-hole recombination, but the mechanisms involved are different. In the case of metal-doped TiO_2, the electrons are transferred from the conduction band of TiO_2 to the metal, whereas on a dye-sensitized photocatalyst, the dye injects electrons into the conduction band of TiO_2.

1.8.3 Isolated Ti-species acting as active sites for CO_2 photoreduction in micro/mesoporous materials

As discussed in Table 1-1, isolated tetrahedral Ti^{+4} species in zeolites or mesoporous sieves were used as catalysts by Anpo and coworkers[13,37,38,39] as well as Frei and coworkers[14, 15]. The location of the Ti atoms in mesoporous silica depend on the synthetic technique used[87]. Framework Ti-substituted MCM-41 is prepared when the Ti precursors are included in the MCM-41 synthesis gel (Lin et al.[15]). On the other hand, Ti-grafted MCM-41 is prepared by post-synthesis grafting (e.g., Lin and Frei[16]). In such Ti-

grafted MCM-41, the Ti atoms are located at the surface of the silicate wall and are not a part of the framework. They are therefore more accessible to reactants. However, this might also make them more susceptible to leaching in aqueous solutions. Moreover, depending on the titanium content, a variety of configurations for Ti species is possible[88].

Using in situ X-ray fluorescence spectroscopy (XAFS) studies to probe the local environment around an isolated Ti atom, Yamashita et al.[40] studied the effects of the hydrophobic–hydrophilic properties of Ti-β zeolites in the photocatalytic reduction of CO_2 with H_2O. Adsorption of CO_2 did not change the XANES spectra of Ti-β zeolite catalysts. On the other hand, the addition of water increased the coordination number of Ti atom from 4 to 6. Therefore, in the ground state, H_2O interacted more strongly with Ti-β zeolites compared to CO_2. In situ photoluminescence (PL) spectroscopy measurements on irradiated Ti-β zeolites indicated that the lifetime of the charge transfer excited state decreased in the presence of CO_2 and/or H_2O molecules. Therefore, while CO_2 interacted with the excited state of the Ti-β zeolite, water interacted with the Ti-centers in both excited and ground electronic states. Additionally, using in situ FT-IR spectroscopy to study the initial steps of CO_2 photoreduction with methanol as a sacrificial oxidant in a Ti silicalite molecular sieve, Ulagappan and Frei[89] recorded the formation of formic acid as the primary electron transfer product. They proposed that the initial step in this reaction involved electron transfer from the photoexcited LMCT state of the catalyst to CO_2 concurrent with methanol oxidation to form CO_2^- and CH_3OH^+ species which react further to produce formic acid and formaldehyde.

Although the above isolated tetrahedral Ti-centers in zeolites/mesoporous materials are active towards CO_2 photoreduction, the absorption of these materials lies in

the deep-UV (UV-C) region of the electromagnetic spectrum. To activate CO_2 using visible light, Frei's research group demonstrated metal-metal charge transfer (MMCT), involving two different metal ions grafted in a mesoporous material[16]. Examples include Ti-O-Cu(I) and Ti-O-Sn(II) as well as Zr-O-Cu(I) grafted in Mobil crystalline material (MCM)-41 molecular sieve. Irradiation of the binuclear Zr-O-Cu(I)/MCM-41 catalyst under a CO_2 atmosphere resulted in the growth of IR signals corresponding to CO and H_2O[90]. Only Zr-O-Cu(I) complexes showed CO formation. CO_2 dissociation was not observed on Ti-O-Cu(I) complexes. Lin and Frei attributed this to the higher reducing power of the Zr^{3+} transient ion. Similar studies using various other redox couples (ex: Ti^{4+}/Fe^{2+}, Ti^{4+}/Mn^{2+}) could reveal visible light-absorbing catalysts active towards CO_2 photoreduction.

Although the primary charge transfer mechanism in isolated-Ti species is localized, overall reactivity is also affected by the bulk properties. For example, Yamashita et al. [37] attributed higher C_1 photoproduct yields using Ti-MCM-48 compared to Ti-MCM-41 or TS-1 to the larger pore size and the three-dimensional channel structure of the MCM-48 catalyst. Additionally, electrostatic fields in the zeolite/mesoporous material could stabilize the $CO_2^{\bullet-}$ radical ion and thereby affect the product yield and selectivities.[91]

1.8.4 Effect of oxygen vacancies created by cation doping or thermal treatment of TiO_2 on the activity towards CO_2

CO_2 does not interact with stoichiometric rutile TiO_2 surfaces. The band gaps of rutile and anatase are not widely different; therefore, this might also be expected to apply

to anatase TiO_2. Defects such as oxygen vacancies control most of the chemistry at many metal oxide surfaces. These defects could be created either by doping TiO_2 with other anions or cations or by thermal treatments of stoichiometric TiO_2.

One example of this defect creation due to thermal treatments is the work of Yamashita et al.[52], who studied the photoreduction of CO_2 with H_2O on rutile TiO_2 (100) and TiO_2 (110) single crystals. Structure-dependent reactivity was observed, with the TiO_2 (100) surface being more active towards CO_2 photoreduction compared to the TiO_2 (110) surface. Yamashita et al.[52] explained this by stating that the Ti:O atomic ratio on the (100) surface was greater than the (110) surface. A pretreatment procedure involving degassing at 725 K, followed by a 4h reoxidation in O_2 at 725 K, followed by subsequent catalyst degassing at 725 K for 4h at ~10^{-6} Torr was used in the study. We note that this pretreatment procedure might create oxygen vacancies on the TiO_2 surface. For example: Thompson et al.[92] note that surface oxygen vacancies could be created with annealing temperatures as low as 600 K with rutile TiO_2 under ultra-high vacuum (UHV) conditions. Additionally, stoichiometric reactions between CO_2 and water on oxygen-deficient rutile surfaces to yield reduced C_1-C_2 products are well known in the literature[93]. In such cases, in situ surface characterization of the catalyst under light irradiation would provide information on the oxidation state of the surface, because the surface-Ti^{4+} and Ti^{3+} can be differentiated using XPS 2p core-level spectra[94].

In addition to creating oxygen vacancies, transition metal doping of TiO_2 also may create specific surface structures affecting the CO_2 photoreduction activity. Tseng et al.[43] and Wu et al.[95] found that Cu(I) doped TiO_2 promoted the formation of CH_3OH compared to undoped TiO_2. Pathak et al.[45] also observed selectivity for CH_3OH

formation over HCOOH using Ag-coated nanoscale TiO_2 immobilized in Nafion ionomer membranes. Apart from influencing the electron-hole recombination rates (as noted in the discussion on surface states) and affecting product specificity and yields, transition metal doping of TiO_2 also results in red-shifting of the absorption spectrum of TiO_2. This apparent bandgap-narrowing is attributed to transitions from localized surface states above the conduction band of TiO_2 and not due to bulk band-gap modification[96].

1.8.5 Discussion

One of the major factors limiting CO_2 photoreduction is the electron-hole recombination in semiconducting materials under band-gap illumination. The use of isolated Ti-species partly resolves this issue, but most Ti-O LMCT transitions occur at UV-C wavelengths (~ 270 nm). Both local as well as bulk factors influence the activity of catalysts mediating CO_2 photoreduction. For example: cation doping of TiO_2 not only creates oxygen vacancies, but also creates localized intra-bandgap states which contribute to charge transfer transitions by absorbing light wavelengths below the bandgap.

Both *collective* and *local* approaches are required to understand such light-induced electron transfer reactions. The collective, surface state approach indicates that pure TiO_2 is likely to be a poor photocatalyst for CO_2 activation. On the other hand, localized surface sites such as oxygen vacancies have been implicated in CO_2 activation.Using the surface state and surface site approaches, we have shown that both bulk and local variables affect the photoreduction of CO_2. Fundamental understanding of the initial steps of CO_2 activation on TiO_2 surfaces and a detailed knowledge of how

these bulk and local phenomena affect photoreactivity is required to design better catalysts.

1.9 Challenges for CO_2 photoreduction on Ti-based catalysts

As discussed in the earlier sections, significant improvements in the quantum yields and selectivities of Ti-based catalysts is required to bring CO_2 photoreduction using these materials closer to commercialization. Materials not based on Ti have been used to mediate CO_2 photoreduction. For example, metal chalcogenides (CdS, CdSe, ZnS) and other metal oxides (ZnO, MgO) have also been used as photocatalysts (see Usubharatana et al.[10] and references therein). In most cases, the improvements in efficiency are incremental at best. On the other hand, higher quantum efficiencies are possible with homogeneous metal complexes, but a sacrificial reagent is often required to regenerate the photosensitizer[35]. Breakthroughs in related fields such as solar-electric conversion, solar production of hydrogen using water and catalytic CO_2 activation will enable the further development of this field.

Essentially, the main challenges for CO_2 photoreduction using Ti-based catalysts involve finding suitable photosensitizers that can absorb visible light to produce electron-hole pairs and transfer the electrons to CO_2 with minimal losses. Additionally, the photosensitizer has to be regenerated with a relatively inexpensive reductant such as water. Choi et al.[97] noted that interfacial electron/hole transfer involves charged pair generation, followed “trapping” of the charged particles, their subsequent release and migration to the surface prior to the transfer. Electron-hole recombination occurs parallel

to the interfacial charge transfer, at all stages of this process. As pointed out in a report on solar energy utilization[98], potential breakthroughs in CO_2 photoreduction can result from significantly increasing the lifetime of the charge-separated state, designing materials that can work under visible light, catalyzing proton-coupled multi-electron transfer to CO_2. This requires a combination of experimental and computational studies.

1.10 Conclusions

In this chapter we provided a review of the mechanistic aspects of CO_2 photoreduction using TiO_2-based metal oxides or Ti-species in micro/mesoporous materials. CO_2 utilization has a significant role in mitigating CO_2 emissions, especially in comparison to other means of CO_2 abatement. The conversion of CO_2 to fuels using solar energy is one of the "grand challenges" for a variety of scientific disciplines. Significantly increased specific rates (~tens of millimoles CO_2 converted/g-TiO_2/h) under visible light irradiation are required to make this process economically feasible. Paradigm shifts in TiO_2 photocatalysis such as the use of bimetallic redox species in mesoporous materials, novel reactor design configurations (OFPR), the use of catalysts absorbing visible radiation, decreasing electron-hole recombination rates, surface modifications via doping or other chemical treatments, will continue to be required to drive innovation in this field.

1.11 References

1. Xu, X.; Moulijn, J. A., Mitigation of CO2 by Chemical Conversion: Plausible Chemical Reactions and Promising Products. *Energy & Fuels* **1996,** 10, (2), 305-325.
2. Song, C. S., Global challenges and strategies for control, conversion and utilization of CO2 for sustainable development involving energy, catalysis, adsorption and chemical processing. *Catalysis Today* **2006,** 115, (1-4), 2-32.
3. Sakakura, T.; Choi, J. C.; Yasuda, H., Transformation of Carbon Dioxide. *Chem. Rev.* **2007,** 107, (6), 2365-2387.
4. Aresta, M.; Dibenedetto, A., Utilisation of CO2 as a chemical feedstock: opportunities and challenges. *Dalton Transactions* **2007**, (28), 2975-2992.
5. Mazzotti, M.; Abanades, J. C.; Allam, R.; Lackner, K. S.; Meunier, F.; Rubin, E.; Sanchez, J. C.; Yogo, K.; Zevenhoven, R., Mineral Carbonation and Industrial Uses of Carbon dioxide. In *IPCC 2005: IPCC Special Report on Carbon dioxide Capture and Storage. Prepared by Working Group III of the Intergovernmental Panel on Climate Change.*, Metz, B.; Davidson, O.; de Coninck, H. C.; Loos, M.; Meyer, L. A., Eds. Cambridge University Press: Cambridge, United Kingdom and New York, USA, 2005; p 333.
6. Herzog, H. J.; Drake, E. M., Carbon dioxide recovery and disposal from large energy systems. *Annual Review of Energy and the Environment* **1996,** 21, (1), 145-166.
7. McKinsey&Company, Reducing U.S. Greenhouse Gas Emissions: How Much at What Cost? (http://www.mckinsey.com/clientservice/ccsi/pdf/US_ghg_final_report.pdf), accessed 11/24/2008.
8. Aresta, M.; Dibenedetto, A., The contribution of the utilization option to reducing the CO2 atmospheric loading: research needed to overcome existing barriers for a full exploitation of the potential of the CO2 use. *Catalysis Today* **2004,** 98, (4), 455.
9. Aresta, M.; Quaranta, E.; Tommasi, I., Utilization of carbon dioxide: a strategy for the control of its level in the atmosphere. The role of the photoconversion technology. *Photochem. Convers. Storage Sol. Energy, Proc. Int. Conf., 8th* **1991**, 517-50.
10. Usubharatana, P.; McMartin, D.; Veawab, A.; Tontiwachwuthikul, P., Photocatalytic Process for CO2 Emission Reduction from Industrial Flue Gas Streams. *Industrial & Engineering Chemistry Research* **2006,** 45, (8), 2558-2568.
11. Anpo, M.; Yamashita, H.; Ikeue, K.; Fujii, Y.; Zhang, S. G.; Ichihashi, Y.; Park, D. R.; Suzuki, Y.; Koyano, K.; Tatsumi, T., Photocatalytic reduction of CO2 with H2O on Ti-MCM-41 and Ti-MCM-48 mesoporous zeolite catalysts. *Catalysis Today* **1998,** 44, (1-4), 327-332.
12. Zhang, S. G.; Fujii, Y.; Yamashita, K.; Koyano, K.; Tatsumi, T.; Anpo, M., Photocatalytic reduction of CO2 with H2O on Ti-MCM-41 and Ti-MCM-48 mesoporous zeolites at 328 K. *Chemistry Letters* **1997**, (7), 659-660.
13. Anpo, M.; Yamashita, H.; Ichihashi, Y.; Fujii, Y.; Honda, M., Photocatalytic reduction of CO2 with H2O on titanium oxides anchored within micropores of zeolites: Effects of the structure of the active sites and the addition of Pt. *Journal of Physical Chemistry B* **1997,** 101, (14), 2632-2636.

14. Lin, W.; Frei, H., Photoactivation of Ti centers in mesoporous silicate sieve under visible and UV light. *Studies in Surface Science and Catalysis* **2004,** 153, (Carbon Dioxide Utilization for Global Sustainability), 283-288.
15. Lin, W. Y.; Han, H. X.; Frei, H., CO2 splitting by H2O to CO and O-2 under UV light in TiMCM-41 silicate sieve. *Journal of Physical Chemistry B* **2004,** 108, (47), 18269-18273.
16. Lin, W.; Frei, H., Bimetallic redox sites for photochemical CO2 splitting in mesoporous silicate sieve. *Comptes Rendus Chimie* **2006,** 9, 207-213.
17. Carp, O.; Huisman, C. L.; Reller, A., Photoinduced reactivity of titanium dioxide. *Progress in Solid State Chemistry* **2004,** 32, (1-2), 33-177.
18. Xu, Y.; Schoonen, M. A. A., The absolute energy positions of conduction and valence bands of selected semiconducting minerals. *American Mineralogist* **2000,** 85, (3-4), 543-556.
19. Diebold, U., The surface science of titanium dioxide. *Surface Science Reports* **2003,** 48, (5-8), 53-229.
20. Gong, X.-Q.; Selloni, A.; Batzill, M.; Diebold, U., Steps on anatase TiO2(101). *Nature Materials* **2006,** 5, (8), 665.
21. Gong, X. Q.; Selloni, A.; Dulub, O.; Jacobson, P.; Diebold, U., Small au and pt clusters at the anatase TiO2(101) surface: Behavior at terraces, steps, and surface oxygen vacancies. *Journal Of The American Chemical Society* **2008,** 130, 370-381.
22. Gong, X. Q.; Selloni, A.; Vittadini, A., Density functional theory study of formic acid adsorption on anatase TiO2(001): Geometries, energetics, and effects of coverage, hydration, and reconstruction. *Journal of Physical Chemistry B* **2006,** 110, (6), 2804-2811.
23. Gong, X. Q.; Selloni, A., Reactivity of anatase TiO2 nanoparticles: The role of the minority (001) surface. *Journal of Physical Chemistry B* **2005,** 109, (42), 19560-19562.
24. Diebold, U.; Ruzycki, N.; Herman, G. S.; Selloni, A., One step towards bridging the materials gap: surface studies of TiO2 anatase. *Catalysis Today* **2003,** 85, 93-100.
25. Ruzycki, N.; Herman, G. S.; Boatner, L. A.; Diebold, U., Scanning tunneling microscopy study of the anatase (100) surface. *Surface Science* **2003,** 529, L239-L244.
26. Lazzeri, M.; Selloni, A., Stress-driven reconstruction of an oxide surface: The anatase TiO2(001)-(1x4) surface. *Physical Review Letters* **2001,** 87, (26).
27. Liang, Y.; Gan, S. P.; Chambers, S. A.; Altman, E. I., Surface structure of anatase TiO2(001): Reconstruction, atomic steps, and domains. *Physical Review B* **2001,** 63, (23).
28. Hengerer, R.; Bolliger, B.; Erbudak, M.; Gratzel, M., Structure and stability of the anatase TiO2 (101) and (001) surfaces. *Surface Science* **2000,** 460, (1-3), 162-169.
29. Gopel, W.; Rocker, G.; Feierabend, R., Intrinsic defects of titanium dioxide(110): Interaction with chemisorbed oxygen, hydrogen, carbon monoxide, and carbon dioxide. *Physical Review B: Condensed Matter and Materials Physics* **1983,** 28, (6), 3427-38.
30. Nerlov, J.; Christensen, S. V.; Weichel, S.; Pedersen, E. H.; Moller, P. J., A photoemission study of the coadsorption of CO2 and Na on TiO2(110)-(1x1) and -(1x2) surfaces: Adsorption geometry and reactivity. *Surface Science* **1997,** 371, (2-3), 321-336.

31. Gutiérrez-Sosa, A.; Walsh, J. F.; Lindsay, R.; Wincott, P. L.; Thornton, G., Carbonate co-adsorption geometry on TiO2(110)1×1-Na. *Surface Science* **1999,** 433-435, 538.
32. Krischok, S.; Höfft, O.; Kempter, V., The chemisorption of H2O and CO2 on TiO2 surfaces: studies with MIES and UPS (HeI/II). *Surface Science* **2002,** 507-510, 69.
33. Brause, M.; Kempter, V., CO2 chemisorption on alkalated TiO2(1 0 0)-(1×3) studied with MIES and UPS(HeI). *Surface Science* **2001,** 476, (1-2), 78.
34. Inoue, T.; Fujishima, A.; Konishi, S.; Honda, K., Photoelectrocatalytic reduction of carbon dioxide in aqueous suspensions of semiconductor powders. *Nature (London, United Kingdom)* **1979,** 277, (5698), 637-8.
35. Fujita, E., Photochemical carbon dioxide reduction with metal complexes. *Coordination Chemistry Reviews* **1999,** 186, 373-384.
36. Anpo, M.; Yamashita, H., Photocatalytic Reductions - Photocatalytic Reduction of Carbon Dioxide with Water and Hydrogenation of Unsaturated Hydrocarbons with Water. In *Hetergeneous Photocatalysis*, Schiavello, M., Ed. John Wiley & Sons: Chichester, UK, 1997; p 136.
37. Yamashita, H.; Fujii, Y.; Ichihashi, Y.; Zhang, S. G.; Ikeue, K.; Park, D. R.; Koyano, K.; Tatsumi, T.; Anpo, M., Selective formation of CH3OH in the photocatalytic reduction of CO2 with H2O on titanium oxides highly dispersed within zeolites and mesoporous molecular sieves. *Catalysis Today* **1998,** 45, (1-4), 221.
38. Ikeue, K.; Yamashita, H.; Anpo, M.; Takewaki, T., Photocatalytic Reduction of CO2 with H2O on Ti-Beta Zeolite Photocatalysts: Effect of the Hydrophobic and Hydrophilic Properties. *J. Phys. Chem. B* **2001,** 105, (35), 8350-8355.
39. Ikeue, K.; Nozaki, S.; Ogawa, M.; Anpo, M., Photocatalytic Reduction of CO2 with H2O on Ti-Containing Porous Silica Thin Film Photocatalysts. *Catalysis Letters* **2002,** 80, (3), 111.
40. Yamashita, H.; Ikeue, K.; Takewaki, T.; Anpo, M., In situ XAFS Studies on the Effects of the Hydrophobic–Hydrophilic Properties of Ti-Beta Zeolites in the Photocatalytic Reduction of CO2 with H2O. *Topics in Catalysis* **2002,** 18, (1), 95.
41. Wovchko, E. A.; Yates, J. T., Jr., Photochemical Activation of CO2 on RhI(CO)2/Al2O3-CO2 Dissociation and Oxygen Atom Exchange. *Journal of the American Chemical Society* **1998,** 120, (30), 7544-7550.
42. Yamashita, H.; Nishiguchi, H.; Kamada, N.; Anpo, M.; Teraoka, Y.; Hatano, H.; Ehara, S.; Kikui, K.; Palmisano, L.; Sclafani, A.; Schiavello, M.; Fox, M. A., Photocatalytic Reduction of Co2 With H2o on tiO2 and Cu/TiO2 Catalysts. *Research on Chemical Intermediates* **1994,** 20, 815.
43. Tseng, I. H.; Chang, W.-C.; Wu, J. C. S., Photoreduction of CO2 using sol-gel derived titania and titania-supported copper catalysts. *Applied Catalysis, B: Environmental* **2002,** 37, (1), 37-48.
44. Wu, J. C. S.; Lin, H.-M.; Lai, C.-L., Photo reduction of CO2 to methanol using optical-fiber photoreactor. *Applied Catalysis A: General* **2005,** 296, (2), 194.
45. Pathak, P.; Meziani, M. J.; Castillo, L.; Sun, Y.-P., Metal-coated nanoscale TiO2 catalysts for enhanced CO2 photoreduction. *Green Chemistry* **2005,** 7, (9), 667-670.
46. Ozcan, O.; Yukruk, F.; Akkaya, E.; Uner, D., Dye sensitized CO2 reduction over pure and platinized TiO2. *Topics in Catalysis* **2007,** 44, (4), 523.

47. Lo, C.-C.; Hung, C.-H.; Yuan, C.-S.; Wu, J.-F., Photoreduction of carbon dioxide with H2 and H2O over TiO2 and ZrO2 in a circulated photocatalytic reactor. *Solar Energy Materials & Solar Cells* **2007,** 91, (19), 1765-1774.
48. Nguyen, T.-V.; Wu, J. C. S., Photoreduction of CO2 in an optical-fiber photoreactor: Effects of metals addition and catalyst carrier. *Applied Catalysis, A: General* **2008,** 335, (1), 112-120.
49. Nguyen, T.-V.; Wu, J. C. S., Photoreduction of CO2 to fuels under sunlight using optical-fiber reactor. *Solar Energy Materials & Solar Cells* **2008,** 92, (8), 864-872.
50. Nguyen, T.-V.; Wu, J. C. S.; Chiou, C.-H., Photoreduction of CO2 over Ruthenium dye-sensitized TiO2-based catalysts under concentrated natural sunlight. *Catalysis Communications* **2008,** 9, (10), 2073-2076.
51. Li, G.; Ciston, S.; Saponjic, Z. V.; Chen, L.; Dimitrijevic, N. M.; Rajh, T.; Gray, K. A., Synthesizing mixed-phase TiO2 nanocomposites using a hydrothermal method for photooxidation and photoreduction applications. *Journal of Catalysis* **2008,** 253, (1), 105-110.
52. Yamashita, H.; Kamada, N.; He, H.; Tanaka, K.; Ehara, S.; Anpo, M., Reduction of CO2 with H2O on TiO2(100) and TiO2(110) single-crystals under uv-irradiation. *Chemistry Letters* **1994**, (5), 855-858.
53. Kaneco, S.; Shimizu, Y.; Ohta, K.; Mizuno, T., Photocatalytic reduction of high pressure carbon dioxide using TiO2 powders with a positive hole scavenger. *Journal of Photochemistry and Photobiology A: Chemistry* **1998,** 115, (3), 223.
54. Kaneco, S.; Kurimoto, H.; Shimizu, Y.; Ohta, K.; Mizuno, T., Photocatalytic reduction of CO2 using TiO2 powders in supercritical fluid CO2. *Energy* **1999,** 24, (1), 21.
55. Nguyen, T.-V.; Wu, J. C. S., Photoreduction of CO2 to fuels under sunlight using optical-fiber reactor. *Solar Energy Materials and Solar Cells* **2008,** 92, (8), 864.
56. Tseng, I. H.; Wu, J. C. S., Chemical states of metal-loaded titania in the photoreduction of CO2. *Catalysis Today* **2004,** 97, (2-3), 113-119.
57. MCI, Mitsui Chemicals to Establish a Pilot Facility to Study a Methanol Synthesis Process from CO2 (http://www.mitsuichem.com/release/2008/080825e.htm), accessed 01/09/2008.
58. Zeman, F. S.; Keith, D. W., Carbon neutral hydrocarbons. *Philosophical Transactions of the Royal Society A: Mathematical, Physical and Engineering Sciences* **2008**.
59. Solymosi, F., The bonding, structure and reactions of CO2 adsorbed on clean and promoted metal surfaces. *Journal of Molecular Catalysis* **1991,** 65, (3), 337.
60. Wang, S. G.; Cao, D. B.; Li, Y. W.; Wang, J. G.; Jiao, H. J., Chemisorption of CO2 on nickel surfaces. *Journal Of Physical Chemistry B* **2005,** 109, (40), 18956-18963.
61. Gibson, D. H., Carbon dioxide coordination chemistry: metal complexes and surface-bound species. What relationships? *Coordination Chemistry Reviews* **1999,** 185-186, 335-355.
62. Freund, H. J.; Roberts, M. W., Surface chemistry of carbon dioxide. *Surface Science Reports* **1996,** 25, (8), 227-273.

63. Keene, R. F., Thermodynamic, Kinetic, and Product Considerations in Carbon Dioxide Reactivity. In *Electrochemical and Electrocatalytic Reactions of Carbon Dioxide*, Sullivan, B. P.; Krist, K.; Guard, H. E., Eds. Elsevier Science: 1993; pp 1-17.
64. Rasko, J.; Solymosi, F., Infrared spectroscopic study of the photoinduced activation of CO2 on TiO2 and Rh/TiO2 catalysts. *Journal of Physical Chemistry* **1994,** 98, (29), 7147-7152.
65. Hartman, K. O.; Hisatsune, I. C., Infrared spectrum of carbon dioxide anion radical. *Journal of Chemical Physics* **1966,** 44, (5), 1913-18.
66. Perissinotti, L. L.; Brusa, M. A.; Grela, M. A., Yield of carboxyl anion radicals in the photocatalytic degradation of formate over TiO2 particles. *Langmuir* **2001,** 17, (26), 8422-8427.
67. Morrison, R. S., The Chemical Physics of Surfaces. 1990, pp 1-3.
68. Morrison, R. S., The Chemical Physics of Surfaces. 1990, pp 329-331.
69. Koppenol, W. H.; Rush, J. D., Reduction potential of the CO2/CO2.- couple - a comparison with other C1 radicals. *Journal of Physical Chemistry* **1987,** 91, (16), 4429-4430.
70. Bonapasta, A. A.; Filippone, F., Photocatalytic reduction of oxygen molecules at the (100) TiO2 anatase surface. *Surface Science* **2005,** 577, (1), 59-68.
71. Krischok, S.; Hofft, O.; Kempter, V., The chemisorption of H2O and CO2 on TiO2 surfaces. Studies with MIES and UPS (HeI/II). *Surface Science* **2002,** 507-510, 69-73.
72. Markovits, A.; Fahmi, A.; Minot, C., A theoretical study of CO2 adsorption on TiO2. *Theochem-Journal of Molecular Structure* **1996,** 371, 219-235.
73. Nowotny, J.; Bak, T.; Nowotny, M. K.; Sheppard, L. R., Titanium dioxide for solar-hydrogen IV. Collective and local factors in photoreactivity. *International Journal of Hydrogen Energy* **2007,** 32, (14), 2651-2659.
74. Busca, G.; Lorenzelli, V., Infrared spectroscopic identification of species arising from reactive adsorption of carbon oxides on metal oxide surfaces. *Materials Chemistry* **1982,** 7, (1), 89-126.
75. Ramis, G.; Busca, G.; Lorenzelli, V., Low-temperature carbon dioxide adsorption on metal oxides: spectroscopic characterization of some weakly adsorbed species. *Materials Chemistry and Physics* **1991,** 29, (1-4), 425-35.
76. Rasko, J., FTIR study of the photoinduced dissociation of CO2 on titania-supported noble metals. *Catalysis Letters* **1998,** 56, (1), 11-15.
77. Schmidt, M., The thermodynamics of CO_2 conversion. In *Carbon dioxide chemistry: Environmental issues*, Paul, J. P., Claire-Marie, Ed. The Royal Society of Chemistry: Cambridge, 1994; pp 22-30.
78. Chen, M. S.; Goodman, D. W., Interaction of Au with titania: the role of reduced Ti. *Topics in Catalysis* **2007,** 44, (1-2), 41-47.
79. Pala, R. G. S.; Liu, F., Nature of reactive O[sub 2] and slow CO[sub 2] evolution kinetics in CO oxidation by TiO[sub 2] supported Au cluster. *The Journal of Chemical Physics* **2006,** 125, (14), 144714.
80. Raj Ganesh, S. P.; Feng, L., Nature of reactive O[sub 2] and slow CO[sub 2] evolution kinetics in CO oxidation by TiO[sub 2] supported Au cluster. *The Journal of Chemical Physics* **2006,** 125, (14), 144714.

81. Remediakis, I. N.; Lopez, N.; Nørskov, J. K., CO Oxidation on Rutile-Supported Au Nanoparticles13. *Angewandte Chemie International Edition* **2005,** 44, (12), 1824-1826.
82. Chrétien, S.; Metiu, H., Density Functional Study of the CO Oxidation on a Doped Rutile TiO2(110): Effect of Ionic Au in Catalysis. *Catalysis Letters* **2006,** 107, (3), 143.
83. Colombo, D. P., Jr.; Bowman, R. M., Does Interfacial Charge Transfer Compete with Charge Carrier Recombination? A Femtosecond Diffuse Reflectance Investigation of TiO2 Nanoparticles. *Journal of Physical Chemistry* **1996,** 100, (47), 18445-18449.
84. Xie, T.-f.; Wang, D.-j.; Zhu, L.-j.; Li, T.-j.; Xu, Y.-j., Application of surface photovoltage technique in photocatalysis studies on modified TiO2 photo-catalysts for photo-reduction of CO2. *Materials Chemistry and Physics* **2001,** 70, (1), 103.
85. McConnell, R. D., Assessment of the dye-sensitized solar cell. *Renewable and Sustainable Energy Reviews* **2002,** 6, (3), 271.
86. Bak, T.; Nowotny, J.; Rekas, M.; Sorrell, C. C., Photo-electrochemical hydrogen generation from water using solar energy. Materials-related aspects. *International Journal of Hydrogen Energy* **2002,** 27, (10), 991.
87. Chen, L. Y.; Chuah, G. K.; Jaenicke, S., Ti-containing MCM-41 catalysts for liquid phase oxidation of cyclohexene with aqueous H2O2 and tert-butyl hydroperoxide. *Catalysis Letters* **1998,** 50, (1-2), 107-114.
88. Yuan, Q.; Hagen, A.; Roessner, F., An investigation into the Ti-grafting structure on MCM-41 and epoxidation catalysis. *Applied Catalysis A: General* **2006,** 303, (1), 81.
89. Ulagappan, N.; Frei, H., Mechanistic Study of CO2 Photoreduction in Ti Silicalite Molecular Sieve by FT-IR Spectroscopy. *Journal of Physical Chemistry A* **2000,** 104, (33), 7834-7839.
90. Lin, W. Y.; Frei, H., Photochemical CO2 splitting by metal-to-metal charge-transfer excitation in mesoporous ZrCu(I)-MCM-41 silicate sieve. *Journal of The American Chemical Society* **2005,** 127, (6), 1610-1611.
91. Sogabe, K.; Hasegawa, A.; Yamada, Y.; Miura, M., Electron spin resonance studies of the carbon dioxide anion radical absorbed on X-type zeolites. *Bulletin of the Chemical Society of Japan* **1972,** 45, (11), 3362-6.
92. Thompson, T. L.; Diwald, O.; Yates, J. T., Jr., CO2 as a Probe for Monitoring the Surface Defects on TiO2(110)-Temperature-Programmed Desorption. *Journal of Physical Chemistry B* **2003,** 107, (42), 11700-11704.
93. Wilson, J. N.; Senanayake, S. D.; Idriss, H., Carbon coupling on titanium oxide with surface defects. *Surface Science* **2004,** 562, (1-3), L231-L237.
94. Kumar, P. M.; Badrinarayanan, S.; Sastry, M., Nanocrystalline TiO2 studied by optical, FTIR and X-ray photoelectron spectroscopy: correlation to presence of surface states. *Thin Solid Films* **2000,** 358, (1-2), 122.
95. Wu, J. C. S.; Lin, H.-M., Photoreduction of CO2 to methanol via TiO2 photocatalyst. *International Journal of Photoenergy* **2005,** 7, (3), 115-119.
96. Serpone, N., Is the Band Gap of Pristine TiO2 Narrowed by Anion- and Cation-Doping of Titanium Dioxide in Second-Generation Photocatalysts? *The Journal of Physical Chemistry B* **2006,** 110, (48), 24287-24293.

97. Choi, W. Y.; Termin, A.; Hoffmann, M. R., The Role Of Metal-Ion Dopants In Quantum-Sized TiO2 - Correlation Between Photoreactivity And Charge-Carrier Recombination Dynamics. *Journal of Physical Chemistry* **1994,** 98, (51), 13669-13679.
98. Lewis, N.; Crabtree, G., Report on the Basic Energy Sciences Workshop on Solar Energy Utilization (http://www.sc.doe.gov/bes/reports/files/SEU_rpt_print.pdf), accessed 11/30/2008.

Chapter 2

Quantum Chemical Modeling of Ground States of CO_2 Chemisorbed on Anatase (001), (101) and (010) TiO_2 Surfaces

2.1 Introductory Comment

"We are reaching the stage where the problems we must solve are going to become insoluble without computers. I do not fear computers. I fear the lack of them."

- Issac Asimov

The previous chapter discussed some challenges to developing better CO_2 photoreduction catalysts. Breakthroughs in solar photoconversion of CO_2 to fuels require a combination of computational and experimental studies. In this and the following three chapters, results using computational modeling of CO_2 interactions with anatase TiO_2 surfaces are presented. Whereas both local and bulk factors affect the photocatalytic activity towards CO_2 photoreduction, the primary charge transfer event likely involves chemisorbed CO_2 species. Using a surface site approach, the ground states of CO_2 are modeled using density functional theory calculations in this chapter. Modeling the ground states is important, because understanding excited states of CO_2 on TiO_2 surfaces requires a comprehensive knowledge of the surface adsorption complexes formed by CO_2.

2.2 Abstract

To design efficient CO_2 photoreduction catalysts, we need to understand the intermediates and energetics of various reactions involved in the photoreduction of CO_2 in greater detail. As a first step in this process, the ground states of CO_2 chemisorbed on small clusters from various anatase surface planes are modeled in this study. We show that large basis sets with diffuse functions and high levels of electron correlation are needed to model the electron attached states of CO_2, which may play a role in its photoreduction. Density functional theory (DFT) calculations of CO_2 adsorbed on small TiO_2 clusters ($Ti_2O_9H_{10}$) extracted from the (010), (001) and (101) surface plane structures point to the formation of different adsorbed species depending on crystal face atomic structure. The calculated infrared (IR) spectral properties of these species are compared against experimental data. We find favorable agreement for the existence of three different surface complexes. The formation of different surface species correlates well with the acid-base strength of the coordinatively unsaturated atoms. The implications of carbonate formation for CO_2 photoreduction are discussed.

2.3 Introduction

The interaction of small molecules such as CO_2 on titania (TiO_2) surfaces plays a significant role in chemical processes. For example, TiO_2 is used as a support for catalysts reducing nitrogen oxides, oxidizing carbon monoxide and ammonia[1]. Mixed oxide titania-zirconia is also used as catalyst and as a catalyst support[2]. CO_2 is used as a probe molecule for characterizing weakly basic surface sites on metal oxides[3]. TiO_2 is

also widely used as a photocatalyst affecting the mineralization of organic compounds[4], where CO_2 is often the end product of photooxidation. Moreover, TiO_2 has been shown to mediate the photoreduction of CO_2 to useful organic compounds[5-10]. Photocatalytic activation of CO_2 to produce renewable carbon feedstocks holds promise to utilize intermittent solar energy and also lessen the consumption of fossil fuels. At a more fundamental level, the activation of CO_2 in the presence of metal oxides and light is by itself a captivating research problem that could have potential implications for abiotic photosynthesis and future human space exploration.

Titania occurs as three polymorphs, anatase, rutile and brookite; anatase being the most catalytically active polymorph, though not for all applications. CO_2 adsorption on rutile TiO_2 was studied by Markovits et al. using periodic Hartree-Fock calculations[11]. The bare rutile (110) surface was predicted to be very acidic and the most probable model for CO_2 adsorption consisted of a perpendicular CO_2 molecule over a coordinatively undersaturated Ti cation (i.e., a Ti in 5-fold coordination rather than 6-fold as found in bulk rutile, forming a Ti-O=C=O complex). Similar studies of CO_2 adsorption on anatase TiO_2 have not been published.

To develop better CO_2 photoreduction catalysts, we need to understand the interaction of CO_2 with TiO_2 in greater detail. Various forms of CO_2 (adsorbed on surface Lewis acidic and basic sites) have been observed on TiO_2 surfaces[12, 13]. For example: Ramis et al.[13] assigned solid CO_2, linearly adsorbed CO_2, bent CO_2 and carbonate species to bands observed in low-temperature IR spectroscopic studies. Martra observed distinct carbonate and bicarbonate species on P25 TiO_2[14]. Hadjiivanov et al.[15] proposed the existence of Ti cation sites varying in electrophilic character, on different surface planes

of TiO_2 from their studies of probe molecule adsorption on anatase[15]. They suggested that the heterogeneity of surface acidic and basic sites resulted in various adsorbed species. The extent to which similar surface specificity influences the adsorption of CO_2 on anatase TiO_2 is not known. Knowledge of intermediate species in the TiO_2-catalyzed photoreduction of CO_2 will help us understand the reaction mechanism on a molecular level. Quantum chemical modeling can help identify intermediates by corroborating data from in situ spectroscopic measurements.

To accurately depict the surface processes occurring during CO_2 photoreduction, a detailed knowledge of the specific surface planes exposed is significant because different crystal faces can have different reactivities. For example: Hadjiivanov et al.[15] suggested that the coordinatively undersaturated Ti cations exposed on the (010) and (101) surface planes are more electrophilic than similar cations on the (001) surface plane. A high-resolution transmission electron microscopy (HRTEM) investigation of the surface morphology of P25 TiO_2 (consisting of ~80% anatase) found that it mainly exposed the (001) and (010) surface planes[14]. The most common surfaces for anatase are generally the (001) and (101) planes[16]. Amongst (100), (001), (101) and (110) surface planes, quantum chemical calculations[17] have shown that the (101) surface plane has the lowest surface energy. The (101) surface plane exposes both cations and anions having coordinative undersaturation (5-coordinate Ti (5-c Ti) and 2-coordinate O (2-c O)), as well as bulk (6-c Ti and 3-c O) atoms, whereas the (001) surface exposes 5-c Ti and 2-c O atoms. The (010) surface is isostructural with (100), exposing 2-c, and 3-c O atoms and 5-c and 6-c Ti atoms. The 3 surfaces modeled in this study are all possible under different conditions. For some anatase particles, only 2 of them may exist, but this does not

preclude us from comparing different faces. To compare reactivities among 5-c Ti atoms, only the (101), (010) and (001) surfaces will be discussed in this study. The results for the (110) surface are shown in Appendix A.

As an initial step in the process of understanding mechanisms of CO_2 photoreduction, this study aims at identifying ground states of CO_2 chemisorbed on various surface planes of anatase. Previous experimental results from in situ IR spectroscopic studies of CO_2 adsorption on TiO_2 are compared with DFT calculations of predicted vibrational frequencies of CO_2 adsorbed on 2 Ti atom clusters from the (001), (010) and (101) surface planes of anatase TiO_2.

2.4 Computational Methods

Small clusters of TiO_2 have been used in previous computational studies[18] to understand reactions on titania surfaces. Although the use of 2 atom clusters does not model the bulk band gap of the solid, it allows us to understand the local chemistry of the system at a lower computational cost. Note that it is not unrealistic to model the reaction of CO_2 on small TiO_2 clusters. For example, Anpo's research group has used Ti exchanged zeolites as photocatalysts to activate CO_2[5, 8, 9]. Their X-ray absorption extended fine structure spectroscopy (EXAFS) studies show that the active site is comprised of tetrahedrally coordinated Ti atoms in the zeolite cage. These Ti atoms typically have titanol (Ti-OH) or titanosilane (Ti-O-Si) linkages. Our calculations on two atom clusters may not be the same as a Ti atom in a zeolite cage, but there are precedents for modeling materials with molecular clusters for certain purposes[19]. For example,

comparisons of similar clusters and periodic DFT calculations have shown good agreement with each other and experimental results for adsorption of oxyanions on Fe-hydroxide surfaces[20].

In order to assess the level of theory suitable for modeling CO_2 photoreduction, we have performed free energy calculations for the CO_2-$CO_2^{\bullet-}$ system using different levels of theory (accounting more accurately for configuration interaction) and basis sets (Table **2-1**). The optimized geometries using quadratic configuration interaction with single and double excitations (QCISD(T))[21, 22] are shown in Figure **2-1** .

As shown in Table **2-1** quantum mechanical calculations at the QCISD(T)/6-311+G(3df) level of theory model the structure and vibrational frequencies of $CO_2^{\bullet-}$. (Within this chapter, the symbol $CO_2^{\bullet-}$ has been used to refer to carbon dioxide radical anion.) The calculated value of electron affinity for CO_2 (-0.62 eV) from QCISD(T)/6-311+G(3df) is consistent with the experimental value of -0.6 ± 0.2 eV[23] and agrees with the value calculated by Yu et al. using the G2 method (-0.62 eV)[24].

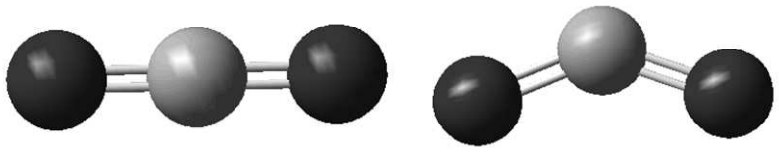

CO_2

C-O = 1.165 Å

<OCO = 180°

$CO_2^{\bullet-}$

C-O = 1.234 Å

<OCO = 137.7°

Figure **2-1**: Optimized geometries of CO_2 and $CO_2^{\bullet-}$ calculated at the QCISD(T)/6-311+G(3df) level

Ideally, all CO_2-TiO_2 calculations would be performed at this level of theory, but such high-level calculations are not practical for the larger models necessary in this study. Consequently, Møller-Plessett (e.g., MP2/6-311+G(3df)) and hybrid molecular orbital/density functional theory (MO/DFT; e.g., B3LYP/6-31G(d)) calculations were performed to test their ability to reproduce results obtained for the higher level and more accurate theoretical methods. The results shown in Table **2-1** indicate that the B3LYP calculations with a diffuse basis set (6-31+G(d)) reproduce the bond angle, distance, atomic spin densities and IR vibrational frequencies of $CO_2^{\bullet-}$ as accurately as the more time-consuming QCISD methods. MP2 calculations with a large basis set also produce similar results. However, these lower levels of theory are not sufficient to reproduce the electron affinity of CO_2. While the B3LYP/6-31+G(d) method underestimates the electron affinity, the MP2 method overestimates this value. The use of larger basis set (B3LYP/6-311+G(3df) over B3LYP/6-31+G(d) does improve the value of the electron affinity, but does not predict the bond angles and bond lengths of the carbon dioxide anion well. Diffuse functions (the "+" in the basis set description) are clearly needed to estimate the electron affinity or model the vibrational frequencies of the radical anion to any extent.

We therefore used the B3LYP/6-31+G(d) model chemistry for ground state geometry optimizations and frequency calculations. Higher level calculations will be necessary to accurately model the energetics of the photoreduction reaction and any radical or excited states that occur as intermediates. The B3LYP/6-31+G(d) results are useful as a starting point, however, because we can constrain which reaction pathways are most probable by comparing observed and modeled vibrational spectra.

Table **2-1**: Comparisons of B3LYP, MP2 and QCISD results with the observed properties of $CO_2^{\bullet-}$, the highlighted results indicate the model chemistries whose results (IR frequencies, C-O bond lengths) are consistent with experimental values (shown at the bottom of the table)

(Method/basis set) or reference	Adiabatic Electron Affinity (at 0 K), eV	<OCO in $CO_2^{\bullet-}$	C-O , Å	Frequencies, scaled,cm^{-1}	Atomic spin densities of $CO_2^{\bullet-}$
B3LYP/6-31G(d)	-1.30	133.64	1.252	704, 1291, 1639	C: 0.677 O: 0.161
B3LYP/6-31+G(d)	-0.22	137.13	1.239	651, 1191, 1690	C:0.967 O: 0.016
B3LYP/ 6-311+G(3df)	-0.38	138.25	1.227	647, 1178, 1711	C:1.160 O:-0.08
MP2/6-311+G(3df)	-0.82	137.50	1.233	651, 1158, 1682	C: 0.944 O: 0.028
QCISD/ 6-311+G(3df)	-0.62	137.70	1.234	651, 1167, 1680	C:0.944 O: 0.028
Experimental values (Hartman and Hisatsune,1966)	-0.6±0.2	134		1671	

Cluster models containing 2 Ti atoms were constructed from the (010), (001) and (101) faces of anatase using the Cerius[2] software suite (Accelrys Inc., San Diego, CA). Figure **2-2** shows the principal atoms in the clusters, as located in the anatase crystal lattice. The coordination of the dangling bonds was saturated by adding protons and hydroxyl groups, resulting in a (formally) neutral $Ti_2O_9H_{10}$ cluster. To form a 2 Ti atom

cluster from the (010) surface plane, the bridging oxygen was made 2-c. The ground-state of stoichiometric TiO_2 is a singlet. Therefore, the ground state of the 2 atom cluster was modeled as a zero-charge singlet.

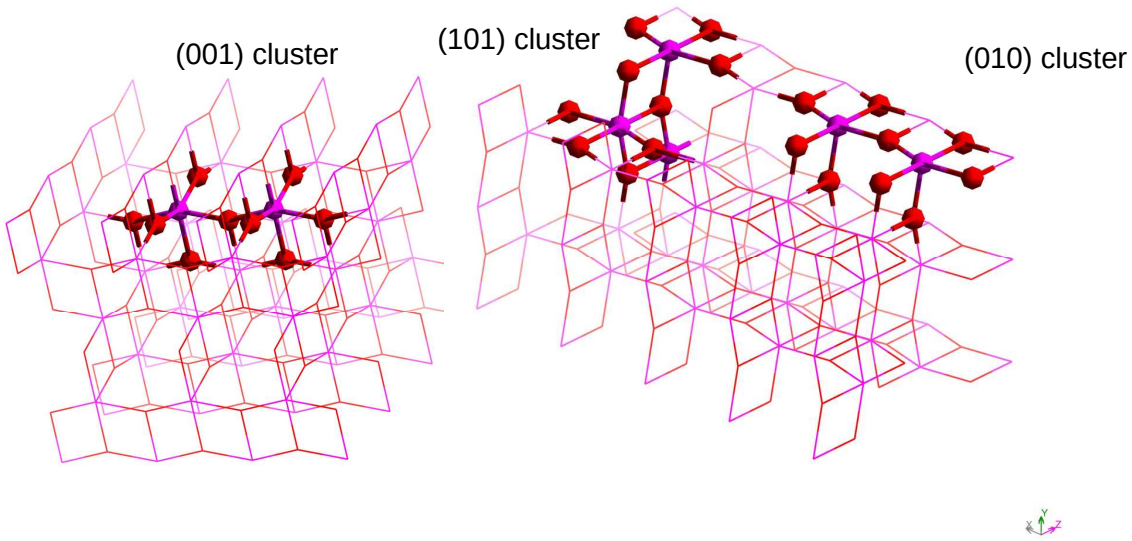

Figure **2-2**: Ball-and-stick representations of the clusters (showing nearest neighboring atoms to titanium atoms) from the (001), (101) and (010) surfaces of anatase TiO_2 considered in this study. Red atoms represent O, pink atoms represent Ti.

All quantum calculations were performed using the computational chemistry package Gaussian 03[25]. The ground states of the cluster were modeled using Becke's 3-parameter hybrid method[26] with the LYP correlation functional[27] (B3LYP). The following procedure was used to prepare a relaxed $Ti_2O_9H_{10}CO_2$ cluster:

i. Ground-state bare cluster ($Ti_2O_9H_{10}$) geometries were initially calculated with a 3-21G* basis set, the H atoms were relaxed while the Ti,O atoms of the cluster were fixed.

ii. B3LYP/6-31+G(d) calculations with fixed Ti,O geometries were subsequently performed with tight optimization convergence criteria and

ultra-fine DFT integration grids. Two-center electron integrals of magnitude less than 10^{-12} (default: 10^{-10}) were discarded. In this chapter, the term “bare constrained cluster” will be used to refer to this geometry.

iii. Neutral, singlet CO_2 was optimized using similar method/basis set combination.

iv. Subsequently, the CO_2 molecule was located over the $Ti_2O_9H_{10}$ cluster and its geometry was optimized (with constraints on the Ti, O atoms of the $Ti_2O_9H_{10}$ cluster) in the neutral, singlet state using B3LYP/6-31+G(d) model chemistry.

v. In a subsequent B3LYP/6-31+G(d) optimization, the molecule from the above step was allowed to relax freely, removing all constraints.

To validate the choice of the B3LYP/6-31+G(d) basis set, harmonic vibrational frequencies were calculated using the fully converged, relaxed geometry and are compared with vibrational frequencies from in situ studies of CO_2 adsorption on TiO_2. The vibrational frequency scaling factor and the uncertainty in its estimation for the B3LYP/6-31+G(d) method/basis set combination were assumed to be the same as that for B3LYP/6-31+G(d,p) (0.964), taken from the NIST Computational Chemistry Comparison and Benchmark Database (CCCBDB). The scaling factors for B3LYP/6-311+G(3df), MP2/6-311+G(3df) and QCISD(T)/6-311+G(3df) were taken to be 0.967, 0.950 and 0.963 respectively. All results reported in this paper except for the interaction energies used fully relaxed, optimized (cluster+CO_2) geometries where no negative frequencies were calculated for the final structures.

The interaction energies of the CO_2 and $Ti_2O_9H_{10}$ moieties are calculated using electronic energies of the bare constrained ($Ti_2O_9H_{10}$) and constrained ($Ti_2O_9H_{10}CO_2$) clusters and free energies of the relaxed clusters as:

$$\Delta E^{interaction} = E_{CO_2} + E_{Ti_2O_9H_{10}} - E_{Ti_2O_9H_{10}CO_2} \qquad \textbf{2.1}$$

In Eq. **2.1**, E could represent either electronic energy of the constrained cluster or the Gibbs free energy of the relaxed cluster. Counterpoise corrected[28] interaction energies (i.e., the basis set superposition error induced by bringing two molecules in proximity) were estimated . The free energies of interaction reported in Table **2-3** were derived from the energies of relaxed bare $Ti_2O_9H_{10}$, CO_2 and $Ti_2O_9H_{10}CO_2$ clusters (and hence cannot be compared with the (electronic) interaction energies reported in the same table). Population analyses and Wiberg bond indices in the natural atomic (NAO) basis and "natural" bonding orbitals (NBO) were calculated using the NBO program[29] included in Gaussian 03. The use of "natural" atomic orbitals has been shown[30] to decrease the basis set dependence of these quantities, which are not actual quantum mechanical observables and therefore cannot be extracted directly from the wave function.

2.5 Results

The ground state atomic structure of the $Ti_2O_9H_{10}CO_2$ clusters from (001), (010) and (101) surface planes are shown in Figure **2-3**, Figure **2-4** and Figure **2-5** respectively**.** As shown in Figure **2-3**, CO_2 located ~2.5 Å from the surface (Ti-O-Ti) atoms on the

(001) $Ti_2O_9H_{10}$ fixed cluster adsorbed to form a bridged carbonate geometry with $r(C\text{-}O)^{(CO_2)}$ = 1.275 Å.

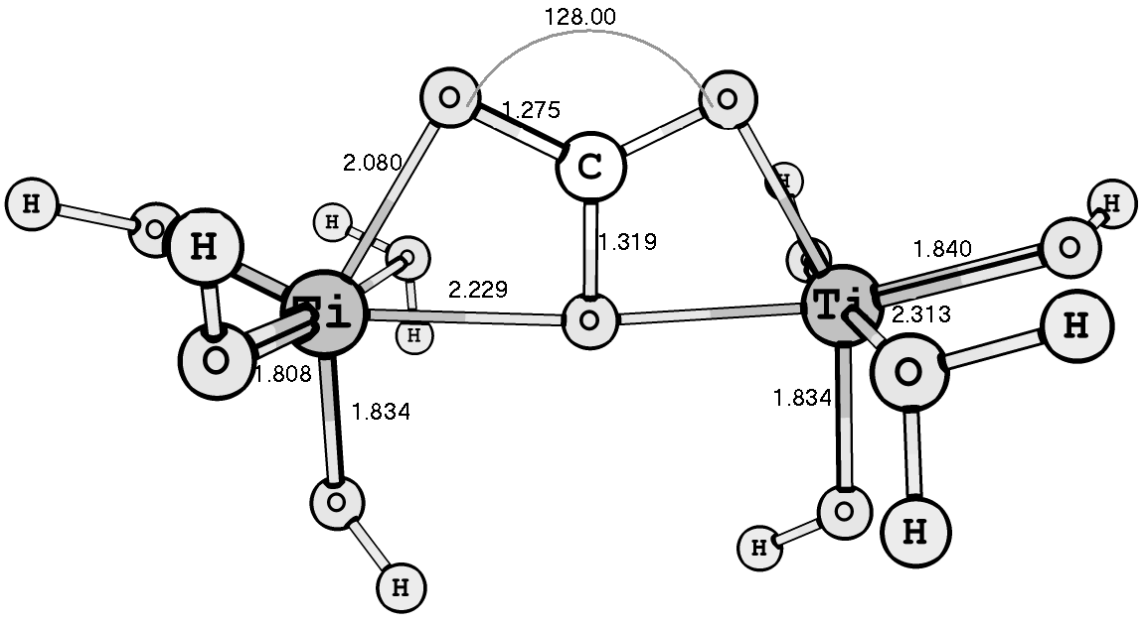

Figure **2-3**: Ground state (001) C_2 symmetric $Ti_2O_9H_{10}CO_2$ cluster optimized at B3LYP/6-31+G(d) level of theory, bond distances in Å, angles in degrees. The C-O bond lengths and O-C-O bond angles are different from other clusters shown in Figure **2-4** , and Figure **2-5**.

The H_2O groups which were fixed at the bottom of the Ti atoms in the initial fixed cluster relaxed to a C_2 symmetric cluster (undergoing rotation to be on opposite sides).The asymmetric and symmetric C-O stretch IR frequencies are consistent with those reported by Martra[14] for surface carbonate species (1580, 1360 cm^{-1}).

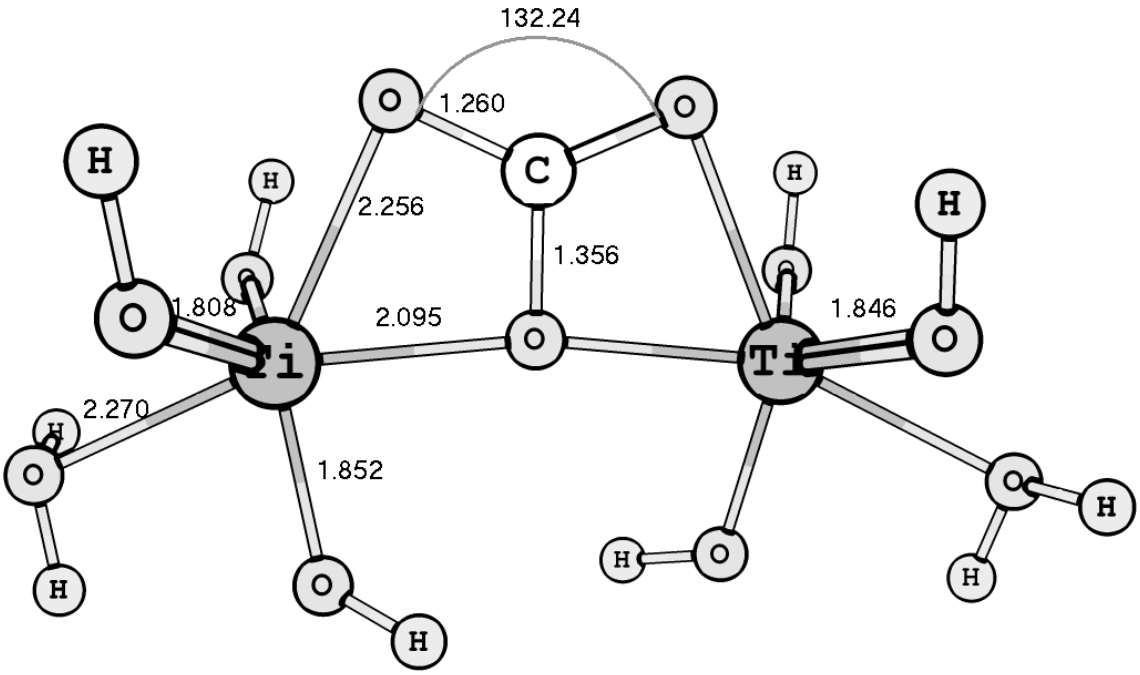

Figure **2-4**: Ground state (010) C_2 symmetric $Ti_2O_9H_{10}CO_2$ cluster optimized at B3LYP/6-31+G(d) level of theory, bond distances in Å, angles in degrees.

The (010) $Ti_2O_9H_{10}CO_2$ cluster (Figure **2-4**) is distinct from the (001) cluster (Figure **2-3**) because CO_2 forms another carbonate-like species with $r(C\text{-}O)^{(CO_2)}$ = 1.259 Å. As mentioned earlier, the bridging oxygen of the cluster was made 2-coordinate to prepare a $Ti_2O_9H_{10}$ cluster. (Cluster geometries with 2 bridging oxygen atoms on the (010) surface, were not investigated in this study).The relaxed cluster is C_2 symmetric about the $C\text{-}O^{bridging}$ axis. Initial (fixed) geometries with H_2O at the bottom (attached to Ti atoms) resulted in the cluster breaking apart and losing its symmetry upon relaxation. The C-O vibrational frequencies are similar to those found during in situ low temperature adsorption studies and assigned to "bent" CO_2 species on TiO_2[13]. The $(C\text{-}O^{(CO_2)})$ bond distances of the (001) cluster (Figure **2-3**) are longer than corresponding distances in the

(010) cluster (Figure 2-4), which is consistent with the lower IR frequencies observed in (001) cluster. Ti-$O^{bridging}$ bond lengths are also longer in the (001) cluster.

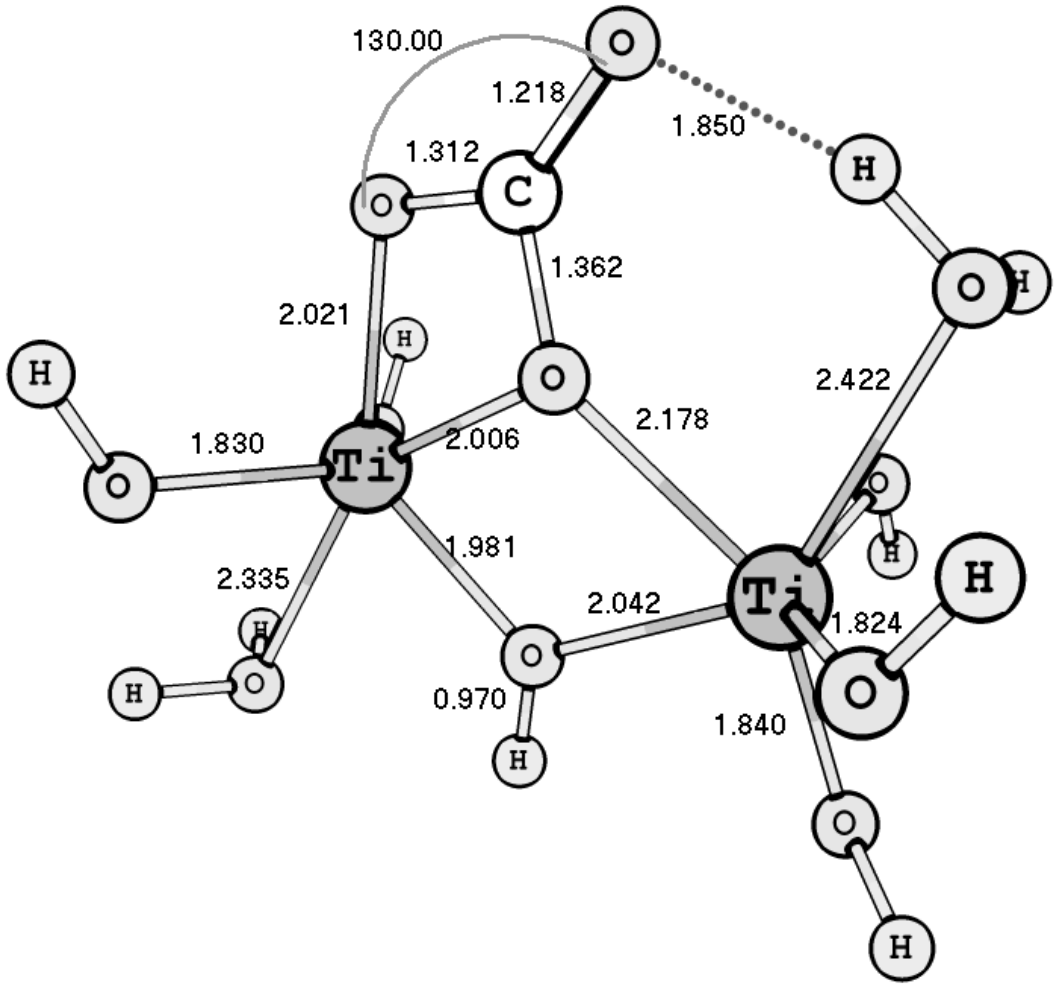

Figure 2-5: Ground state (101) $Ti_2O_9H_{10}CO_2$ cluster optimized at B3LYP/6-31+G(d) level of theory, bond distances in Å, angles in degrees.

In comparison to the (001) and (010) surfaces, the (101) surface plane forms a corrugated structure exposing a 2-c oxygen and 5-c and 6-c Ti atoms. The fixed C_s symmetric (101) $Ti_2O_9H_{10}CO_2$ cluster upon relaxation reached a saddle point. Extremely tight optimization convergence criteria and calculations without symmetry constraints were used to move away from this saddle point resulting in a C_1 symmetric cluster with

some H-bonding between the O of CO_2 and one of the H atoms added for coordinative saturation. The optimized ground state geometry is shown in Figure **2-5**.

Table **2-2**: Comparisons of scaled IR frequencies and the intensity ratios for CO_2 adsorbed on anatase TiO_2 (1800-1100 cm^{-1} region).

Reference	Experimental vibrational frequencies, cm^{-1}	Scaled IR frequencies, computational, cm^{-1}		Intensity ratio, experimental	Normalized intensity ratio, from computations	Raw IR intensities, km/mol	Comments
Ramis et al.,1991[13]	1750, 1150	1724	1203	1.96	2.52	737.25, 292.20	IR frequencies calculated for (101) $Ti_2O_9H_{10}CO_2$ cluster
Ramis et al.,1991[13]	1668, 1312	1659	1322	1.23	4.46	805.19, 180.51	(010) cluster
Martra, 2000[14]	1580, 1360	1582	1377	2.96	4.80	993.04, 206.71	(001) cluster

Similar to the (010) surface plane, the C-O IR frequencies are consistent with those observed by Ramis et al.[13]. The calculated C-O stretch frequencies for each configuration and the experimental IR frequencies are compared in Table **2-2**. Each pair of calculated C-O stretch frequencies corresponds to a different CO_2 species adsorbed on TiO_2. In all three cases, CO_2 forms a carbonate-like species on the surface, but these configurations are different enough to be distinguished by their vibrational frequencies. C-O (scaled) IR vibrational frequencies at the B3LYP/6-31+G(d) level for the $Ti_2O_9H_{10}CO_2$ clusters from (001), (101) and (010) surface planes are shown in Figure **2-**

6, and there is good agreement between the IR frequencies predicted by computations and those derived from experiments.

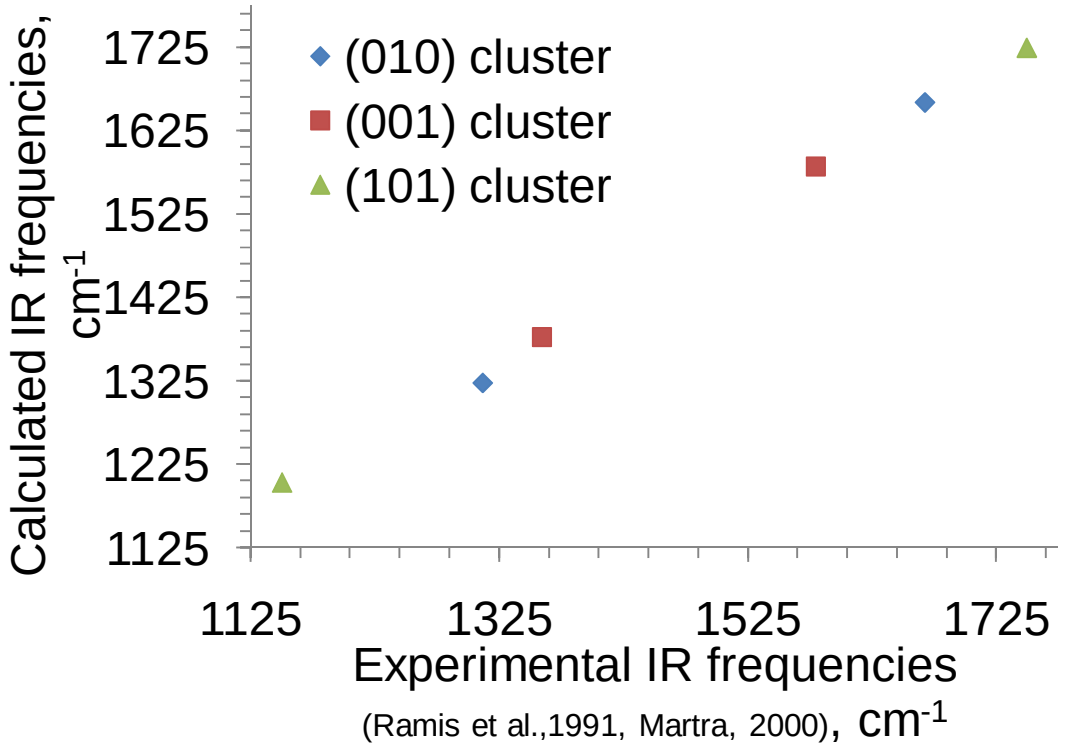

Figure **2-6**: Comparison of experimental C-O IR frequencies to those calculated using B3LYP/6-31+G(d) calculations on the (001), (010) and (101) $Ti_2O_9H_{10}CO_2$ clusters.

The (101) cluster shown in Figure **2-5** exhibits some hydrogen bonding between the water and carbonate groups. While this might shift the observed (C-O) stretch frequencies, this effect may not be entirely artificial. Real anatase surfaces (even under high vacuum) may have adsorbed water vapor that may form hydrogen bonds with (electron-rich) carbonate-like species. In this case, the anatase pre-treatment Ramis et al.[13] adopted prior to adsorption studies is not clear. Moreover, the agreement between the calculated and experimental frequencies suggests that this effect may be of the same

order of magnitude as the error in scaling these frequencies itself (~± 20 cm^{-1}), so this effect should not alter our interpretation.

The interaction energies along with other calculated properties of the $Ti_2O_9H_{10}CO_2$ clusters are shown in Table **2-3**. Analysis of the "natural" atomic charges of the three clusters as shown in Table **2-4** shows that the CO_2 moiety gains ~ 0.4 electrons of charge upon adsorption and further relaxation.

Table **2-3**: Counterpoise corrected interaction energies (based on electronic energy of fixed geometries and Gibbs free energy of relaxed geometries) of CO_2 on (001), (010) and (101) $Ti_2O_9H_{10}$ clusters (positive values indicate exergonic reaction).

	(001)	(010)	(101)
$\Delta E^{electronic\ (0\ K)}$, fixed geometry, kJ/mol	51	83	70
ΔG^0, relaxed geometry, kJ/mol	-110	-134	-86

End-on configurations of CO_2 on the $Ti_2O_9H_{10}$ cluster were formed upon constrained geometry optimization. (The geometry of the (010) $Ti_2O_9H_{10}CO_2$ constrained cluster with CO_2 adsorbed linearly is included in Appendix A) However, it was not feasible to follow the procedure described for the carbonate-like species to optimize the linear species since they desorbed from the bare cluster upon relaxation. Although linearly adsorbed species are also important species for CO_2 photoreduction, only carbonate-like species will be discussed in this work.

Table 2-4: Natural atomic charges, bond distances and $\Delta\nu_3$ splittings of (010), (001) and (101) $Ti_2O_9H_{10}CO_2$ clusters calculated with the B3LYP/6-31+G(d) model chemistry.

	(001) $Ti_2O_9H_{10}CO_2$	(010) $Ti_2O_9H_{10}CO_2$	(101) $Ti_2O_9H_{10}CO_2$
$\Delta\nu_3$ unscaled (scaled), cm^{-1}	213 (205)	350 (338)	540 (521)
IR harmonic frequencies, unscaled, cm^{-1}	1641, 1428	1721, 1371	1788, 1248
$q(CO_3)^{(CO_2+O^{bridging})}$	-1.236	-1.272	-1.207
$q(CO_2)$	-0.42	-0.435	-0.372
$q(O^{bridging})$	-0.82	-0.84	-0.83
$\Sigma q\left(Ti\right)^{(Ti_2O_9H_{10}CO_2)}$	3.78	3.85	3.88
$\Sigma\left(qO^{cluster+CO_2} - qO^{CO2}\right)$	-0.42	-0.43	-0.38
Cluster dipole moment, D	0.77	1.477	4.096
$r(C\text{-}O)^{(CO_2)}$, Å	1.27457	1.25977	1.21827, 1.31205

2.6 Discussion

CO_2 can interact with the Lewis acid centers (Ti^{4+}) and/or with the Lewis base centers (O^{2-}) of TiO_2. The carbon atom in CO_2 is slightly electrophilic while the O atom can interact with Lewis acid sites on metal oxide surfaces. The IR frequencies, bond lengths of the $C\text{-}O^{bridging}$ bonds and the O-C-O bond angles indicate that these clusters correspond to chemisorbed CO_2 species. Moreover, the bond angles and C-O, O-Ti bond

lengths correspond to polydentate carbonate-like species. As shown in Table **2-2** , the C-O vibrational intensity ratios of the two frequencies also match well with experimental IR intensity ratios. However, according Ramis et al.[13], the IR assignments for the species on the (010) and (101) $Ti_2O_9H_{10}CO_2$ clusters correspond to "side-on bent" CO_2 species, bonded on Lewis acid surface cationic centers (Ti^{4+} ions). These authors suggested that these species underwent nucleophilic attack forming surface carbonates upon heating.

Although the CO_2 species adsorbed on all three surface planes in our modeling results are partially negatively charged (~-0.3 to -0.45 e^-, suggesting that they could be precursors to reduction of CO_2), we note that these species correspond more closely to polydentate surface carbonates and do not have C-Ti bonds (C-Ti Wiberg bond indices close to zero, Table **2-5**). This is significant, because as reported by Freund and Roberts[31], the lowest unoccupied molecular orbital (LUMO) of CO_2 is lowered in energy upon decreasing the O-C-O bond angle from 180°. Therefore, it becomes relatively easier to reduce CO_2 as the O-C-O angle is lowered from 180°. One of the ways to achieve this distortion of the O-C-O angle is by CO_2 interacting with the anatase surface. The formation of surface polydentate carbonates reported in this paper can be thought of as a limiting case of such O-C-O angle distortion, where CO_2 gains electronic charge from the bare cluster/surface but the carbon atom does not get reduced.

The number of harmonic C-O vibrational modes calculated for the (010), (001) and (101) clusters (~6-7) (shown in Supporting Information) are consistent with a CO_3^{2-} -like species that has 3N - 6 = 6 total vibrational modes, (where N is the number of atoms) some of which are not IR active. Ramis et al.[12] proposed that (Ti)d-(C-O)π^* electron back-donation would stabilize the "bent" CO_2 species on the surface. However, analysis

of natural charges (calculated from Table **2-4**) shows that most of the charge is transferred to the oxygen atoms of CO_2, not carbon. Moreover, the data shown in Table **2-6** indicates that the anti-bonding C-O NBOs are not occupied. Therefore, the assignments of IR vibrational frequencies (1773, 1750, 1150; 1668, 1312) as reported by Ramis et al.[13] probably correspond to polydentate surface carbonate-like species and not "side-on bent" CO_2 coordinated with surface Ti atoms.

Table **2-5**: Comparison of Wiberg bond indices in the natural atomic orbital (NAO) basis for the (001), (010) and (101) $Ti_2O_9H_{10}CO_2$ clusters at the B3LYP/6-31+G(d) level.

	(001) $Ti_2O_9H_{10}CO_2$	(010) $Ti_2O_9H_{10}CO_2$	(101) $Ti_2O_9H_{10}CO_2$	CO_2
Ti-C	0.02	0.02	0.00, 0.00	----
$C\text{-}O^{bridging}$	1.14	0.99	0.96	----
$(C\text{-}O)^{(CO_2)}$	1.31	1.39	1.17, 1.63	1.89
$Ti\text{-}O^{(OH)}$	0.94, 0.84	0.93, 0.83	0.84, 0.84, 0.79, 0.90, 0.88	----
$(Ti\text{-}O^{(H_2O)})$	0.18	0.22	0.19, 0.18	----
$Ti\text{-}O^{bridging}$	0.22	0.32	0.43, 0.23	----
$(Ti\text{-}O)^{(CO_2)}$	0.36	0.26	0.49, 0.06, 0.01, 0.00	----
$(O^{CO_2}\text{-}H)$	----------	----------	0.057	----

From Table **2-4**, the "natural" charges of Ti and O atoms (involved in bonding with CO_2) on the (010) cluster are higher than corresponding charges for the (001) cluster. This difference can be attributed to the difference in electrophilic character of the Ti cations on the (010) and (001) surface planes[15]. This difference might account for the slightly higher partial charge on the CO_2 moiety adsorbed on the (010) cluster compared

to the (001) cluster. As shown in Table **2-5** and Table **2-4** , the greater charge on the O atoms of the (010) and (101) clusters also results in stronger ($C\text{-}O^{CO_2}$) bonds. In conclusion, the main differences among the three clusters are the relative acidity of Ti atoms (and the basicity of O atoms). The (001) cluster is the least acidic among the three which is reflected by the amount of electrons donated to CO_2. The amount of electrons donated to CO_2 in the (101) cluster is lesser than that for the (010) cluster probably because one of the Ti atoms is 6-c, and is therefore less acidic. Analysis of the natural electronic configurations (from the NBO analysis) indicates that most of this donated charge resides primarily on the O(2p) orbitals of CO_2.

The interaction energies of CO_2 on the three clusters (as calculated by Eq (1)) are shown in Table **2-3** . Fixed geometry $Ti_2O_9H_{10}$ and $Ti_2O_9H_{10}CO_2$ clusters were used in the calculation because the bare cluster ($Ti_2O_9H_{10}$) relaxed more than the cluster with adsorbed CO_2 ($Ti_2O_9H_{10}CO_2$), resulting in positive free energies of reaction (or negative interaction energies), because the fully relaxed reactants had a lower free energy compared to fully relaxed products, $Ti_2O_9H_{10}CO_2$. Using the energetics of the partially constrained cluster is reasonable because lattice constraints will limit the relaxation of surface Ti and O atom on a real crystal face. The interaction energy on the (001) cluster is lower than that on the (010) cluster, which is consistent with the acid/base character of the surface cations and anions on these surface planes.

Table **2-6**: Natural bonding orbital (NBO) analyses showing the occupancies and % C and %Ti contributions to various orbitals of (010), (001) and (101) $Ti_2O_9H_{10}CO_2$ clusters at the B3LYP/6-31+G(d) level. (Asterisk indicates antibonding NBOs.)

	(001) $Ti_2O_9H_{10}CO_2$		(010) $Ti_2O_9H_{10}CO_2$		(101) $Ti_2O_9H_{10}CO_2$	
C-O bonds	Occupancy	%C	Occupancy	%C	Occupancy	%C
$(C\text{-}O)^{(CO_2)}$	1.960	33%	1.993	35%	1.988, 1.994	34%, 35%
$(C{=}O)^{(CO_2)}$	1.955	19%	1.983	21%	1.991	27%
$C\text{-}O^{bridging}$	1.896	28%	1.989	31%	1.989	31%
$C{=}O^{bridging}$	1.900	1%	---	---	---	---
$(C\text{-}O^{(CO_2)})^*$	0.065	67%	0.064	65%	0.080, 0.060	66%, 65%
$(C{=}O^{(CO_2)})^*$	0.472	81%	0.450	79%	0.321	73%
$(C\text{-}O^{bridging})^*$	0.067	72%	0.106	69%	0.117	69%
$(C{=}O^{bridging})^*$	0.191	99%	---	---	---	---
Ti-O bonds	Occupancy	%Ti	Occupancy	%Ti	Occupancy	%Ti
$(Ti\text{-}O^{(CO_2)})$	1.864	6%	1.887	7%	1.924	11%
$Ti\text{-}O^{bridging}$	---	---	1.946	7%	1.944	10%
$Ti{=}O^{bridging}$	---	---	---	---	1.822	3%
$(Ti\text{-}O^{(CO_2)})^*$	0.111	94%	0.148	94%	0.133	90%
$(Ti\text{-}O^{bridging})^*$	---	---	0.123	93%	0.151	90%
$(Ti{=}O^{bridging})^*$	---	---	---	---	0.213	97%

Table **2-4** shows that the carbonate $\Delta\nu_3$ frequency splitting of the three clusters increase from (001) to (101) $Ti_2O_9H_{10}CO_2$. Busca and Lorenzelli[12] have pointed out that $\Delta\nu_3$ carbonate splitting of ~200 cm^{-1} was consistent with bidentate carbonate species whereas higher splitting (~300 cm^{-1}) was observed in bridged $CO_3^{\delta-}$ species. This is

consistent with our observation that the IR frequencies for the (001) cluster correspond to a surface carbonate species. In the previous discussion, we showed that the IR frequencies for these higher $\Delta\nu_3$ splitting (i.e. higher C-O stretch frequencies) corresponded to polydentate CO_3 species whereas Busca and Lorenzelli[12] assigned them to "bent" CO_2 species.

A comparison of Wiberg bond order indices in the NAO basis for (001), (010) and (101) $Ti_2O_9H_{10}CO_2$ clusters is shown in Table **2-5**. These results are consistent with the data from Table **2-4**. C-O bond length of the CO_2 species on the (010) surface is shorter than that formed at the (001) surface plane. Similarly, the C-$O^{bridging}$ bond and the Ti-O^{CO_2} bonds are weaker in CO_2 species at the (010) surface plane. This indicates that the electron density from the C=O bond of CO_2 (which has a C-O Wiberg bond order of 1.89) is more strongly delocalized in the (001) cluster. In addition, NBO analyses shown in Table **2-6** indicate that the occupancy of the C-O and C=O bonding orbitals of CO_2 increases from the (001) to the (101) cluster. The Ti-$O^{bridging}$ bond in the (001) cluster is weaker compared to the (010) and (101) clusters, mainly because of lower electrophilic nature of the Ti cations. This weaker bonding between the Ti and bridging oxygen, (due to their relatively low electrophilic and nucleophilic character) effectively results in a CO_3 group bridged across two Ti cations on the (001) cluster; forming a surface carbonate species.

Ramis et al.[13] suggested that the "bent" CO_2 species converted to surface carbonates and bicarbonates upon heating. From the previous discussion, it is not clear how polydentate carbonates could convert to surface carbonates. One possible mechanism might involve CO_2 desorption and further reaction with traces of adsorbed O_2

and/or surface hydroxyl groups. Another pathway might involve weakening of the Ti-$O^{bridging}$ bond of the cluster upon electron donation to the CO_2 species, as shown in Figure 2-7. As electron density is withdrawn from the O atom towards carbon, the Ti-$O^{bridging}$ bond becomes weaker (and longer, indicated with a dotted line) and the Ti-O^{CO_2} bond becomes stronger. This electron donation could weaken the Ti-O bond and convert the polydentate species to a surface carbonate (effectively a 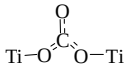 species). This is qualitatively seen in Table 2-5, the Ti-$O^{bridging}$ bonds of the (001) cluster are weaker than similar bonds in the (010) and (101) clusters; while the Ti-O^{CO_2} bonds of the (001) cluster are stronger than similar bonds in the (001) cluster.

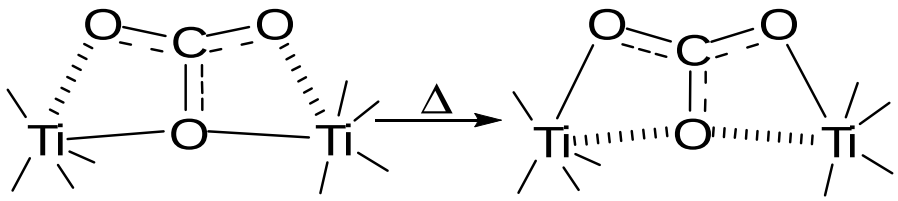

Figure 2-7: One possible pathway for the formation of surface carbonates from polydentate carbonate groups on a Ti-O-Ti cluster. Bridged carbonate-like species upon heating may be transformed to "*free*" carbonate. Singly hashed lines indicate weaker bonds, compared to single solid lines.

2.7 Conclusions

Large basis sets on the atoms of CO_2 (with diffuse functions) and high levels of electron correlation are required to model its anionic attached states. As a starting point for the excited state calculations, we have modeled the ground states of carbonate-like species adsorbed on $Ti_2O_9H_{10}$ surfaces. These B3LYP/6-31+G(d) DFT calculations on

$Ti_2O_9H_{10}CO_2$ have accurately predicted the ground state geometry and vibrational spectra of CO_2 adsorbed onto different faces of anatase. We have shown that the spectra reported in the literature and assigned to "bent CO_2 species" on anatase TiO_2 are more consistent with polydentate carbonate-like species. The fact that significantly different reactions are predicted for the three clusters built from distinct crystal surfaces suggests that all the surface-specific information is not lost when the molecular cluster approximation is made. Furthermore, the results indicate that the dominant control over surface reactivities is local in nature to a first approximation. Consequently, molecular cluster model calculations in conjunction with periodic calculations and experimental studies can be used to effectively understand surface reaction mechanisms.

In addition to coordination, the geometrical arrangement of Ti and O atoms on the surface might also play a role in photoreduction. Yamashita et al.[32] proposed that the atomic Ti/O ratio of top-surface Ti and O atoms capable of directly interacting with CO_2 and H_2O is higher on (rutile) TiO_2 (100) than TiO_2 (110). Similar considerations might play a significant role in affecting photoactivity on anatase surfaces as well. Existing mechanisms proposed for CO_2 photoreduction do not indicate the state of CO_2 adsorbed on TiO_2. This is important, because if the interaction between the surface atoms and CO_2 is very strong, CO_2 becomes irreversibly chemisorbed on the surface, while weak interactions at large inter-atomic distances will not result in efficient charge transfer from the photo-excited surface. Our modeling results show that localized, cluster approach to adsorption processes is helpful in determining the reactive species formed on metal oxide surfaces at a relatively lower computational cost (compared to periodic calculations).

2.8 References

1. Salem, I., Recent studies on the catalytic activity of titanium, zirconium, and hafnium oxides. *Catalysis Reviews-Science And Engineering* **2003,** 45, (2), 205-296.
2. Reddy, B. M.; Khan, A., Recent advances on TiO2-ZrO2 mixed oxides as catalysts and catalyst Supports. *Catalysis Reviews* **2005,** 47, (2), 257 - 296.
3. Lavalley, J. C., Infrared spectrometric studies of the surface basicity of metal oxides and zeolites using adsorbed probe molecules. *Catalysis Today* **1996,** 27, (3-4), 377-401.
4. Carp, O.; Huisman, C. L.; Reller, A., Photoinduced reactivity of titanium dioxide. *Progress in Solid State Chemistry* **2004,** 32, (1-2), 33-177.
5. Zhang, S. G.; Fujii, Y.; Yamashita, K.; Koyano, K.; Tatsumi, T.; Anpo, M., Photocatalytic reduction of CO2 with H2O on Ti-MCM-41 and Ti-MCM-48 mesoporous zeolites at 328 K. *Chemistry Letters* **1997**, (7), 659-660.
6. Rasko, J.; Solymosi, F., Infrared spectroscopic study of the photoinduced activation of CO2 on TiO2 and Rh/TiO2 catalysts. *Journal of Physical Chemistry* **1994,** 98, (29), 7147-7152.
7. Lin, W. Y.; Han, H. X.; Frei, H., CO2 splitting by H2O to CO and O-2 under UV light in TiMCM-41 silicate sieve. *Journal of Physical Chemistry B* **2004,** 108, (47), 18269-18273.
8. Anpo, M.; Yamashita, H.; Ikeue, K.; Fujii, Y.; Zhang, S. G.; Ichihashi, Y.; Park, D. R.; Suzuki, Y.; Koyano, K.; Tatsumi, T., Photocatalytic reduction of CO2 with H2O on Ti-MCM-41 and Ti-MCM-48 mesoporous zeolite catalysts. *Catalysis Today* **1998,** 44, (1-4), 327-332.
9. Anpo, M.; Yamashita, H.; Ichihashi, Y.; Fujii, Y.; Honda, M., Photocatalytic reduction of CO2 with H2O on titanium oxides anchored within micropores of zeolites: Effects of the structure of the active sites and the addition of Pt. *Journal of Physical Chemistry B* **1997,** 101, (14), 2632-2636.
10. Anpo, M.; Yamashita, H.; Ichihashi, Y.; Ehara, S., Photocatalytic reduction of CO2 with H2O on various titanium oxide catalysts. *Journal of Electroanalytical Chemistry* **1995,** 396, (1-2), 21-6.
11. Markovits, A.; Fahmi, A.; Minot, C., A theoretical study of CO2 adsorption on TiO2. *Theochem-Journal of Molecular Structure* **1996,** 371, 219-235.
12. Busca, G.; Lorenzelli, V., Infrared spectroscopic identification of species arising from reactive adsorption of carbon oxides on metal oxide surfaces. *Materials Chemistry* **1982,** 7, (1), 89-126.
13. Ramis, G.; Busca, G.; Lorenzelli, V., Low-temperature carbon dioxide adsorption on metal oxides: spectroscopic characterization of some weakly adsorbed species. *Materials Chemistry and Physics* **1991,** 29, (1-4), 425-35.
14. Martra, G., Lewis acid and base sites at the surface of microcrystalline TiO2 anatase: relationships between surface morphology and chemical behaviour. *Applied Catalysis, A: General* **2000,** 200, (1-2), 275-285.
15. Hadjiivanov, K. I.; Klissurski, D. G., Surface chemistry of titania (anatase) and titania-supported catalysts. *Chemical Society Reviews* **1996,** 25, (1), 61-&.

16. Diebold, U., The surface science of titanium dioxide. *Surface Science Reports* **2003,** 48, (5-8), 53-229.
17. Vittadini, A.; Casarin, M.; Selloni, A., Chemistry of and on TiO2-anatase surfaces by DFT calculations: a partial review. *Theoretical Chemistry Accounts* **2007,** 117, (5-6), 663-671.
18. de Lara-Castells, M. P.; Mitrushenkov, A. O.; Roncero, O.; Krause, J. L., Adsorption and nonadiabatic processes in the photodesorption of molecular oxygen from the reduced TiO2(110) surface. *Israel Journal of Chemistry* **2005,** 45, (1-2), 59-76.
19. Sauer, J.; Ugliengo, P.; Garrone, E.; Saunders, V. R., Theoretical Study of van der Waals Complexes at Surface Sites in Comparison with the Experiment. *Chemical Reviews* **1994,** 94, (7), 2095-2160.
20. Paul, K. W.; Kubicki, J. D.; Sparks, D. L., Sulphate adsorption at the Fe(hydr)oxide-H2O interface: comparison of cluster and periodic slab DFT predictions. *European Journal of Soil Science* **2007,** 58, (4), 978-988.
21. Gauss, J.; Cremer, D., Analytical Evaluation Of Energy Gradients In Quadratic Configuration-Interaction Theory. *Chemical Physics Letters* **1988,** 150, (3-4), 280-286.
22. Salter, E. A.; Trucks, G. W.; Bartlett, R. J., Analytic Energy Derivatives In Many-Body Methods.1. 1st Derivatives. *Journal of Chemical Physics* **1989,** 90, (3), 1752-1766.
23. Koppenol, W. H.; Rush, J. D., Reduction potential of the CO2/CO2.- couple - a comparison with other C1 radicals. *Journal of Physical Chemistry* **1987,** 91, (16), 4429-4430.
24. Sommerfeld, T.; Meyer, H. D.; Cederbaum, L. S., Potential energy surface of the CO2- anion. *Physical Chemistry Chemical Physics* **2004,** 6, (1), 42-45.
25. Frisch, M. J. T., G. W.; Schlegel, H. B.; Scuseria, G. E.; Robb, M. A.; Cheeseman, J. R.; Montgomery, Jr., J. A.; Vreven, T.; Kudin, K. N.; Burant, J. C.; Millam, J. M.; Iyengar, S. S.; Tomasi, J.; Barone, V.; Mennucci, B.; Cossi, M.; Scalmani, G.; Rega, N.; Petersson, G. A.; Nakatsuji, H.; Hada, M.; Ehara, M.; Toyota, K.; Fukuda, R.; Hasegawa, J.; Ishida, M.; Nakajima, T.; Honda, Y.; Kitao, O.; Nakai, H.; Klene, M.; Li, X.; Knox, J. E.; Hratchian, H. P.; Cross, J. B.; Bakken, V.; Adamo, C.; Jaramillo, J.; Gomperts, R.; Stratmann, R. E.; Yazyev, O.; Austin, A. J.; Cammi, R.; Pomelli, C.; Ochterski, J. W.; Ayala, P. Y.; Morokuma, K.; Voth, G. A.; Salvador, P.; Dannenberg, J. J.; Zakrzewski, V. G.; Dapprich, S.; Daniels, A. D.; Strain, M. C.; Farkas, O.; Malick, D. K.; Rabuck, A. D.; Raghavachari, K.; Foresman, J. B.; Ortiz, J. V.; Cui, Q.; Baboul, A. G.; Clifford, S.; Cioslowski, J.; Stefanov, B. B.; Liu, G.; Liashenko, A.; Piskorz, P.; Komaromi, I.; Martin, R. L.; Fox, D. J.; Keith, T.; Al-Laham, M. A.; Peng, C. Y.; Nanayakkara, A.; Challacombe, M.; Gill, P. M. W.; Johnson, B.; Chen, W.; Wong, M. W.; Gonzalez, C.; and Pople, J. A. *Gaussian 03, Revision D.01*, Gaussian Inc.: Wallingford, CT, 2004.
26. Becke, A. D., A New Mixing Of Hartree-Fock And Local Density-Functional Theories. *Journal of Chemical Physics* **1993,** 98, (2), 1372-1377.
27. Lee, C. T.; Yang, W. T.; Parr, R. G., Development of the Colle-Salvetti correlation-energy formula into a functional of the electron-density. *Physical Review B* **1988,** 37, (2), 785-789.

28. Boys, S. F.; Bernardi, F., The calculation of small molecular interactions by the differences of separate total energies. Some procedures with reduced errors. *Molecular Physics* **1970,** 19, (4), 553 - 566.
29. Glendening, E. D.; Reed, A. E.; Carpenter, J. E.; Weinhold, F. *NBO Version 3.1*.
30. Reed, A. E.; Weinstock, R. B.; Weinhold, F., Natural-Population Analysis. *Journal of Chemical Physics* **1985,** 83, (2), 735-746.
31. Freund, H. J.; Roberts, M. W., Surface chemistry of carbon dioxide. *Surface Science Reports* **1996,** 25, (8), 227-273.
32. Yamashita, H.; Kamada, N.; He, H.; Tanaka, K.; Ehara, S.; Anpo, M., Reduction of CO2 with H2O on TiO2(100) and TiO2(110) single-crystals under uv-irradiation. *Chemistry Letters* **1994**, (5), 855-858.

Chapter 3

Quantum mechanical modeling of CO_2 interactions with irradiated stoichiometric and oxygen-deficient anatase TiO_2 surfaces: Implications for the photocatalytic reduction of CO_2

3.1 Introductory Comment

"The thing is: The way I see it, these days there's a war on, right? and, ages ago, there wasn't a war on, right? So, there must have been a moment when there not being a war on went away, right? and there being a war on came along. So, what I want to know is: ***How did we get from the one case of affairs to the other case of affairs?****"*

- Baldrick in Blackadder Goes Forth: Goodbyee

Electron transfer from the TiO_2 surface to neutral CO_2 , forming the carbon dioxide radical anion, constitutes the first step in the activation of CO_2. This chapter examines the feasibility of electron transfer to various forms of CO_2 adsorbed on TiO_2 surfaces. Results from ground state modeling of CO_2 chemisorbed on TiO_2 surfaces were presented in Chapter 2. Using a similar surface site approach, two complementary methodologies to study the excited states of CO_2 (likely formed under light irradiation) are presented in this chapter: (a) Density functional theory calculations of triplet TiO_2-CO_2 model clusters, and (b) Computationally-intensive single-point post-Hartree-Fock calculations of both linear and carbonate-like CO_2 species. It is expected that these results would reveal the roles played by the TiO_2 surface in transferring the photo-generated electron to CO_2.

3.2 Abstract

The conversion of CO_2 using light energy (CO_2 photoreduction) has the potential to produce useful fuels or valuable chemicals while decreasing CO_2 emissions from the use of fossil fuels. Identifying the mechanism and the active sites involved in the formation of negatively charged CO_2 species on TiO_2 surfaces represents a significant advance in our understanding of CO_2 photoreduction. To understand the role of the TiO_2 surface acting as a photocatalyst mediating CO_2 photocatalytic reduction, excited-state ab initio calculations of CO_2 adsorbed on clusters from the (010), (101) and (001) anatase surface planes were performed. Both post-Hartree-Fock calculations on small model surface clusters as well as density-functional theory (DFT) calculations on larger clusters indicate that conduction band electrons in irradiated, stoichiometric TiO_2 surfaces may not be transferred to CO_2. On the other hand, oxygen vacancies may act as the active sites for CO_2 photoreduction.

3.3 Introduction

Increasing anthropogenic CO_2 emissions present an opportunity to use CO_2 as a raw material for producing chemicals such as urea and polycarbonates[1]. In addition to converting CO_2 to such chemicals, CO_2 could also be recycled to fuels (or fuel precursors) such as methane, carbon monoxide or methanol. This conversion of CO_2 to fuels is an endergonic process requiring a hydrogen source and/or energy. The most abundant sources of energy and hydrogen are sunlight and water, respectively. Solar

photocatalytic reduction of CO_2 to produce fuels using water as the hydrogen source thus has the potential to store intermittent solar energy and to recycle CO_2.

Titania (TiO_2) based photocatalysts have been used to convert CO_2 to useful compounds, both in gas and aqueous phase photoreactions. The conversion of CO_2 and water to simple C_1 products such as formic acid and formaldehyde using irradiated aqueous suspensions of titania was first demonstrated by Inoue et al.[2]. The concept of semiconductor-mediated photocatalytic reduction of CO_2 is illustrated in Figure **3-1**. Researchers have also used homogeneous metal complexes in solution to reduce CO_2[3]. Some recent developments in this field have been moves towards rational photocatalyst design, development of catalysts active at longer wavelengths than can be utilized by commercially available titania, and the elucidation of reaction mechanisms through in situ spectroscopic studies[4, 5].

Current photocatalysts for CO_2 reduction are inefficient. State-of-the-art CO_2 photoreduction catalysts do not perform as efficiently as the state-of-the-art catalysts for H_2 photogeneration. For example, doped metal oxide photoelectrodes for solar hydrogen generation have hydrogen evolution rates of 400-700 µmol/h under visible irradiation[7]. This is well in excess of what current catalysts for CO_2 photoreduction have achieved to date (~1% conversion of CO_2 at a rate of ~1 µmol product/h[6-8]). To develop better catalysts, we need to understand the initial steps of the reactions involved in this process. As a step towards that goal, we report excited-state molecular orbital (MO) calculations of CO_2 adsorbed on clusters from various surface planes of anatase TiO_2.

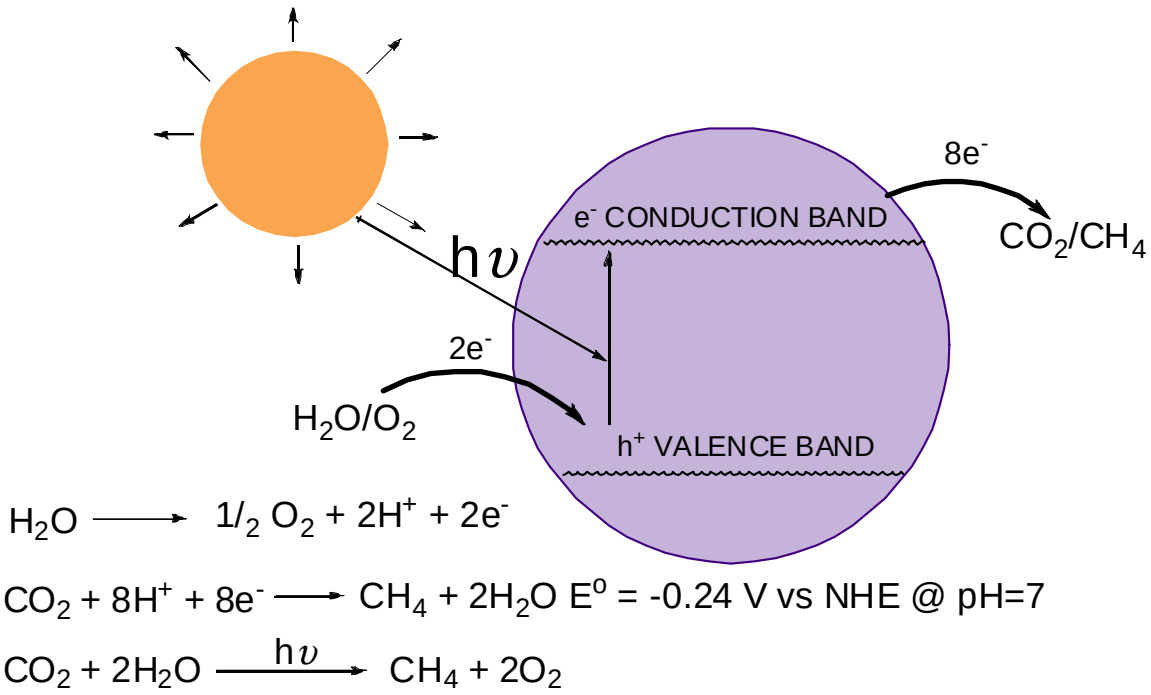

Figure **3-1**: Schematic of semiconductor-mediated CO_2 photoreduction. Photogenerated electrons and holes are transferred to CO_2 and H_2O in a series of reactions leading to the formation of compounds such as CH_4 and O_2 respectively.

The mechanism proposed in the literature to account for CO_2 photoreduction involves the initial photo-excitation of the solid surface, creating electron-hole pairs, followed by their transfer to CO_2 and H_2O[9]. These charge carriers could also recombine or become localized at surface/bulk trapping sites. The surface state approach shown in Figure **3-1** does not indicate whether specific sites exhibiting enhanced reactivity towards the photoinduced activation of CO_2 exist on anatase TiO_2 surfaces. Identification of these surface sites could lead to the design of more effective catalysts for mediating CO_2 photoreduction. Moreover, the exact mechanism by which gaseous CO_2 interacts with the surface electron-hole centers on the TiO_2 surface is unknown. Additionally, although $CO_2^{\bullet-}$, the electron attached state of CO_2, has been proposed as a key intermediate in the

activation of CO_2[10],only a single in situ experimental study presented evidence for $CO_2^{\bullet-}$ on illuminated, undoped TiO_2 catalysts[10]. Gaseous CO_2 also has a negative electron affinity[11-13]. Therefore, identifying the mechanism and the active sites involved in the formation of negatively charged CO_2 species on TiO_2 surfaces represents a significant advance in our understanding of CO_2 photoreduction.

The conduction band of TiO_2 consists mainly of Ti(3d) orbitals, whereas the valence band is comprised of O(2p) orbitals. Xu and Schoonen[14] have pointed out that semiconductor-mediated photo-induced electron transfer reactions require the electrons in the conduction band of the semiconductor to have greater energy than that of the lowest unoccupied molecular orbital (LUMO) of the electron-accepting species. Using the values for the energy of the TiO_2 conduction band and the standard reduction potential for the $HCOOH/H_2CO_3$ couple at pH 5, Xu and Schoonen[14] suggested that the electrons in the conduction band of (bulk) TiO_2 may not be transferred to CO_2. This is contrary to currently proposed mechanisms for CO_2 photoreduction that suggest CO_2 gains electrons from the conduction band of TiO_2[9]. However, electronic interaction between the TiO_2 surface and the adsorbate (CO_2) could facilitate electron transfer by lowering of the LUMO of the adsorbate (for example, by forming a surface state in the band gap). Therefore, it is not known whether chemical interaction with anatase TiO_2 surfaces facilitates charge transfer to CO_2.

In this study, we address the following questions:

1. Does the interaction between CO_2 and anatase TiO_2 surfaces facilitate electron transfer to CO_2?

2. What specific surface sites on the anatase TiO_2 surface promote CO_2 photoreduction?
3. Is there a qualitative difference between different methods of electron correlation for studying excited states of CO_2 adsorbed on TiO_2 surfaces?

To answer these questions, we performed ab initio molecular orbital (MO) calculations of the gas-solid photoreduction of CO_2 on clusters from various low-index anatase TiO_2 surfaces. A combination of small cluster size with a high level of electron correlation and DFT level calculations with larger clusters was used. The results indicate that CO_2 does not gain electrons from defect-free TiO_2 clusters in the excited state.

3.4 Computational Methods

In this study, neutral TiO_2-CO_2 clusters obtained from unreconstructed, stoichiometric surfaces are referred to as being *defect-free.* Two computational tools were used to model excited states of these TiO_2-CO_2 clusters : Gaussian 03 (G03)[15] and Turbomole V5.9[16]. Single-point post-Hartree-Fock (post-HF) Symmetry-Adapted Cluster-Configuration Interaction (SAC-CI)[17] calculations were performed on relatively small clusters containing one or two Ti atoms in G03. The clusters modeled in G03 are: $Ti_2O_9H_{10}$-CO_2 (denoted as Ti2-CO2), $Ti(OH)_4H_2O$-CO_2 (Ti-watCO2), and $Ti(OH)_4$-CO_2 (Ti-4cCO2)). DFT level calculations on larger TiO_2-CO_2 clusters ($Ti_6O_{21}H_{18}$-CO_2, denoted as Ti6-5cCO2) from the (101), (001), (010) surfaces and (110) Ti6- cluster ($Ti_6O_{22}H_{20}$, Ti6-4c) of anatase TiO_2 were performed in Turbomole.

The cluster-based approach has been used in this study because data in the literature suggest that localized processes (such as adsorption) on titania surfaces could be treated using small clusters. de Lara-Castells and Krause[18] compared slab and cluster model calculations for the adsorption of O_2 on reduced TiO_2 (rutile) surfaces and concluded that localized phenomena such as chemisorption could be treated by small clusters. Adsorption of anionic species on oxide surfaces is also well described by hydrogen-saturated cluster models[19]. Cluster calculations of anion adsorption yielded results in agreement with periodic DFT calculations[20]. An alternative technique to model the surface involves the use of embedded point charges instead of the hydrogen atoms. However, as pointed out by Belelli et al.[21], the use of embedded charges leads to varying charges for equivalent atoms in the lattice. In the case of small molecules such as CO_2, long-range electrostatic effects are therefore expected to play a minor role in controlling adsorption. On the other hand, to accurately model the band gap of TiO_2, larger clusters are required. We note that slightly larger Ti_7O_{14} clusters have been used to model the photocatalytic oxidation of water on rutile (110) TiO_2 surface[22]. Ultimately, considering the computational costs, we used clusters comprising of 1-2 Ti atoms for SAC-CI calculations and 6-Ti atom clusters for DFT calculations. A detailed description of the parameters used and the cluster preparation procedures for each method is provided below.

3.4.1 Details of cluster preparation and parameters used for SAC-CI calculations in G03

Clusters of various sizes were cut from the (001), (010) and (110) surface planes of anatase using the Cerius[2] software suite (Accelrys Inc., San Diego, CA). The coordination of the dangling bonds was saturated by adding protons at the same location as the missing Ti atom. All O-H bond distances were initialized to 0.97 Å. ((Full geometry optimizations of a $Ti(OH)_4CO_2$ cluster at the B3LYP/6-31+G(d) level resulted in a O-H bond length of 0.967 Å). TiO_2-CO_2 clusters from the (001) and (110) surface planes containing a single Ti atom were obtained by minimizing the geometry of a cluster having a CO_2 molecule located over the Ti atom. Only Ti, O and CO_2 atoms in the Ti-watCO2 and Ti-4cCO2 clusters were allowed to relax. This resulted in linearly adsorbed CO_2 species. The anatase (110) surface exposes 4-c Ti and 2-c oxygen atoms, whereas the anatase (001) surface exposes 5-c Ti atoms and 2-c and 3-c O atoms[23]. Additionally, 4-c Ti atoms at the interface between anatase and rutile phases have been proposed to act as electron traps in Degussa P-25[24, 25].Therefore, comparing excited state calculations from these two clusters will provide insights into the role of surface coordination on electron transfer to linear CO_2 species.

Excited states of carbonate-like species adsorbed on (010) anatase surface plane (modeled using Ti2-CO2) clusters) were also calculated. Details of methods used to model the ground state of the $Ti_2O_9H_{10}$-CO_2 are given in a previous publication[26]. The ground states of these clusters were modeled using Becke's 3-parameter hybrid method[27] with the LYP correlation functional[28] (B3LYP), and the 6-31+G(d) basis set (as implemented in G03) with default optimization criteria.

For the excited state calculations, the SAC-CI method was chosen to overcome size limitations of the active space and to avoid pitfalls in selecting chemically relevant orbitals. SAC calculations on the ground-state singlet cluster indicate that it can be well described using single determinant wave functions. Therefore, the B3LYP/6-31+G(d) ground-state geometry could be used as a starting point for single point excited-state post-HF calculations. Excited-state calculations used the SD-R version of SAC-CI (with singles and doubles linked excitation operators). The following paragraphs describe the parameters and methods used for excited-state population analysis for clusters containing one and two Ti atoms.

In the case of clusters containing one Ti atom, excited-state calculations were performed without frozen core orbitals. The maximum R2 operators after perturbation selection (MaxR2Op) were set to 10^6. Atomic charges (to be used as one indicator of CO_2 reduction) from the single-point excited-state calculations were calculated using relaxed density natural population analyses (using the NBO program[29] included in G03). It should be noted that the "relaxed density" corresponds to a one-particle density matrix consisting of a HF-contribution with a correlation correction, and does not refer to excited state orbitals. In this study, SAC-CI calculations were performed at the lowest threshold for the selection of double excitation operators. Single-point SAC-CI calculations for the first four excited-states were performed for both (001) Ti-watCO2 and (110) Ti-4cCO2 clusters, using the above criteria. The amount of charge gained by the CO_2 moiety in an excited state, compared to the SAC-ground-state, was calculated as shown in Eq. **3.1**:

$$\% \text{ charge transferred to } CO_2 = (\Delta qCO_2)/ (\Sigma\Delta q(O^{cluster})) \times 100, \quad \textbf{3.1}$$

where ΔqCO_2 refers to the change in charge of CO_2 compared to the SAC-ground-state and $\Sigma\Delta q(O^{cluster})$ refers to the change in the charge of all the oxygen atoms of the cluster.

Excited-state calculations with two Ti atoms (Ti2-CO2) used thirty frozen core orbitals. It was not possible to calculate relaxed density excited-state natural population analyses for the Ti2-CO2 clusters. Instead, unrelaxed excited-state Mulliken population analyses[30] for the first four excited-states are reported. Other parameters were the same as those for the Ti-watCO2 and Ti-4cCO2 clusters described above. We also compared the SAC-CI excitation energies and oscillator strengths to those obtained from time-dependent density functional theory (TD-DFT)[31] calculations at the B3LYP/6-31+G(d) level to examine the possibility of using these computationally more efficient methods to model TiO_2-catalyzed CO_2 photoreduction.

3.4.2 Details of cluster preparation and parameters used for DFT calculations in Turbomole

To complement these SAC-CI calculations on small TiO_2-CO_2 clusters, we also performed DFT level calculations on larger TiO_2-CO_2 clusters (Ti6-5cCO2) using Turbomole. Similar to the smaller clusters, larger (Ti6-) clusters from bulk-terminated (101), (010) (001) and (110) surfaces were cut with Cerius[2] and the coordination of dangling bonds was saturated by adding protons at O-H distances of 0.97 Å. All Ti atoms in the clusters thus prepared have the same coordination as that of the defect-free surface. All added H atoms were fixed during geometry optimizations in Turbomole. In addition

to CO_2, only surface atoms and their next nearest neighbors were allowed to relax. This meant that different numbers of atoms were constrained for different surfaces.

The geometry of the ground-state neutral singlet bare cluster (without CO_2) was optimized with B3LYP/def2-SV(P) model chemistry using default optimization criteria. (The def2-SV(P) basis set[32] is approximately equivalent to the Pople 6-31G(d) basis set. The implementation of the B3-LYP functional (incorporating the VWN(V) correlation) in Turbomole differs from that in G03 (VWN(III) correlation).) Henceforth, in this paper, TM-B3LYP denotes the Turbomole implementation, while G03-B3LYP will be used to refer to the G03 implementation. All Turbomole calculations used the Multipole-Accelerated-Resolution-of-Identity-*J* (MARI-*J*) approximation[33] with the def2-SV(P) auxiliary basis set on Ti, O and C atoms. The error in single point self-consistent-field (SCF) energy with the MARI-*J* approximation for a TiO_2 cluster containing 47 atoms was calculated at the TM-B3LYP/def2-SV(P) level of theory to be 1.2 mH.

Upon optimizing the ground-state, similar constraints were used to model the triplet state of the cluster. Subsequently, a CO_2 molecule (with r(C-O) = 1.167 Å and <OCO = 180°) was located at a distance of ~2.2-1.9 Å from the Ti atom where the photogenerated electron was localized. A similar procedure has been reported in the literature for a study of O_2 and H_2O interactions on irradiated TiO_2[21]. Geometry optimization of the triplet Ti6-CO2 clusters was performed using constraints and model chemistry similar to that as the “bare” cluster. Atomic charges were calculated using natural population analysis (NPA)[29] for singlet and triplet states of the bare and CO_2-containing clusters.

The adsorption of CO_2 on non-stoichiometric anatase surfaces containing oxygen vacancies was also performed, to compare the results with those from defect-free clusters. An earlier modeling study of O_2 photoreduction on surface oxygen vacancies has shown that O_2^- species could be formed on and desorbed from illuminated defective (100) anatase TiO_2 surfaces[34]. Therefore, CO_2 adsorption on a bridging oxygen vacancy on the (010) surface (isostructural with the anatase (100) surface) was investigated. After removing one of the bridging 2-coordinate (2-c) oxygen atoms on the (010) surface, the ground state geometry (triplet) was optimized, with constraints similar to the defect-free Ti6-cluster. Two different configurations of CO_2 adsorbed on the vacancy were modeled, resulting in linear and bent CO_2 species. The geometry of the ground-state neutral singlet cluster was optimized at the TM-B3LYP/def2-SV(P) level of theory. The optimized Ti6-cluster with CO_2 adsorbed on the oxygen vacancy ($Ti_6O_{20}H_{18}$-CO_2) is denoted as (010) Ti6(Vo)-5cCO2-linear and (010) Ti6(Vo)-5cCO2-bent. Counterpoise uncorrected interaction energies between the Ti6-stoichiometric cluster and CO_2 in both singlet and triplet states are calculated as shown in Eq. **3.2**:

$$\Delta E^{inter} = E(\text{Ti6-5cCO2}) - E(\text{Ti6-5c}) - E(CO_2) \qquad \textbf{3.2}$$

Interaction energies for non-stoichiometric clusters and CO_2 are calculated as shown in Eq. **3.3**:

$$\Delta E^{inter} = E(\text{Ti6(Vo)-5cCO2}) - E(\text{Ti6(Vo)-5c}) - E(CO_2) \qquad \textbf{3.3}$$

In the above equations, E refers to the electronic energy of the cluster. Reasonable values for the basis set superposition error (BSSE) in the energies for the triplet state clusters could not be obtained. The BSSE values for the singlet state clusters were

typically 8-13 mH. For the sake of uniformity, we present energies without the counterpoise correction.

The gOpenMol program[35, 36] (v3.0) was used to display molecular orbitals and spin densities. The ChemCraft program (Plimus Corporation, San Diego, CA) was used to display cluster geometries.

3.5 Results

The optimized geometries of the (110) Ti-4cCO2 and (001) Ti-watCO2 clusters are shown in Figure 3-2. CO_2 adsorbs linearly at the Ti Lewis acid sites. The O-C-O bond angle of CO_2 is not significantly distorted from its gas-phase value of 180°, which indicates that the electronic interaction between the unoccupied orbitals of CO_2 and the occupied orbitals of the "bare" cluster in the ground state is weak.

Table 3-1 shows the excitation energies and symmetries of the first four excited states of these two clusters, calculated from single-point calculations at the SAC-CI/6-31+G(d) level of theory. These vertical excitation energies lie in the (UV-B)–(UV-C) region of the electromagnetic spectrum. Additionally, the excitation energies for the (4-c) Ti-4cCO2 cluster are significantly higher than the (5-c) Ti-watCO2 cluster. This is consistent with the trends in the ligand-to-metal charge transfer (LMCT) transition energies for tetrahedral (4-c) and octahedral (6-c) Ti atoms[37].

In the next step, excited states of a cluster ((010) Ti2-CO2) with significant electronic interaction between the bare cluster and CO_2 (in the ground-state) were

studied. This represented carbonate-like species adsorbed on the (010) surface plane of anatase.

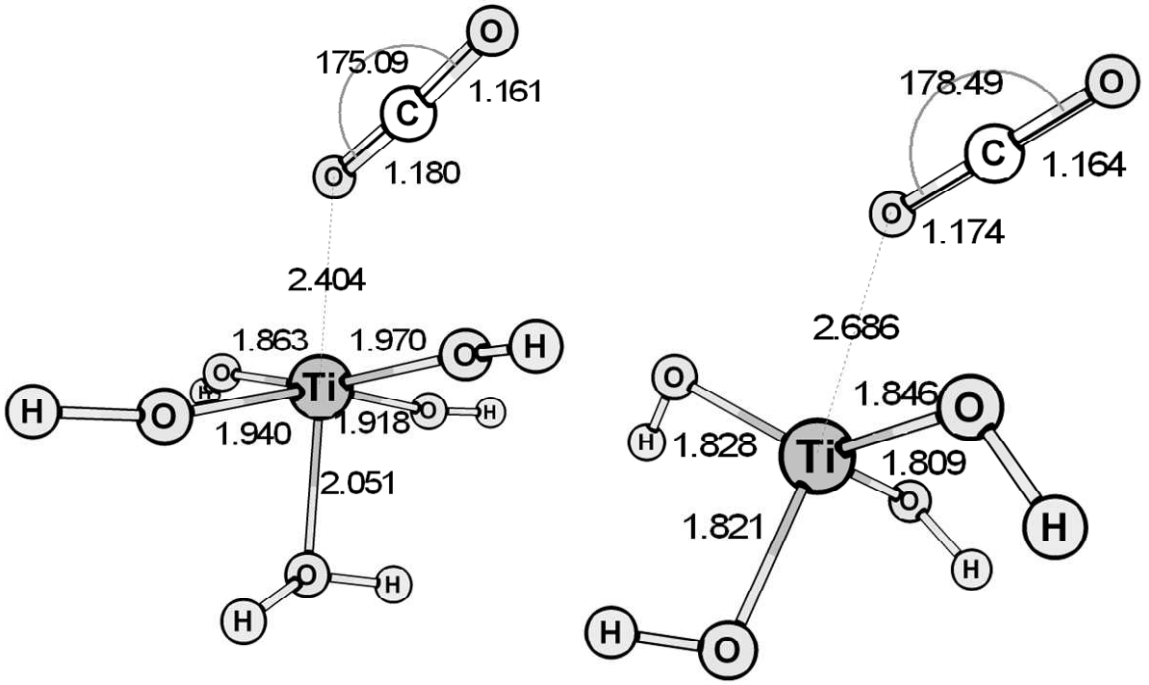

Figure **3-2**: Left, (001) Ti-watCO2 ($Ti(OH)_4H_2O$-CO_2) cluster, right, Ti-4cCO2 ($Ti(OH)_4H_2O$-CO_2) cluster, optimized at the G03-B3LYP/6-31+G(d) level of theory. The bond lengths are in Å, the angles are in degrees.

Table **3-1**: Excitation energies (for the first 4 excited-states) of CO_2 linearly adsorbed on clusters from (110) and (001) anatase TiO_2 surfaces (Ti-4cCO2, Ti-watCO2), calculated at the SAC-CI/6-31+G(d) level of theory. Excitation energies for the (4-c) Ti-4cCO2 cluster are significantly higher than the (5-c) Ti-watCO2 cluster.

	(110) Ti-4cCO2	(001) Ti-watCO2
	Excitation energy, eV	Excitation energy, eV
1	4.27	2.19
2	4.88	2.51
3	5.11	2.96
4	5.30	3.16

Comparisons of the SAC-CI/6-31+G(d) adiabatic excitation energies for the (010) Ti2-CO2 cluster (shown in Figure **3-3**) with those obtained from TD-DFT calculations at the G03-B3LYP/6-31+G(d) level are shown in Table **3-2**. Clearly, TD DFT excitation energies are within 0.5 eV of those obtained with SAC-CI. Therefore, although significant errors exist in TD-DFT values, TD-DFT could be used to estimate the trends in vertical excitation energies for larger clusters. However, the oscillator strengths predicted by the less expensive TD-DFT calculations do not agree with those from SAC-CI calculations. Moreover, the excited state symmetries predicted by TD-DFT do not agree with those predicted by SAC-CI. Therefore, even qualitative comparisons of TD-DFT absorption spectra with experimental spectra will be complicated by the fact that the oscillator strengths are inaccurate. This indicates the need for post-HF methods rather than TD-DFT to study excited states of chemisorbed carbonate-like species.

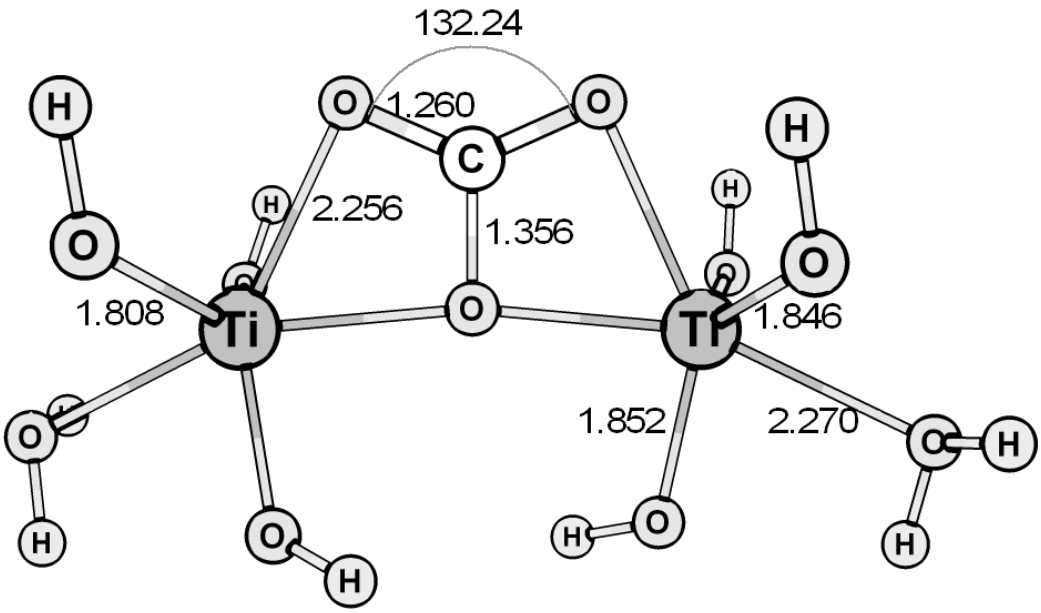

Figure **3-3**: Ground-state (1A) (010) C_2 symmetric $Ti_2O_9H_{10}CO_2$ cluster optimized with G03-B3LYP/6-31+G(d) model chemistry, bond distances in Å, angles in degrees. CO_2 forms a carbonate-like species on the (010) anatase surface.

Table 3-2: Excited-state symmetries, excitation energies and oscillator strengths for the first four excited singlet states of the (010) $Ti_2O_9H_{10}CO_2$ cluster (carbonate-like species) calculated by SAC-CI and TD-DFT using 6-31+G(d) basis set.

Excited-state symmetry		Excitation Energy, eV		Oscillator strength, $f*10^3$	
SAC-CI	TD-DFT	SAC-CI	TD-DFT	SAC-CI	TD-DFT
B	B	4.256	4.723	7.2	6.8
A	A	4.263	4.754	3.4	0.4
B	A	4.413	4.865	61.8	0.2
A	B	4.493	4.894	1.5	12.7

The excitation energies predicted by TD-DFT calculations are within 0.5 eV of those from SAC-CI calculations. However, TD-DFT calculations neither predict correct oscillator strengths nor correct excited-state symmetries, making TD-DFT qualitatively incorrect.

The percentage of charge transferred from the oxygen atoms of the cluster to the CO_2 moiety in the Ti-watCO2 and Ti-4cCO2 clusters is shown in Figure 3-4. Figure 3-5 shows the change in the charge (from unrelaxed Mulliken population analyses of the excited-states) of various moieties (CO_2, $CO_2+O^{bridging}$, (referred to as CO3), and $Ti_2O_9H_{10}$) of the Ti2-CO2 cluster. In Figure 3-5, the results are shown as the difference of the charge of the moiety between the SAC-ground-state and the excited-state. In addition to these criteria, charge transfer to CO_2 can be indicated by examining the excited states and the type of (canonical) molecular orbitals comprising various configurations of the wavefunction. From the analysis of the ground state molecular orbitals of the linear CO_2 species Ti-watCO2 and Ti-4cCO2 that are involved in various excited state configurations (presented in Appendix B), it is clear that the majority of the contribution to the unoccupied orbitals comes from the Ti 3d atomic orbitals and not π^* C-O orbitals of

CO_2. Therefore, most of the charge transferred from the oxygen atoms is localized on the Ti atoms. These SAC-CI results indicate that the amount of charge transfer from the bare cluster to CO_2 is insignificant compared to the charge gained by Ti atoms, for both linearly adsorbed CO_2 as well as carbonate-like chemisorbed species.

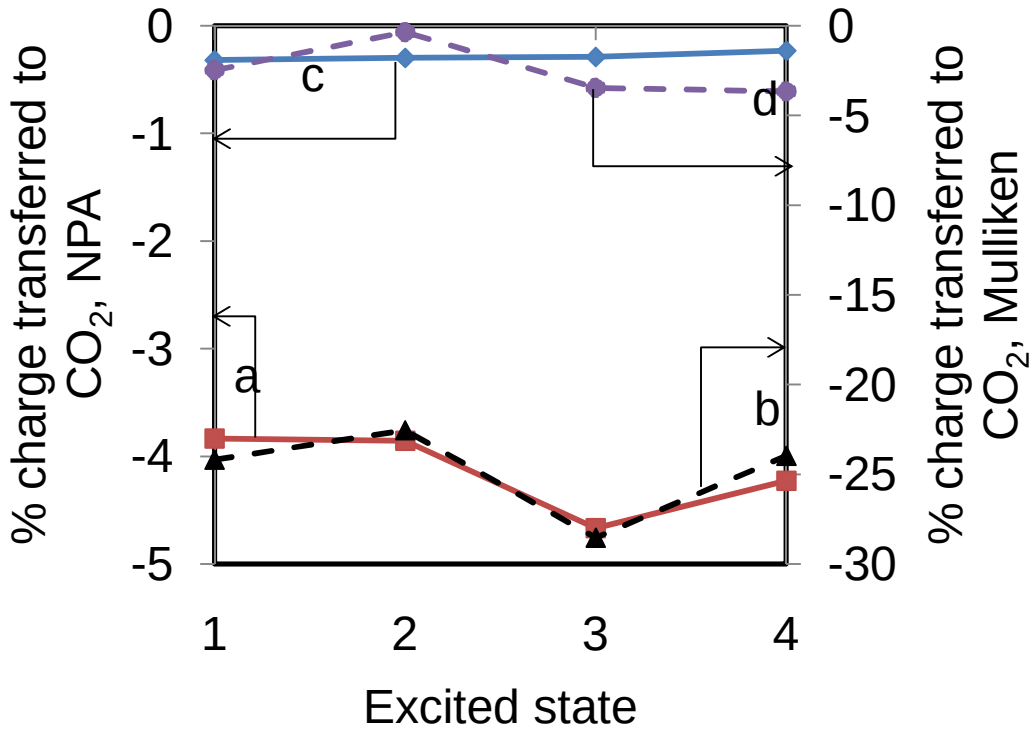

Figure 3-4: Percentage of charge transferred to CO_2, calculated from single point excited-state relaxed density population analyses. Negative values indicate a net gain in the charge of the CO_2 moiety. (a): (001) Ti-watCO2,NPA, (b): (001) Ti-watCO2,Mulliken (c): (110) Ti-4cCO2,NPA, (d): (110) Ti-4cCO2,Mulliken. The NPA analyses for both (001) Ti-watCO2 and (110) Ti-4cCO2 clusters indicate insignificant charge transfer to CO_2. The lines are shown for clarity and are not meant to indicate charge transfer trends among different excited-states.

The results in Figure 3-4 indicate a large discrepancy between Mulliken and natural population analyses for the Ti-watCO2 cluster. Mulliken population analyses are not independent of the basis set and the method used for the calculations. In contrast,

atomic charges obtained by NPA analysis are known to vary less with the choice of the basis set. NPA analysis is therefore a better indicator of the real charge of the species in various excited states.

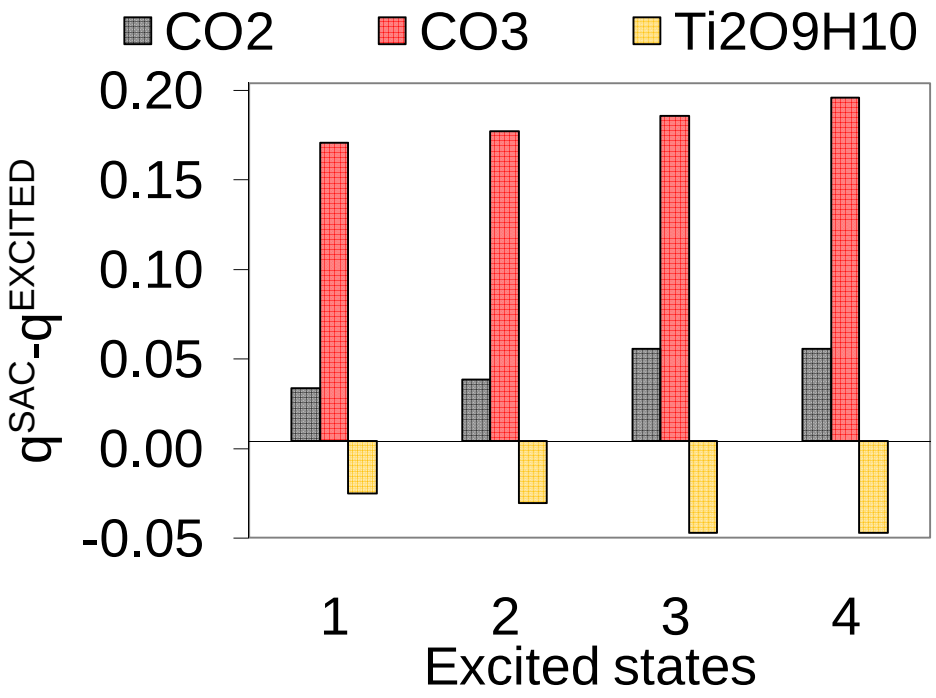

Figure **3-5**: Changes in summed atomic charges of the CO_2 (CO2), surface species (CO3) and the bare cluster (Ti2O9H10) over the SAC ground-state, calculated with unrelaxed excited-state SAC-CI densities (from single point calculations) using the 6-31+G(d) basis set. The amount of charge transferred from/to the CO_2 moiety in various excited states is minimal.

In the next part of this study, we modeled the adsorption of CO_2 on triplet (Ti6-) clusters from various surface planes. Various starting configurations were used for the interaction of CO_2 with the electron-center (Ti^{3+}), and the lowest energy configurations are shown in Figure **3-6**. Additional details, including the local geometry around the Ti atom interacting with the CO_2 species are shown in. Figure **3-7**. The overall nature of CO_2 adsorption on triplet Ti6- clusters modeled using Turbomole is similar to that

observed with the smaller ground-state clusters modeled in G03. The interaction is mainly weak acid-base in character. On the (010) and (101) triplet Ti6-5c clusters, CO_2 adsorbs with the oxygen end-on Ti atom.

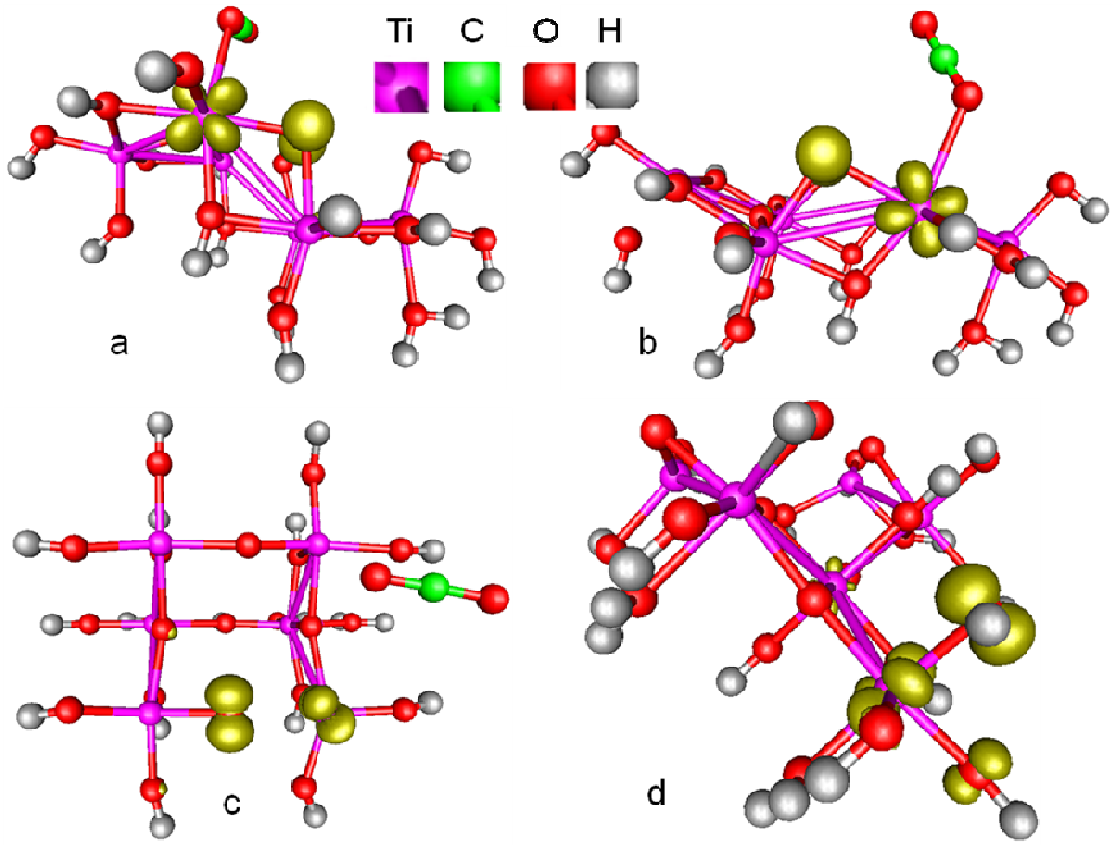

Figure **3-6**: Location of the photogenerated electron and hole in various triplet Ti6-clusters. (a): (010) Ti6-5cCO2 cluster, (b): (101) Ti6-5cCO2 cluster, (c) (001) Ti6-5cCO2 cluster, (d) Ti6-4c cluster without CO_2. The difference in spin densities (alpha-beta) is plotted at an isocontour value of 0.03 e/Å^3. In (a), (b) and (c), the photogenerated electrons are localized on the 3d orbitals of the Ti atoms and are not transferred to CO_2. In (d), the photogenerated electrons on the (110) surface are not available to surface Ti atoms and are localized on (6-coordinate) Ti atoms in the bulk. Therefore CO_2 adsorption and further electron transfer on this surface was not investigated. (Plotted with the gOpenMol visualization program[35, 36])

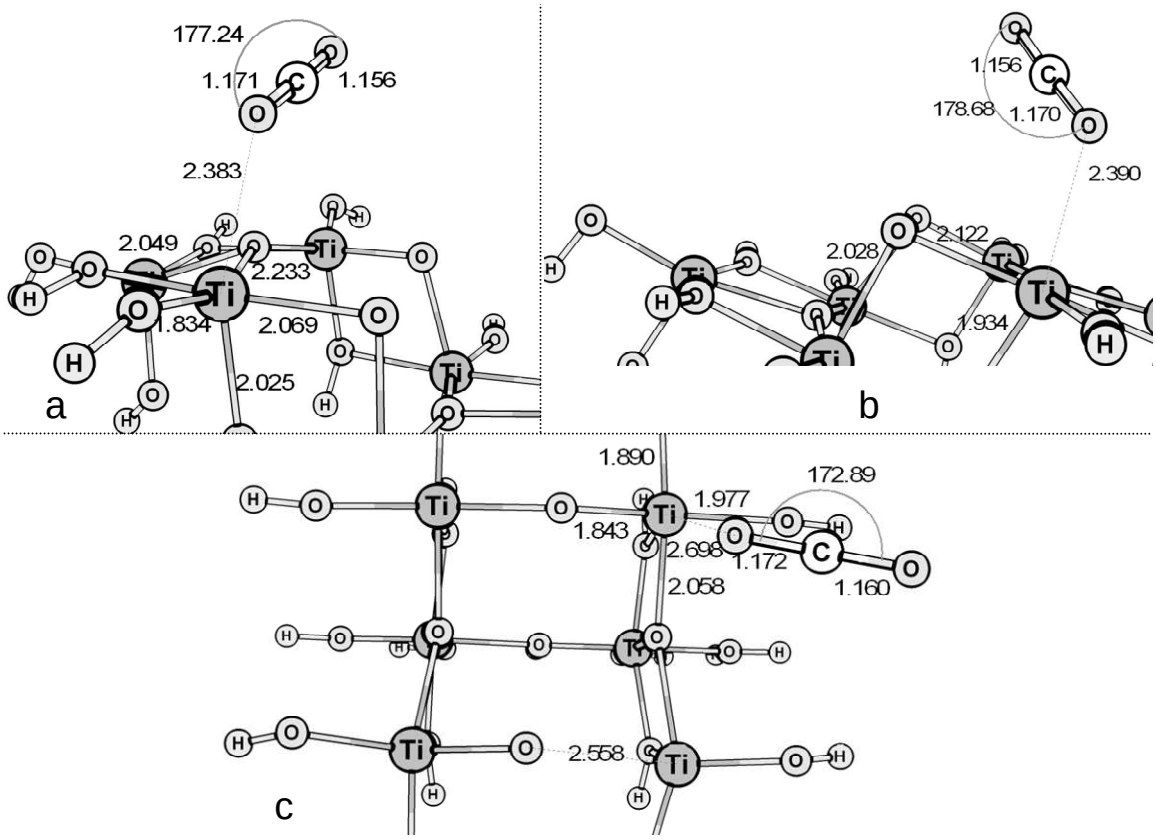

Figure **3-7**: Local geometry around the Ti atom interacting with CO_2 in various triplet Ti6-CO_2 clusters, from TM-B3LYP/def2-SV(P) calculations; (a): (010) Ti6-5cCO2, (b): (101)Ti6-5cCO2 cluster, (c) (001) Ti6-5cCO2 cluster. Only linear CO_2 species are shown in the figure. CO_2 is not significantly distorted from its linear geometry in all three cases. The bond lengths are in Å, the angles are in degrees. Only Ti, O (and CO_2) atoms on and adjacent to the (010), (101), (001) and (110) surfaces were relaxed from their positions in the bulk TiO_2 anatase crystal.

In the case of the triplet (001) Ti6-5c cluster, one of the (Ti-2c O) bonds is broken (shown in Figure **3-7**), and CO_2 is more loosely bound. We also observed the formation of carbonate species on the (001) TiO_2 surface. However, electron transfer was not predicted for these carbonate species to or from the TiO_2 surface in the triplet state. The difference between the alpha and beta spin densities of the triplet (010), (101) and (001)

Ti6-5cCO2 clusters, shown in Figure **3-6**, indicates that the photogenerated electron is not transferred to CO_2.

In the limit of the cluster sizes used in this study, we find that photogenerated electrons are available for surface reactions on (010), (001) and (101) surfaces (Figure **3-7** a-c). The photogenerated electrons are localized on the *terrace* 5-c Ti atoms of the (101) surface. On the (110) surface exposing 4-c Ti atoms, the photogenerated electron and hole were localized in the bulk. Therefore, CO_2 adsorption on this surface in the triplet state was not modeled.

Both SAC-CI and DFT calculations have shown that clusters from defect-free anatase TiO_2 surfaces do not transfer the photogenerated electron to CO_2. Because oxygen vacancies are among the most common defects on metal oxide surfaces, CO_2 adsorption on oxygen-deficient clusters was modeled. The ground-state of the (010) oxygen-deficient bare anatase cluster (Ti6(Vo)-5c) is a triplet. However, upon CO_2 adsorption, the ground-state of the (010) Ti6(Vo)-5cCO2 cluster was found to be a singlet. As shown in Figure **3-8**, CO_2 adsorbs on the oxygen vacancy, forming a negatively charged $CO_2^{\delta\bullet-}$ species, which resembles a η^2_{CO}-(metal-CO_2) complex[38]. Additionally, linear CO_2 adsorbed on the Ti^{3+} electron centers (formed as a result of the oxygen vacancy formation) (Figure **3-9**) were also modeled. Triplet states of the oxygen-deficient CO_2-TiO_2 clusters were also studied.

The charges on the CO_2 moieties from DFT level calculations on oxygen-deficient and defect-free clusters are shown in Figure **3-10** Counterpoise uncorrected electronic interaction energies of CO_2 adsorption on the (010), (101) and (001) Ti6-5c defect-free and oxygen-deficient clusters are shown in Table **3-3**. Table **3-4** shows the

energies of electrons in the highest occupied orbitals of the (010) Ti6-5c triplet defect-free and oxygen-deficient clusters compared to the energy of the LUMO of CO_2.

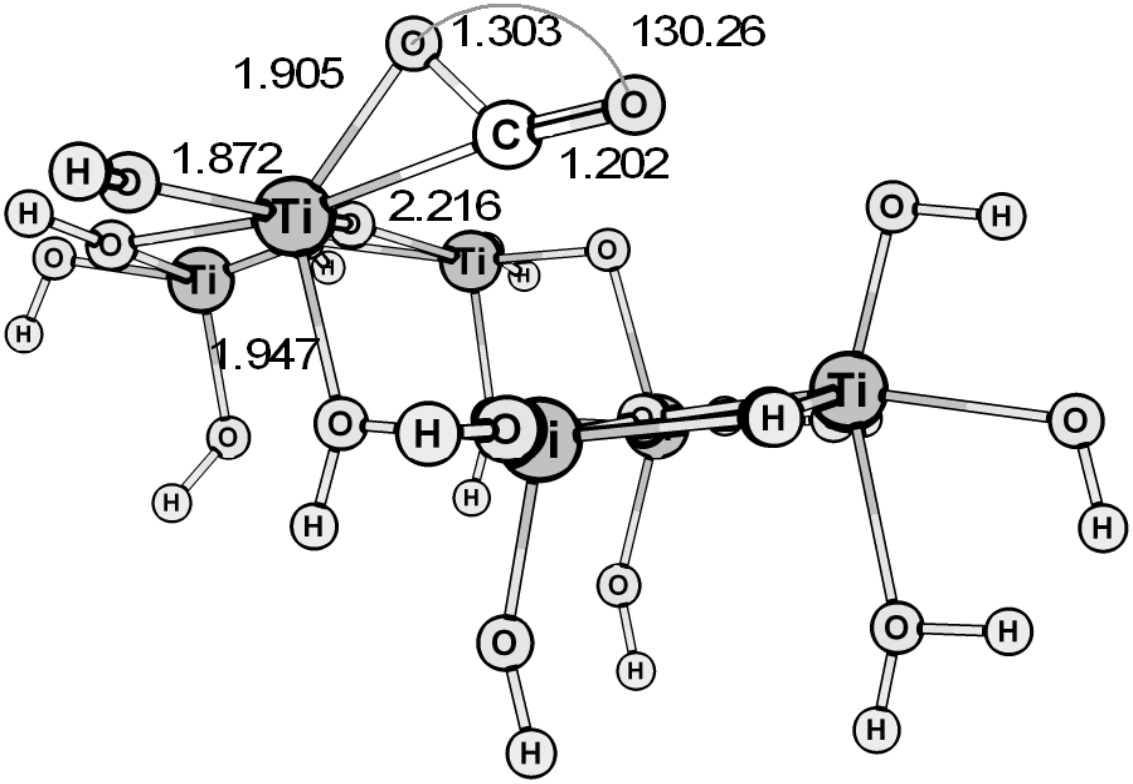

Figure **3-8**: TM-B3LYP/def2-SV(P) optimized geometry of the singlet (010) Ti6(Vo)-5cCO2-bent ($Ti_6O_{20}H_{18}$-CO_2) cluster. CO_2 adsorbs on the reduced (010) surface with bridging oxygen vacancies forming a negatively charged $CO_2^{\delta\bullet-}$ species, which resemble η^2-(transition metal-CO_2) complexes. The bond lengths are in Å, the angles are in degrees. Only Ti, O (and CO_2) atoms on and adjacent to the (010), (101), (001) and (110) surfaces were relaxed from their positions in the bulk TiO_2 anatase crystal.

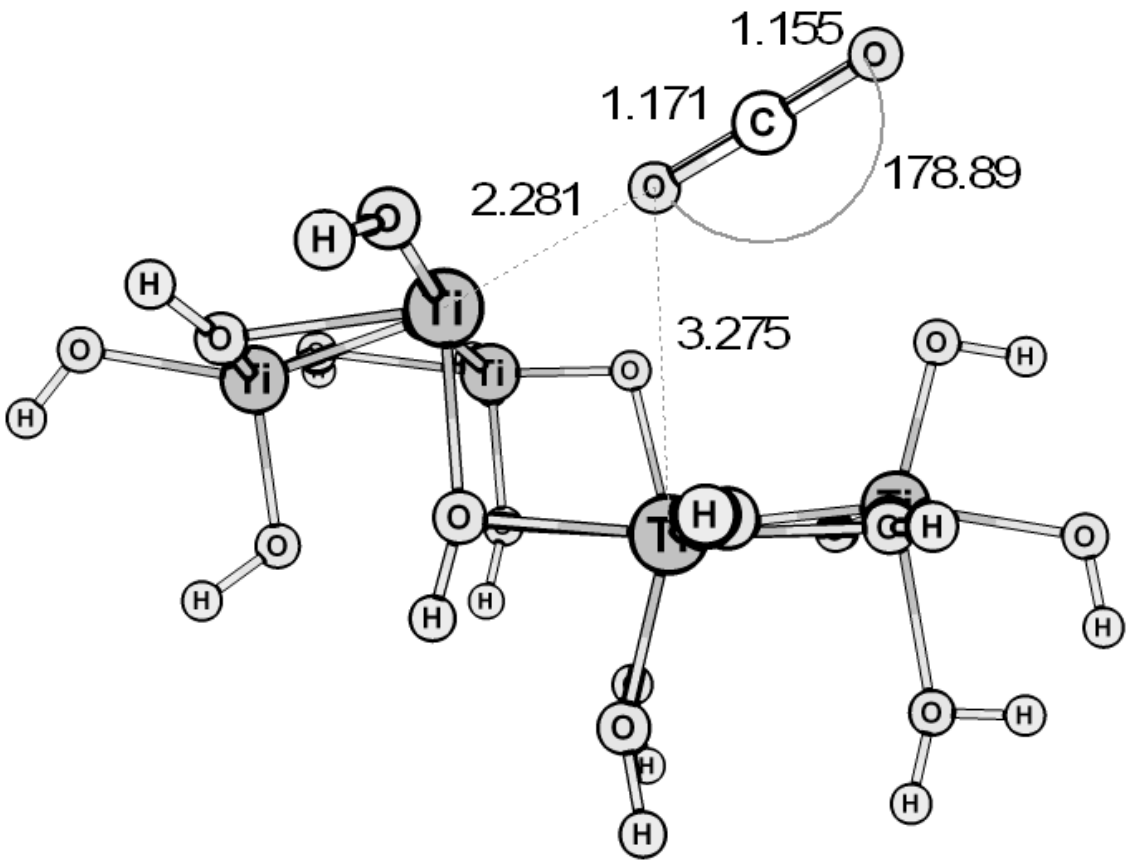

Figure **3-9**: TM-B3LYP/def2-SV(P) optimized geometry of the singlet (010) Ti6(Vo)-5cCO2-linear ($Ti_6O_{20}H_{18}$-CO_2) cluster. CO_2 adsorbs linearly the reduced (010) surface with bridging oxygen vacancies. The linear complex is not stable compared to the bent-adsorption mode, shown in the previous figure. The bond lengths are in Å, the angles are in degrees. Only Ti, O (and CO_2) atoms on and adjacent to the (010), (101), (001) and (110) surfaces were relaxed from their positions in the bulk TiO_2 anatase crystal.

Table **3-3**: Counterpoise uncorrected electronic interaction energies of CO_2 adsorption on various singlet and triplet (010), (101) and (001) defect-free clusters and those of singlet and triplet (010) oxygen-deficient cluster, calculated at the TM-B3LYP/def2-SV(P) level.

Cluster	Spin multiplicity	ΔE^{inter}, kJ/mol	Spin multiplicity	ΔE^{inter}, kJ/mol
(001) Ti6-5cCO2	3	-38		
(101) Ti6-5cCO2	3	-33		
(010) Ti6-5cCO2	3	-41	1	-43
(010) Ti6(Vo)-5cCO2–linear	3		1	-58
(010) Ti6(Vo)-5cCO2–bent	3	11	1	-123

Table **3-4**: Comparison of energies of LUMO of CO_2 with the highest SOMO of defect-free and oxygen-deficient Ti6- clusters and the highest SOMO of the surface complex ((010) Ti6(Vo)-5cCO2).

Molecular orbital	Energy, eV
$^1CO_{2(g)}$, LUMO	0.91
^{3}(010) Ti6(Vo)-5c highest SOMO	-3.73
^{3}(010) Ti6-5c highest SOMO	-4.29
^{3}(010) Ti6(Vo)-5cCO2-bent highest SOMO	-4.38

The electrons in the highest SOMO of the bare, oxygen-deficient cluster are higher in energy compared to those in the highest SOMO of the bare, defect-free cluster. Calculations were performed using the TM-B3LYP/def2-SV(P) model chemistry.

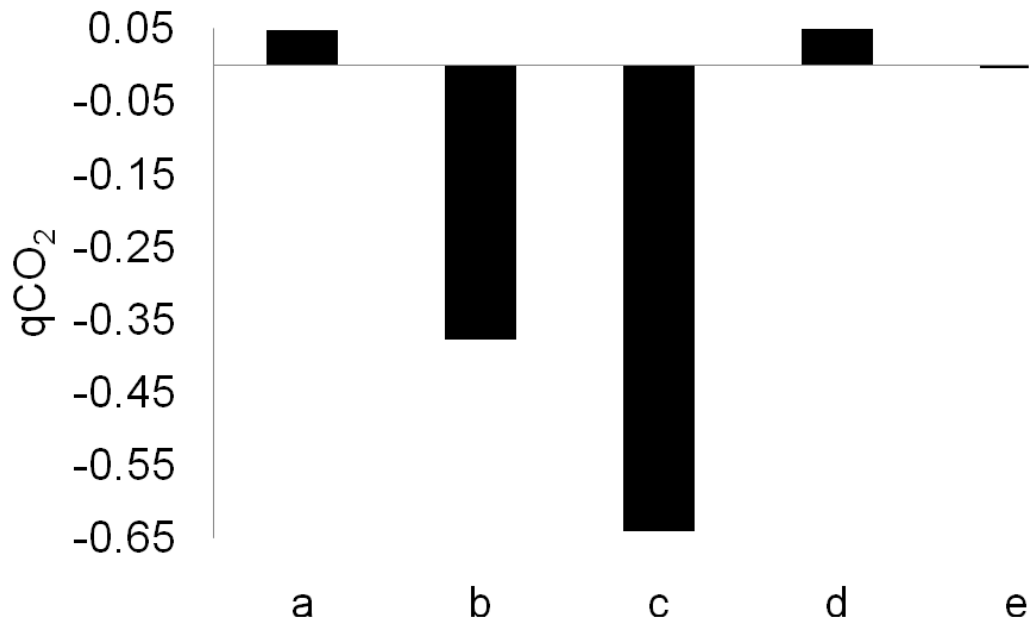

Figure **3-10**: Natural charges of CO_2 species calculated from TM-B3LYP/def2-SV(P) level calculations on Ti6-5cCO2 clusters from various surface planes. a: triplet (010) Ti6-5cCO2, b: triplet (010) Ti6(Vo)-5cCO2-bent, c: singlet (010) Ti6(Vo)-5cCO2-bent, d: triplet (101) Ti6-5cCO2, e: triplet (001) Ti6-5cCO2. CO_2 gains electrons only from oxygen-deficient TiO_2 clusters.

3.6 Discussion

Why was no electron transfer to CO_2 from defect-free TiO_2 in the excited state predicted by these calculations? One reason is the energy level of the LUMO and HOMO of CO_2 with respect to those of TiO_2. As shown in Figure **3-11**, the LUMO of the clusters is far below the LUMO of CO_2. Increasing the size of the cluster (as shown in the (001) $Ti_{15}O_{41}H_{22}$ cluster) decreases the band (HOMO-LUMO) gap, but does not increase the energy of the LUMO. However, chemical interaction between the surface and the gas-phase species (CO_2) can alter the energy level of the CO_2 LUMO. The interaction

energies between CO_2 and the triplet defect-free (Ti6-5c) clusters shown in Table **3-3** do not indicate significant interaction. Therefore, due to this weak acid-base interaction (in the defect-free cluster models), the LUMO of CO_2 does not contribute strongly to the LUMO of the (CO_2+TiO_2) surface complex.

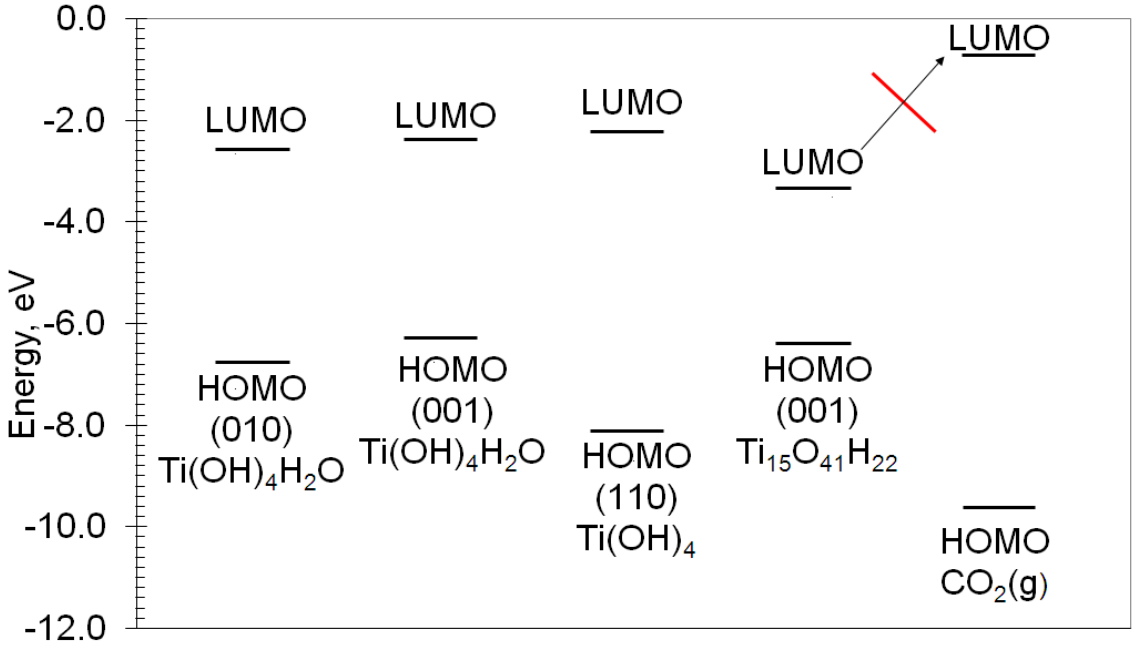

Figure **3-11**: Positions of the bottom of the conduction band (LUMO) and top of the valence band (HOMO) for singlet $Ti(OH)_4H_2O$ (010), $Ti(OH)_4H_2O$ (001) clusters compared with those of a CO_2 molecule in the gas phase at the G03-B3LYP/6-31+G(d) level. A single point G03-B3LYP/GenECP calculation (LANL2DZ on Ti atoms, 6-31+G(d) on O, H) with the larger $Ti_{15}O_{41}H_{22}$ cluster was performed to calculate the HOMO and LUMO energies.

Another reason why no charge transfer is observed from excited-state cluster to CO_2 is the negative electron affinity of a single CO_2 molecule[11, 12, 39]. $CO_{2(g)}^{\bullet-}$ is metastable with respect to electron detachment[40]. Factors such as solvation could change the electron affinity of CO_2. For example: recent high-level ab initio calculations have shown that $(CO_2)_4^{\bullet-}$ clusters, where the CO_2 essentially acts as a solvent stabilizing the

$(CO_2)_4^{\bullet-}$ species, could have a positive vertical electron affinity[39]. The implications of this cluster formation, in terms of selecting appropriate temperature and pressure conditions, as well as the choice of theoretical methods for modeling these reactions on the surface, are currently not well understood.

Mechanisms of CO_2 photocatalysis in the literature indicate that CO_2 gains electrons from the conduction band of TiO_2. However, as shown in Figure **3-10**, such transfer from defect-free surfaces is unlikely. Using larger clusters will further reduce the energy of the LUMO of the bare cluster. Therefore, any electrons in the conduction band produced by photoexcitation cannot be transferred to the LUMO of gas-phase CO_2.

The photocatalyst surface plays a role in activating CO_2 by lowering the LUMO of CO_2 from its gas-phase value, possibly via decreasing the O-C-O bond angle. In one limiting case, this corresponds to the formation of carbonate-like species on the surface. However, the results from SAC-CI single point calculations on the carbonate-like species on the (010) anatase surface indicate that even the carbonate species do not gain appreciable electron density from the TiO_2 cluster in various excited states. Therefore, excited-state calculations on both linear and the bent-carbonate species indicate that they do not undergo charge transfer from the cluster.

Why does CO_2 gain electrons from oxygen-deficient clusters? The Ti^{n+} ion has stable (formal) oxidation numbers of n= 2, 3 and 4. A missing oxygen atom would leave two extra electrons at the site of the vacancy. These electrons then reduce the adjacent two surface Ti^{4+} sites to Ti^{3+}, creating surface electron-centers. As shown in Table **3-4**, the energies of the highest singly occupied molecular orbital (SOMO) of the (010) Ti6-5c cluster is ~0.5 eV larger than that of the (010) Ti6(Vo)-5c cluster (with the bridging

oxygen vacancy). Therefore, electrons in the highest SOMO of the (010) Ti6(Vo)-5c cluster have more energy, compared to the defect-free cluster. Nevertheless, this energy difference is not the primary reason for the formation of the negatively charged species.

Electron transfer also requires that orbitals of similar symmetries overlap. Therefore, CO_2 should be located close to the Ti^{3+} atoms to form a surface complex where the CO_2 moiety gains electrons. Only initial configurations where CO_2 was located in the Ti-O-Ti plane, bridging the two Ti atoms, resulted in the formation of bent-CO_2 species. The presence of O atoms on a defect-free surface does not permit these interactions, due to the repulsion between the large oxide ions on the surface and the lone electron pairs on the oxygen atoms of CO_2. This is further shown in a comparison of the highest occupied molecular orbitals of the oxygen-deficient and defect-free clusters, shown in Figure **3-12**. Overlap between the (C-O) π^* antibonding orbitals and the Ti(3d) orbitals is possible only when oxygen vacancies are present.

The bonding between CO_2 and the oxygen-deficient cluster leading to the bent-adsorbed state resembles a η^2_{CO}(metal-CO_2) homogeneous complex[38]. Therefore, overlap between the 3d-orbitals of the reduced Ti atom and the π^* antibonding orbitals of CO_2 may lead to such species[41]. The interaction energies (Table **3-3**) of bent-CO_2 species adsorbed on clusters containing oxygen vacancies are higher than those for the linearly adsorbed CO_2 on singlet defect-free clusters. This indicates that the singlet bent-CO_2 species are strongly bound to the surface. However, compared to the singlet bent-CO_2 species, the triplet bent-CO_2 species are weakly bound to the surface. Additionally, CO_2 adsorbed linearly on regular 5-c Ti^{4+} sites ((010) Ti6-5cCO2) interacts less strongly with the surface compared to the linear CO_2 species adsorbed on reduced 4-c Ti^{3+} sites ((010)

Ti6(Vo)-5cCO2). This is consistent with the evidence for two-peak desorption of CO_2 obtained from thermal desorption spectroscopic (TDS) studies of CO_2 on reduced rutile (110) surfaces[42]. Moreover, the interaction energies in Table **3-3** indicate that the bent-CO_2 species (010 Ti6(Vo)-5cCO2-bent) is more stable than the CO_2 species linearly adsorbed at the oxygen vacancies (010 Ti6(Vo)-5cCO2-linear). Bent-CO_2 species have been observed on reduced polycrystalline powdered TiO_2 at low temperatures[10].

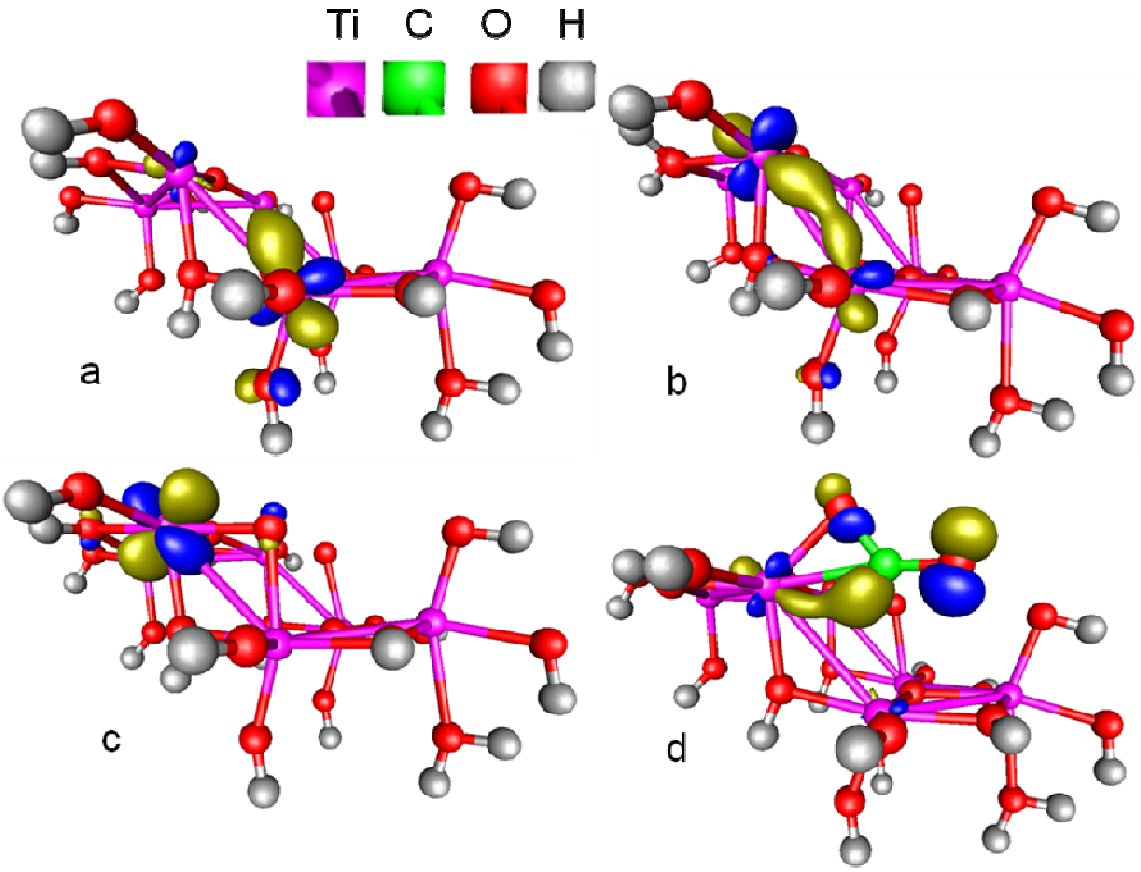

Figure **3-12**: The highest occupied molecular orbitals of various (010) Ti6- clusters with and without CO_2. (Plotted with the gOpenMol visualization program[35, 36]) (a): triplet oxygen-deficient (Ti6(Vo)-5c) bare cluster,(b): singlet oxygen-deficient (Ti6(Vo)-5c) bare cluster, (c): triplet defect-free (Ti6-5c) bare cluster, (d): singlet bent-CO_2 species adsorbed on the oxygen-deficient cluster (Ti6(Vo)-5cCO2-bent) plotted at an isocontour value of 0.1 $e^{1/2}/Å^{3/2}$. The HOMO of cluster (d) consists of both the Ti(3d) orbital (similar to those in (a) and (b)) and the π^* (C-O) orbitals of CO_2.

Whether or not the original Ti^{3+} centers could be regenerated by interaction with light, or whether $CO_2^{\delta\bullet-}$ formation is a stoichiometric reaction is an open question. Using infrared spectroscopic studies on reduced polycrystalline rutile powders, Raskó and Solymosi[10] found that CO_2 adsorbed on the oxygen vacancies forming a bent-CO_2 species. The intensity of the bands corresponding to C-bent CO_2 species increased upon irradiation, indicating further charge transfer from reduced TiO_2 to CO_2 upon irradiation, but no CO formation via CO_2 dissociation was observed. On the other hand, experiments at higher temperatures by Raupp and Dumesic[43] as well as recent surface studies by Wilson et al.[44] showed that CO_2 underwent dissociation and further reactions on reduced TiO_2 surfaces, leading to stoichiometric consumption of the oxygen vacancy. Further work is therefore required to compare the geometries, IR frequencies and other characteristics of these species to the ones observed during previous experimental studies.

Experimental studies of well defined anatase surfaces have begun only in the past ten years, whereas rutile TiO_2 surfaces are relatively better understood. Because real crystalline surfaces always have defects, studies of anatase surface reconstructions and steps[45-50] will help identify other surface features that could promote CO_2 photoreduction. Anatase surfaces have a lower concentration of oxygen vacancies compared to rutile[51]. However, doping, either with cations or anions, could result in the formation of oxygen vacancies/other defects. In contrast to O_2 photoreduction, which has been modeled on defect-free anatase surfaces[21], CO_2 photoreduction likely requires surface/bulk defects.

3.7 Conclusions

Using a combination of both post-HF calculations on small model (TiO_2:CO_2) clusters, as well as DFT calculations on larger CO_2-TiO_2 clusters, we have shown that charge transfer from defect-free TiO_2 surfaces to CO_2 is energetically unfavorable. DFT calculations on triplet defect-free clusters indicate that the interaction between CO_2 and the excited stoichiometric TiO_2 surface do not lead to charge transfer to CO_2. CO_2 photoreduction mechanisms in the literature assume that CO_2 gains electrons from the conduction band of TiO_2. However, our results show that such electron transfer may only be mediated by surface defects. This work therefore underscores the significance of defects such as steps, kinks and vacancies on anatase TiO_2 surfaces in promoting electron transfer to CO_2 in the excited state. The role of defects in catalytically promoting CO_2 photoreactions needs to be investigated. These computations will serve as guidelines for in situ irradiated single crystal studies of CO_2 on anatase, by which structures of adsorbates at well-defined surfaces can be obtained.

3.8 References

1. Aresta, M.; Dibenedetto, A., Utilisation of CO2 as a chemical feedstock: opportunities and challenges. *Dalton Transactions* **2007**, (28), 2975-2992.
2. Inoue, T.; Fujishima, A.; Konishi, S.; Honda, K., Photoelectrocatalytic reduction of carbon dioxide in aqueous suspensions of semiconductor powders. *Nature (London, United Kingdom)* **1979,** 277, (5698), 637-8.
3. Fujita, E., Photochemical carbon dioxide reduction with metal complexes. *Coordination Chemistry Reviews* **1999,** 186, 373-384.
4. Lin, W.; Frei, H., Photoactivation of Ti centers in mesoporous silicate sieve under visible and UV light. *Studies in Surface Science and Catalysis* **2004,** 153, (Carbon Dioxide Utilization for Global Sustainability), 283-288.

5. Wovchko, E. A.; Yates, J. T., Jr., Photochemical Activation of CO2 on RhI(CO)2/Al2O3-CO2 Dissociation and Oxygen Atom Exchange. *Journal of the American Chemical Society* **1998,** 120, (30), 7544-7550.
6. Anpo, M.; Yamashita, H.; Ikeue, K.; Fujii, Y.; Zhang, S. G.; Ichihashi, Y.; Park, D. R.; Suzuki, Y.; Koyano, K.; Tatsumi, T., Photocatalytic reduction of CO2 with H2O on Ti-MCM-41 and Ti-MCM-48 mesoporous zeolite catalysts. *Catalysis Today* **1998,** 44, (1-4), 327-332.
7. Zhang, S. G.; Fujii, Y.; Yamashita, K.; Koyano, K.; Tatsumi, T.; Anpo, M., Photocatalytic reduction of CO2 with H2O on Ti-MCM-41 and Ti-MCM-48 mesoporous zeolites at 328 K. *Chemistry Letters* **1997**, (7), 659-660.
8. Anpo, M.; Yamashita, H.; Ichihashi, Y.; Fujii, Y.; Honda, M., Photocatalytic reduction of CO2 with H2O on titanium oxides anchored within micropores of zeolites: Effects of the structure of the active sites and the addition of Pt. *Journal Of Physical Chemistry B* **1997,** 101, (14), 2632-2636.
9. Usubharatana, P.; McMartin, D.; Veawab, A.; Tontiwachwuthikul, P., Photocatalytic Process for CO2 Emission Reduction from Industrial Flue Gas Streams. *Industrial & Engineering Chemistry Research* **2006,** 45, (8), 2558-2568.
10. Rasko, J.; Solymosi, F., Infrared spectroscopic study of the photoinduced activation of CO2 on TiO2 and Rh/TiO2 catalysts. *Journal of Physical Chemistry* **1994,** 98, (29), 7147-7152.
11. Schroder, D.; Schalley, C. A.; Harvey, J. N.; Schwarz, H., On the formation of the carbon dioxide anion radical CO2-.bul. in the gas phase. *International Journal of Mass Spectrometry* **1999,** 185/186/187, 25-35.
12. Sommerfeld, T., A fresh look at the (2)A(1) CO2- potential energy surface. *Journal of Physics B-Atomic Molecular And Optical Physics* **2003,** 36, (7), L127-L133.
13. Sommerfeld, T.; Meyer, H. D.; Cederbaum, L. S., Potential energy surface of the CO2- anion. *Physical Chemistry Chemical Physics* **2004,** 6, (1), 42-45.
14. Xu, Y.; Schoonen, M. A. A., The absolute energy positions of conduction and valence bands of selected semiconducting minerals. *American Mineralogist* **2000,** 85, (3-4), 543-556.
15. Frisch, M. J. T., G. W.; Schlegel, H. B.; Scuseria, G. E.; Robb, M. A.; Cheeseman, J. R.; Montgomery, Jr., J. A.; Vreven, T.; Kudin, K. N.; Burant, J. C.; Millam, J. M.; Iyengar, S. S.; Tomasi, J.; Barone, V.; Mennucci, B.; Cossi, M.; Scalmani, G.; Rega, N.; Petersson, G. A.; Nakatsuji, H.; Hada, M.; Ehara, M.; Toyota, K.; Fukuda, R.; Hasegawa, J.; Ishida, M.; Nakajima, T.; Honda, Y.; Kitao, O.; Nakai, H.; Klene, M.; Li, X.; Knox, J. E.; Hratchian, H. P.; Cross, J. B.; Bakken, V.; Adamo, C.; Jaramillo, J.; Gomperts, R.; Stratmann, R. E.; Yazyev, O.; Austin, A. J.; Cammi, R.; Pomelli, C.; Ochterski, J. W.; Ayala, P. Y.; Morokuma, K.; Voth, G. A.; Salvador, P.; Dannenberg, J. J.; Zakrzewski, V. G.; Dapprich, S.; Daniels, A. D.; Strain, M. C.; Farkas, O.; Malick, D. K.; Rabuck, A. D.; Raghavachari, K.; Foresman, J. B.; Ortiz, J. V.; Cui, Q.; Baboul, A. G.; Clifford, S.; Cioslowski, J.; Stefanov, B. B.; Liu, G.; Liashenko, A.; Piskorz, P.; Komaromi, I.; Martin, R. L.; Fox, D. J.; Keith, T.; Al-Laham, M. A.; Peng, C. Y.; Nanayakkara, A.; Challacombe, M.; Gill, P. M. W.; Johnson, B.; Chen, W.; Wong, M. W.; Gonzalez, C.; and Pople, J. A. *Gaussian 03, Revision D.01*, Gaussian Inc.: Wallingford, CT, 2004.

16. Ahlrichs, R.; Bär, M.; Häser, M.; Horn, H.; Kölmel, C., Electronic structure calculations on workstation computers: The program system Turbomole. *Chemical Physics Letters* **1989,** 162, (3), 165.
17. Zhanpeisov, N. U.; Fukumura, H., Oxygen vacancy formation on rutile TiO2(110) and its interaction with molecular oxygen. A theoretical density functional theory study. *Journal of Physical Chemistry C* **2007,** 111, (45), 16941-16945.
18. de Lara-Castells, M. P.; Mitrushenkov, A. O.; Roncero, O.; Krause, J. L., Adsorption and nonadiabatic processes in the photodesorption of molecular oxygen from the reduced TiO2(110) surface. *Israel Journal of Chemistry* **2005,** 45, (1-2), 59-76.
19. Kubicki, J. D.; Kwon, K. D.; Paul, K. W.; Sparks, D. L., Surface complex structures modelled with quantum chemical calculations: carbonate, phosphate, sulphate, arsenate and arsenite. *European Journal Of Soil Science* **2007,** 58, (4), 932-944.
20. Paul, K. W.; Kubicki, J. D.; Sparks, D. L., Sulphate adsorption at the Fe(hydr)oxide-H2O interface: comparison of cluster and periodic slab DFT predictions. *European Journal of Soil Science* **2007,** 58, 978-988.
21. Belelli, P. G.; Ferullo, R. M.; Branda, M. M.; Castellani, N. J., Theoretical modeling of photocatalytic active species on illuminated TiO2. *Applied Surface Science* **2007,** 254, (1), 32-35.
22. Shapovalov, V.; Stefanovich, E. V.; Truong, T. N., Nature of the excited states of the rutile TiO2(1 1 0) surface with adsorbed water. *Surface Science* **2002,** 498, (1-2), L103.
23. Hadjiivanov, K. I.; Klissurski, D. G., Surface chemistry of titania (anatase) and titania-supported catalysts. *Chemical Society Reviews* **1996,** 25, (1), 61-&.
24. Hurum, D. C.; Gray, K. A.; Rajh, T.; Thurnauer, M. C., Recombination Pathways in the Degussa P25 Formulation of TiO2: Surface versus Lattice Mechanisms. *Journal of Physical Chemistry B* **2005,** 109, (2), 977-980.
25. Hurum, D. C.; Agrios, A. G.; Gray, K. A.; Rajh, T.; Thurnauer, M. C., Explaining the enhanced photocatalytic activity of Degussa P25 mixed-phase TiO2 using EPR. *Journal of Physical Chemistry B* **2003,** 107, (19), 4545-4549.
26. Indrakanti, V. P.; Kubicki, J. D.; Schobert, H. H., Quantum Chemical Modeling of Ground States of CO2 Chemisorbed on Anatase (001), (101), and (010) TiO2 Surfaces. *Energy & Fuels* **2008,** 22, (4), 2611-2618.
27. Becke, A. D., A New Mixing Of Hartree-Fock And Local Density-Functional Theories. *Journal of Chemical Physics* **1993,** 98, (2), 1372-1377.
28. Lee, C. T.; Yang, W. T.; Parr, R. G., Development of the Colle-Salvetti correlation-energy formula into a functional of the electron-density. *Physical Review B* **1988,** 37, (2), 785-789.
29. Reed, A. E.; Weinstock, R. B.; Weinhold, F., Natural-Population Analysis. *Journal of Chemical Physics* **1985,** 83, (2), 735-746.
30. Mulliken, R. S., Electronic Population Analysis on LCAO[Single Bond]MO Molecular Wave Functions. I. *The Journal of Chemical Physics* **1955,** 23, (10), 1833.
31. Neese, F.; Olbrich, G., Efficient use of the resolution of the identity approximation in time-dependent density functional calculations with hybrid density functionals. *Chemical Physics Letters* **2002,** 362, (1-2), 170-178.

32. Schafer, A.; Horn, H.; Ahlrichs, R., Fully optimized contracted Gaussian basis sets for atoms Li to Kr. *The Journal of Chemical Physics* **1992,** 97, (4), 2571.
33. Sierka, M.; Hogekamp, A.; Ahlrichs, R., Fast evaluation of the Coulomb potential for electron densities using multipole accelerated resolution of identity approximation. *The Journal of Chemical Physics* **2003,** 118, (20), 9136.
34. Bonapasta, A. A.; Filippone, F., Photocatalytic reduction of oxygen molecules at the (100) TiO2 anatase surface. *Surface Science* **2005,** 577, (1), 59-68.
35. Laaksonen, L., A Graphics Program For The Analysis And Display Of Molecular-Dynamics Trajectories. *Journal of Molecular Graphics* **1992,** 10, (1), 33-&.
36. Bergman, D. L.; Laaksonen, L.; Laaksonen, A., Visualization of solvation structures in liquid mixtures. *Journal of Molecular Graphics & Modelling* **1997,** 15, (5), 301-306.
37. Capel-Sanchez, M. C.; Peña-O'Shea, V. A. d.; Barrio, L.; Campos-Martin, J. M.; Fierro, J. L. G., TD-DFT analysis of the electronic spectra of Ti-containing catalysts. *Topics in Catalysis* **2006,** 41, (1), 27.
38. Gibson, D. H., Carbon dioxide coordination chemistry: metal complexes and surface-bound species. What relationships? *Coordination Chemistry Reviews* **1999,** 185-186, 335-355.
39. Sommerfeld, T.; Posset, T., Electron attachment to CO2 clusters. *Journal of Chemical Physics* **2003,** 119, (15), 7714-7724.
40. Freund, H. J.; Roberts, M. W., Surface chemistry of carbon dioxide. *Surface Science Reports* **1996,** 25, (8), 227-273.
41. Busca, G.; Lorenzelli, V., Infrared spectroscopic identification of species arising from reactive adsorption of carbon oxides on metal oxide surfaces. *Materials Chemistry* **1982,** 7, (1), 89-126.
42. Thompson, T. L.; Diwald, O.; Yates, J. T., Jr., CO2 as a Probe for Monitoring the Surface Defects on TiO2(110)-Temperature-Programmed Desorption. *Journal of Physical Chemistry B* **2003,** 107, (42), 11700-11704.
43. Raupp, G. B.; Dumesic, J. A., Adsorption of carbon monoxide, carbon dioxide, hydrogen, and water on titania surfaces with different oxidation states. *Journal of Physical Chemistry* **1985,** 89, (24), 5240-6.
44. Wilson, J. N.; Senanayake, S. D.; Idriss, H., Carbon coupling on titanium oxide with surface defects. *Surface Science* **2004,** 562, (1-3), L231-L237.
45. Gong, X. Q.; Selloni, A.; Batzill, M.; Diebold, U., Steps on anatase TiO2(101). *Nature Materials* **2006,** 5, (8), 665-670.
46. Gong, X. Q.; Selloni, A., Reactivity of anatase TiO2 nanoparticles: The role of the minority (001) surface. *Journal of Physical Chemistry B* **2005,** 109, (42), 19560-19562.
47. Diebold, U.; Ruzycki, N.; Herman, G. S.; Selloni, A., One step towards bridging the materials gap: surface studies of TiO2 anatase. *Catalysis Today* **2003,** 85, 93-100.
48. Ruzycki, N.; Herman, G. S.; Boatner, L. A.; Diebold, U., Scanning tunneling microscopy study of the anatase (100) surface. *Surface Science* **2003,** 529, L239-L244.
49. Lazzeri, M.; Selloni, A., Stress-driven reconstruction of an oxide surface: The anatase TiO2(001)-(1x4) surface. *Physical Review Letters* **2001,** 87, (26).

50. Hengerer, R.; Bolliger, B.; Erbudak, M.; Gratzel, M., Structure and stability of the anatase TiO2 (101) and (001) surfaces. *Surface Science* **2000,** 460, (1-3), 162-169.
51. Ganduglia-Pirovano, M. V.; Hofmann, A.; Sauer, J., Oxygen vacancies in transition metal and rare earth oxides: Current state of understanding and remaining challenges. *Surface Science Reports* **2007,** 62, (6), 219.

Chapter 4

A density functional theory of CO_2 adsorption on oxygen vacancies on rutile (110) and anatase (010), (001) surfaces: Implications for spectroscopic studies and photoreduction of CO_2 on irradiated TiO_2

4.1 Abstract

Defects, such as oxygen vacancies, are responsible for many chemical reactions on metal oxide surfaces. The role of oxygen vacancies in promoting the light-induced conversion of CO_2 (CO_2 photoreduction) on TiO_2 surfaces is discussed in this chapter. In the first part of this study, we modeled various ground-state configurations of CO_2 adsorbed on reduced TiO_2, a model oxide surface, using clusters from several TiO_2 surface planes. Initially, ground-state CO_2 adsorption on clusters from oxygen-deficient rutile (110) TiO_2 surfaces was studied. The results were compared against available experimental data. Subsequently, CO_2 adsorption on clusters from oxygen-deficient anatase surface planes was studied. Both linear and bent-CO_2 species were modeled on all surfaces. Two different side-on bonded CO_2 (bridging Ti-$CO_2^{\delta\bullet-}$-Ti species) were formed on the rutile (110) and the anatase (010) surfaces. We did not find evidence for C-bonded CO_2 species on the anatase (010), (001) and rutile (110) surface planes. These results call for a re-interpretation of experimental Fourier transform infra red (FTIR) data of CO_2 adsorption on reduced TiO_2 surfaces.

In the next part of this chapter, plausible photocatalytic reactions of the bent CO_2 species that lead to reduced C_1 compounds are discussed. Consistent with CO_2 adsorption

on other n-type metal oxides such as ZrO_2, the bent-CO_2 species do not gain further charge from the TiO_2 surface under illumination. Subsequently, pathways involving the formation of C_1 compounds via reaction of the bent-CO_2 species with water were investigated. Although the formation of species such as CO and HCHO is thermodynamically possible, we find that the energy needed to regenerate the oxygen vacancy on TiO_2 surfaces is greater than that available through band-gap illumination. Therefore, CO_2 reactions with water on irradiated TiO_2 surfaces are likely to be stoichiometric.

4.2 Introduction

> *"..an important issue in TM oxide-based heterogeneous catalysis is the role of surface defects in determining the activity and selectivity of the catalyst. The existence of reduced surface centers — and hence the presence of neutral oxygen vacancies — is sometimes necessary for any activity."*
>
> - Ganduglia-Pirovano et al.[1]

Oxygen vacancies are among the most common defects on metal oxide surfaces. A good overview on oxide catalysts, and the role of defects in their catalytic activity, is provided by Haber[2]. In the past, different probe molecules, (such as O_2, CO_2, or small organic molecules) have been used to characterize defect sites. Most studies have been reported on the well-defined surfaces from the rutile phase of TiO_2. At elevated temperatures, TiO_2 forms a variety of sub-oxides such as $TiO_{1.985}$[3, 4]. The surface defect structure of TiO_2 and related oxides, and the importance of so-called dangling bonds to the surface properties, is summarized by Masel[5] . On the other hand, anatase is the more

common catalytically active polymorph, and is extensively used in paints and pigments[3] and supports for industrial catalysts. Anatase is also a major component of the Degussa P25 formulation of TiO_2, used in many photocatalytic studies. The focus of this chapter is the activation of CO_2 at oxygen vacancies on rutile (110) and anatase (010), (001) and (101) surfaces. Our previous computational studies showed that CO_2 photoreduction may be promoted at defects such as oxygen vacancies on TiO_2[6]. Moreover, experimental studies by Raskó and Solymosi[7] and Chen et al.[8] also pointed to a role for oxygen vacancies. The role of oxygen vacancies in activating CO_2 may not be limited to TiO_2 alone. For example, using a hybrid quantum mechanics/molecular mechanics (QM/MM) approach to study the conversion of CO_2 to methanol, French et al.[9] proposed oxygen vacancies on ZnO surfaces to be the active sites for its hydrogenation to methanol.

While it is known that anatase is more difficult to reduce than rutile, the exact electronic state of reduced anatase surfaces is a subject of debate and research[1]. The use of gradient-corrected functionals has been shown to result in metallic conducting ground-states, whereas hybrid functionals such as B3LYP result in the excess electrons being localized on the nearest or next- nearest Ti atoms.

Using periodic DFT calculations, Wu et al.[10] demonstrated that oxygen-deficient rutile (110) surfaces mediate the stoichiometric oxidation of CO to CO_2. They noted that both oxygen adsorption as well as CO oxidation required the presence of surface oxygen vacancies (SOVs). However, the reaction was not catalytic and resulted in the consumption of the SOV, leading to a stoichiometric surface. On the other hand, similar calculations for the adsorption of O_2 on anatase (100) surfaces containing SOVs showed

that $O_2^{\bullet-}$ could be desorbed from the surface upon photoexcitation[11], thus making the process photocatalytic.

DFT calculations have also been used to study CO_2 interactions with other metal oxide surfaces as well. Florez et al.[12] used embedded-cluster DFT calculations to study the dissociative adsorption of CO_2 on MgO surfaces. In contrast to MgO, TiO_2 is a less ionic metal oxide (with Ti and O atomic "*natural*" charges of approximately +2 and -1). (A good review of various "types" of oxides is provided by Cotton et al.[13]). Due to this, studies by Bredow et al.[14] and de Lara-Castells and Krause[15] have shown that even hydrogen-saturated two-Ti atom clusters could model the local adsorption of O_2 on the oxygen vacancy.

CO_2 has been used as a probe to study the oxygen vacancies on (rutile) TiO_2 surfaces. Henderson[16] observed only linearly adsorbed CO_2 species with vibrational high resolution electron energy loss spectrometry on vacuum-annealed rutile (110) surfaces. A *precursor-mediated* reaction between CO_2 and H_2O to form bicarbonate on the oxygen-deficient surface was proposed. Temperature-desorption spectroscopy studies showed that CO_2 interacted with the oxygen vacancies and the normal Ti^{4+} sites differently. Surface oxygen vacancies bound CO_2 slightly more strongly than regular Ti^{4+} sites. Similar results were obtained by Funk and Burghaus[17].

On the other hand, low-temperature studies by Raskó and Solymosi[7] offered evidence for *bent* CO_2 species interacting with electron centers (Ti^{3+}) to form negatively charged $CO_2^{\bullet-}$ species. These authors, however, did not observe evidence for CO formation on reduced TiO_2 surfaces at low temperatures (195 K). Both *C-end bonded* as well as *side-on bent* CO_2 species were observed after CO_2 adsorption on TiO_2. The exact

form by which CO_2 adsorbs on reduced TiO_2 surfaces is important, because, if further reactions were to occur at the SOV site, CO_2 must not be bound too strongly. On the other hand, weak acid-base interaction between the Ti^{3+} center and CO_2 molecule will not result in effective charge transfer to CO_2. This is common to many photocatalytic processes[18].

Using surface-sensitive techniques at temperatures higher than those used by Raskó and Solymosi[7], Raupp and Dumesic[19] found that CO_2 dissociatively adsorbed on a polycrystalline reduced TiO_2. This is consistent with the findings of Wu et al.[10], that CO_2 dissociation to CO on a defective TiO_2 (110) surface is exothermic by ~0.8 eV. Therefore CO oxidation to CO_2 on the reduced rutile (110) surface is stoichiometric. Bent-CO_2 species ($CO_2^{\delta\bullet-}$) have been observed as intermediates in CO oxidation to CO_2. It is, however, not clear whether the interaction of light with bent-CO_2 species adsorbed on reduced TiO_2 surfaces could make the process catalytic.

Raskó and Solymosi[7] studied the adsorption of CO_2 on TiO_2 surfaces prepared with various pretreatment procedures. The exact composition of their TiO_2 sample is somewhat under question, because they reportedly used Degussa P25 TiO_2 in the rutile phase. However, Degussa P25 is commonly ~80% anatase and 20% rutile. The pretreatment temperatures reported in reference 7 did not exceed 673 K. Therefore, if the original sample was a mixed-phase titania, the anatase phase would have still been present during experiments. The exact phase (as well as exact surface plane) is important, because it controls the surface activity. Moreover, it will also help understand which phase of P25 is the more active towards the activation of CO_2.

Raskó and Solymosi[7] assigned (1674, 1310 cm^{-1}) to bent CO_2 species side-on bonded to Ti^{3+} (side-on bonded CO_2) and (1640-1630, 1219 cm^{-1}) to bent CO_2 species bonded with the C-end to Ti^{3+} (referred to as C-end bonded CO_2). Upon evacuation, only the C-end bonded species were stable, whereas the peaks at 1674-1676 and 1244-1241 cm^{-1} disappeared. While it is possible that the side-on bonded species would have a higher vibrational frequency compared to the less strongly bound C-end bonded species, it is difficult to imagine how the C-end bonded species would be more stable than the side-on bonded species. We note that in the case of homogeneous metal-CO_2 complexes, CO_2 species with C-bonded to a metal center are considered to be less stable than η^2-CO-(metal-CO_2) complexes[20] exhibiting a metal-(CO) coordination (similar to the *side-on bent* species proposed in to in reference 7). Therefore, if C-bonded $CO_2^{\delta\bullet-}$ forms on TiO_2 surfaces, it might desorb more readily compared to the side-on bent species, contrary to the assignments of Raskó and Solymosi[7].

We previously found evidence for the formation of side-on bent CO_2 species on anatase (010) SOVs[21]. The relative reactivities of both side-on bent as well as C-bonded bent species on TiO_2 surfaces are not well known.

The questions addressed in this study are:

a) Is there a difference CO_2 adsorption (IR frequencies) as bent CO_2 between anatase and rutile model clusters?

b) Can DFT methods model the formation of C-end bonded bent CO_2 on SOVs of rutile (110), anatase (001), anatase (101) and anatase (010) clusters?

c) What is the fate of the bent CO_2 species thus formed on these surfaces?

In an earlier study, we have shown that defect-free anatase TiO_2 surfaces are highly unlikely to mediate CO_2 photoreduction[21]. In the present study, we therefore performed ground-state CO_2 adsorption studies on oxygen-deficient clusters from rutile (110), anatase (010), (001) and (101) surfaces. We compare the results—especially, the predicted vibrational frequencies of various CO_2 species and their relative CO_2-bare cluster interaction energies—with those from single-crystal studies (e.g., those of Henderson[16]) as well as polycrystalline studies[7] using the rutile polymorph of TiO_2. Subsequently, similar calculations were performed on the anatase (010), (001) and (101) surfaces. Finally, the implications of CO_2 adsorption on SOVs for CO_2 photoreduction are discussed.

4.3 Computational Methods

All computations were performed in Turbomole V5.9[22]. The B3LYP functional and the def2-SV(P) basis set were used. The calculations on small clusters with the def2-SV(P) basis set were performed without using the Resolution-of-Identity (RI) approximation. Basis set effects were tested by a B3LYP/TZVPP calculation using the multipole-accelerated-resolution-of-identity-*J* (MARI-*J*) approximation and the TZVPP auxiliary basis set and a similar behavior was observed. Atomic charges for all clusters were calculated using natural population analysis[23] (NPA). All geometry optimizations were performed using default optimization criteria and the m3 grid.

4.3.1 Adsorption of CO_2 on oxygen vacancies on the rutile (110) surface

de Lara-Castells and Krause[15] used a non-stoichiometric $Ti_2O_9H_{11}^{-1}$ cluster to model the reduced rutile (110) surface, while Bredow used a non-stoichiometric neutral $Ti_2O_9H_{12}$ cluster to simulate the oxygen vacancy. However, the cluster used by Bredow had a two-coordinate (2-c) bridging O atom at the bottom, whereas that used by de Lara-Castells and Krause had correct coordination for the bridging O atoms. Combining these two features, a neutral, non-stoichiometric, $Ti_2O_9H_{12}$ cluster (denoted as Ti2Vo_110) was used in this study. Cerius[2] (MSI Inc.) was used to generate the (110) surface from the rutile bulk crystallographic data. Dangling bonds were saturated by adding hydrogen atoms at similar positions to Ti atoms in the bulk.

All O-H bond distances were initially kept at 0.97 Å. Only atoms on and adjacent to the (110) surface were optimized. (Only four atoms, bridging oxygens and the Ti atoms, in addition to CO_2, were relaxed.) Initially, neutral bare cluster geometries were studied. The singlet state of the oxygen-deficient cluster was the ground state. Subsequently, nine different configurations for CO_2 adsorption were modeled, and five unique configurations obtained. The $Ti_2O_9H_{12}$:CO_2 clusters are denoted as Ti2Vo_110_CO2(a-e).

Counterpoise uncorrected electronic interaction energies were calculated for these clusters using the following formula Eq. **4.1** :

$$\Delta E_{inter} = (E_{Ti2\_110} + E_{CO2} - E_{Ti2\_110\_CO2}) * 27.2116 * 96.485 \text{ kJ/mol} \quad \textbf{4.1}$$

To calculate vibrational frequencies, all atoms of selected clusters were relaxed and harmonic vibrational frequencies were calculated. The results did not have any imaginary frequencies. The frequencies thus obtained were scaled by 0.9614[24].

4.3.2 Adsorption of CO_2 on oxygen vacancies on the anatase (010) and (001) surfaces

A neutral, stoichiometric (010) $Ti_2O_8H_{10}$ cluster was used to model the oxygen vacancies on the anatase (010) surface. CO_2 adsorption on the oxygen vacancy was studied by varying the initial configurations of CO_2. CO_2 adsorption on larger clusters, containing six Ti atoms, $Ti_6O_{20}H_{18}$ (denoted Ti6Vo_010 and Ti6Vo_001), were also modeled in this study. The IR frequencies and electronic interaction energies were calculated using procedures similar to those used for the rutile Ti2Vo_110 clusters, described above.

4.3.3 Excited state calculations of various bent-CO_2 species on anatase surface planes

Frontier orbital analysis of various bent-CO_2 species was performed by plotting the highest occupied molecular orbital (HOMO) and the lowest unoccupied molecular orbital (LUMO) using gOpenmol[25, 26] at an isocontour value of 0.1 $e^{1/2}/Å^{3/2}$. Subsequently, geometry optimization was performed on selected clusters.

4.4 Results and Discussion

4.4.1 Adsorption of CO_2 on oxygen vacancies on the rutile (110) surface

Due to the break in symmetry, different configurations for the location of the twelfth atom (H atom) in the bare cluster are possible. The H atom was placed on the O atom, resulting in the cluster with the least single-point energy. The five starting configurations used are shown in Figure 4-1(a-e). They are mainly determined by the position of the CO_2 with respect to the Ti-O-Ti plane of the cluster. Partially relaxed geometries of these configurations (where only four atoms of the cluster and CO_2 were relaxed) are shown in Figure 4-2 (a-e). Only the titanium and the bridging two-coordinate (2-c) O atoms of the cluster were relaxed.

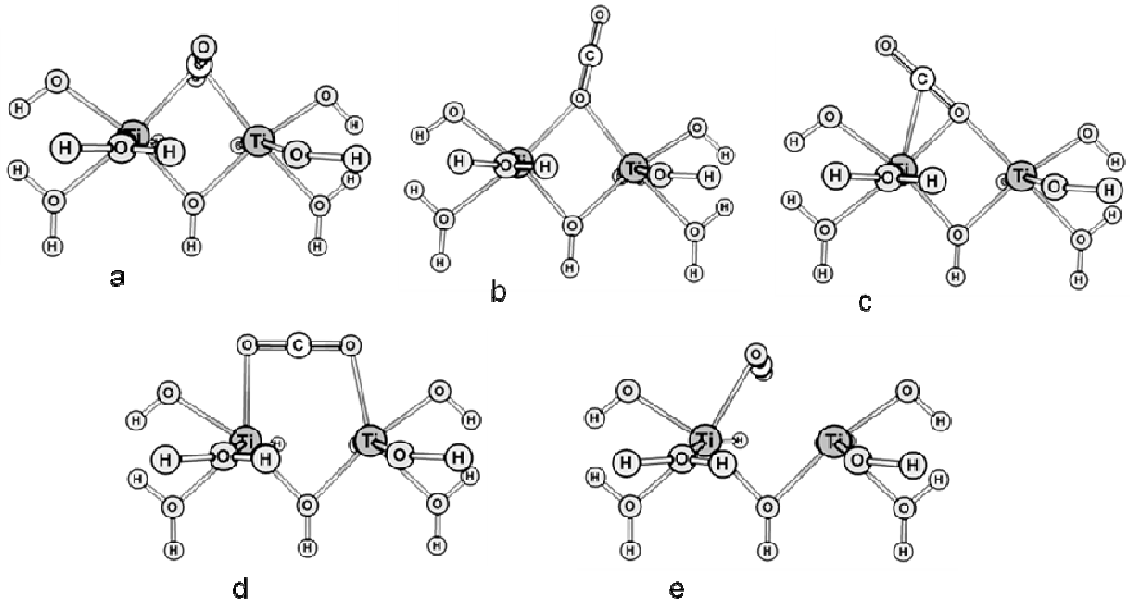

Figure 4-1: Initial configurations for CO_2 adsorption on reduced rutile Ti2Vo_110 - clusters. The C atom was located 2.2 Å from Ti atom. Only configurations shown in (c-d) resulted in bent-CO_2 species. Configuration e resulted in a surface bicarbonate species.

The mode of binding affects whether charge transfer occurs to CO_2. In Figure **4-2** (a-b), CO_2 primarily adsorbs as a linear species, in which the OCO bond angle is slightly more distorted in (b) compared to (a). Two bent-CO_2 species were modeled, shown in Figure **4-2**c and Figure **4-2**d. The notation for metal-CO_2 complexes used by Gibson[20] is used to differentiate between bent-CO_2 species Ti2Vo_110_CO2c-d. Accordingly, the Ti2Vo_110_CO2c species is assigned as a μ_2-η^4 species (because it has four bonds involving CO_2 and the two Ti atoms) and the Ti2Vo_110_CO2d is assigned as a μ_2-η^3 species (three bonds involving CO_2 and two Ti atoms). The Ti-Ti bond distance also increased slightly from 2.78 Å in the case of the linearly bonded CO_2 species to 2.88-2.92 Å for the bent-CO_2 species. Additionally, although the OCO bond angle in Figure **4-2**d is lower than that shown in Figure **4-2**c, the charge of the $CO_2^{\delta\bullet-}$ moiety is almost the same in both cases, as shown in Table **4-1**.

Interaction of CO_2 with the oxygen (3-c) atoms leads to the formation of the bicarbonate-like species shown in Figure **4-2**e. From the interaction energies presented in Table **4-2**, it is clear that among the bent-CO_2 species, the μ_2-η^3 species is more stable than the μ_2-η^4 bent-CO_2 species. Both of these bent-CO_2 species are more stable than the linearly adsorbed CO_2. The bicarbonate-like species, in turn, is more stable than the bent-CO_2 species

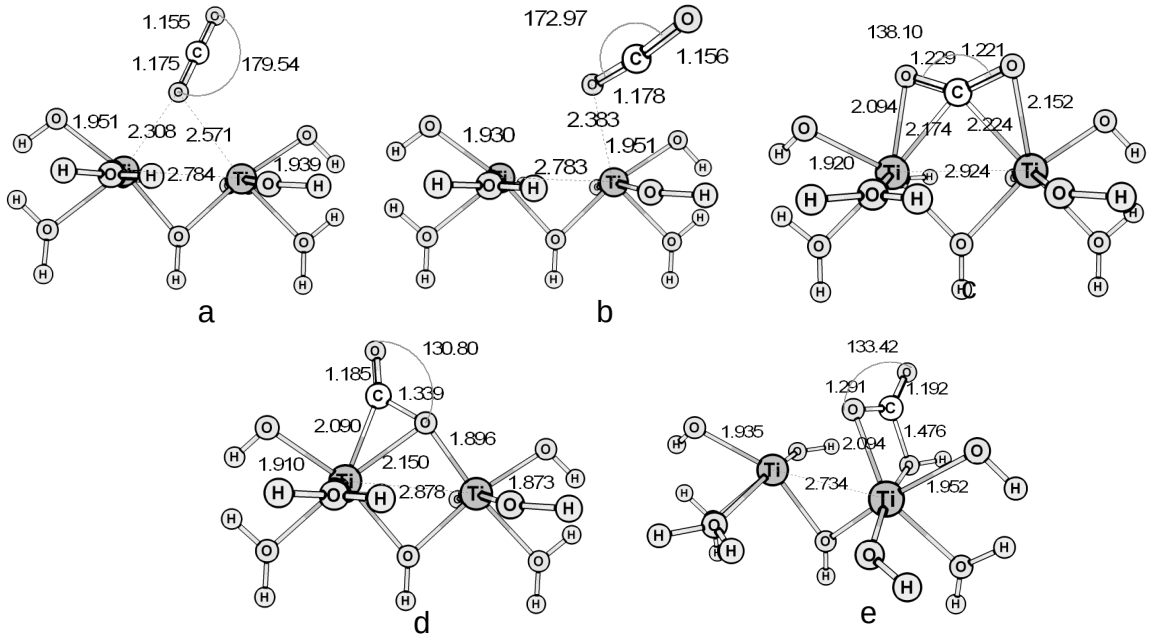

Figure **4-2**: Partially relaxed geometries, using initial configurations shown in Figure **4-1** , (denoted as Ti2Vo_110_CO2(a-e)), from B3LYP/def2-SV(P) calculations. Configurations shown in (c-d) resulted in bent-CO_2 species. The bond distances are in Å, the angles are in degrees.

Table **4-1**: Type of bonding, C-O bond lengths, OCO bond angles and $CO_2^{\delta\bullet-}$ natural charges for bent-CO_2 species on anatase and rutile TiO_2 clusters. The results indicate that the structure of the surface plays a primary role in determining the amount of charge transferred to CO_2.

Cluster	Type of bonding	C-O, Å		<O-C-O, degrees	Natural charge of the $CO_2^{\delta\bullet-}$ moiety
Ti6Vo_010_CO2_a	μ_1-η^2	1.202	1.303	130.3	-0.64
Ti2Vo_010_CO2_1	μ_1-η^2	1.206	1.282	133.1	-0.61
Ti2Vo_010_CO2_2	μ_2-η^3	1.197	1.316	131.8	-0.62
Ti6Vo_001_CO2	μ_2-η^3	1.249	1.285	126.2	-0.70
Ti2Vo_110_CO2c	μ_2-η^4	1.221	1.229	138.1	-0.45
Ti2Vo_110_CO2d	μ_2-η^3	1.185	1.339	130.8	-0.45

Table 4-2: Counterpoise uncorrected electronic interaction energies of various configurations of CO_2 adsorbed on rutile (110), obtained by B3LYP/def2-SV(P) calculations. The interaction energies of the bent-CO_2 species are higher than those of the linear-CO_2 species, while the bicarbonate-like species is the most stable of all.

Cluster	Description	ΔE^{inter}, kJ/mol
Ti2Vo_110_CO2a	Linear	-34
Ti2Vo_110_CO2b	Linear	-46
Ti2Vo_110_CO2c	Bent, μ_2-η^4	-73
Ti2Vo_110_CO2d	Bent, μ_2-η^3	-96
Ti2Vo_110_CO2e	Bicarbonate	-109

This non-exhaustive conformation search did not result in configurations that could lead to C-bonded CO_2 species, which represent η^1-C coordination between CO_2 and the metal center. However, Ramis et al.[27] and Raskó and Solymosi[7] both assigned bands in the IR spectrum to side-on bent and C-bonded CO_2 species upon CO_2 adsorption on TiO_2. We note here that the most stable structures for CO_2 adsorption on the Co(110) surface from DFT studies[28] also correspond to structures somewhat similar to μ_2-η^3 and μ_2-η^4 configurations shown in Figure 4-2. The "short-bridge" configuration on the Co(110) surface shown by de la Peña O'Shea et al.[28] is similar to the Ti2Vo_110_CO2c (μ_2-η^4) species observed in this study.

4.4.2 Adsorption of CO_2 on oxygen vacancies on the anatase (010) and (001) surfaces

Bent-CO_2 species formed on anatase surfaces are shown in Figure 4-3. Similar to the rutile (110) surface, two kinds of bent-CO_2 species, (μ_1-η^2) and (μ_2-η^3), were observed on the anatase (010) surface. The (μ_1-η^2) species (Ti6Vo_010_CO2_1 and Ti2Vo_010_CO2_2) converted to bridged (μ_2-η^4) bent-CO_2 species similar to Ti2Vo_110_CO2_c (from Figure 4-2) upon relaxing all cluster atoms. Various configurations did not result in the formation of the C-bonded CO_2 species. The geometries of bent CO_2 species in Figure 4-3a (Ti6Vo_010_CO2_1 cluster) are somewhat similar to those in Figure 4-3b (Ti2Vo_010_CO2_2 cluster). The OCO bond angles (130° for the Ti6Vo_010_CO2_1 cluster and 133° for Ti2Vo_010_CO2_2 cluster) are different, but the O-C bond lengths (1.303 Å and 1.202 Å for the Ti6Vo_010_CO2_1 cluster, and 1.282 Å and 1.206 Å for the Ti2Vo_010_CO2_2 cluster, from Table 4-1) are comparable. This indicates that small two-Ti-atom clusters could be used in place of the larger, more computationally expensive Ti6- clusters.

CO_2 forms a (μ_2-η^3) complex on the anatase (001) surface, similar to the "long-bridge" configuration of de la Peña O'Shea et al.[28], but the bond angles and O-C bond lengths observed for the Ti6Vo_001_CO2 cluster in Figure 4-3d are different from those calculated on the Co(110) surface. The O-C bond lengths are ~1.25 and 1.29 Å for the Ti6Vo_001_CO2 cluster, compared to 1.24 Å for "long-bridged" CO_2 species on the Co(110) surface. Similarly, the OCO bond angle for the Ti6Vo_001_CO2 cluster is significantly smaller compared to the 135° bond angle of "long-bridged" CO_2 on the Co(110) surface.

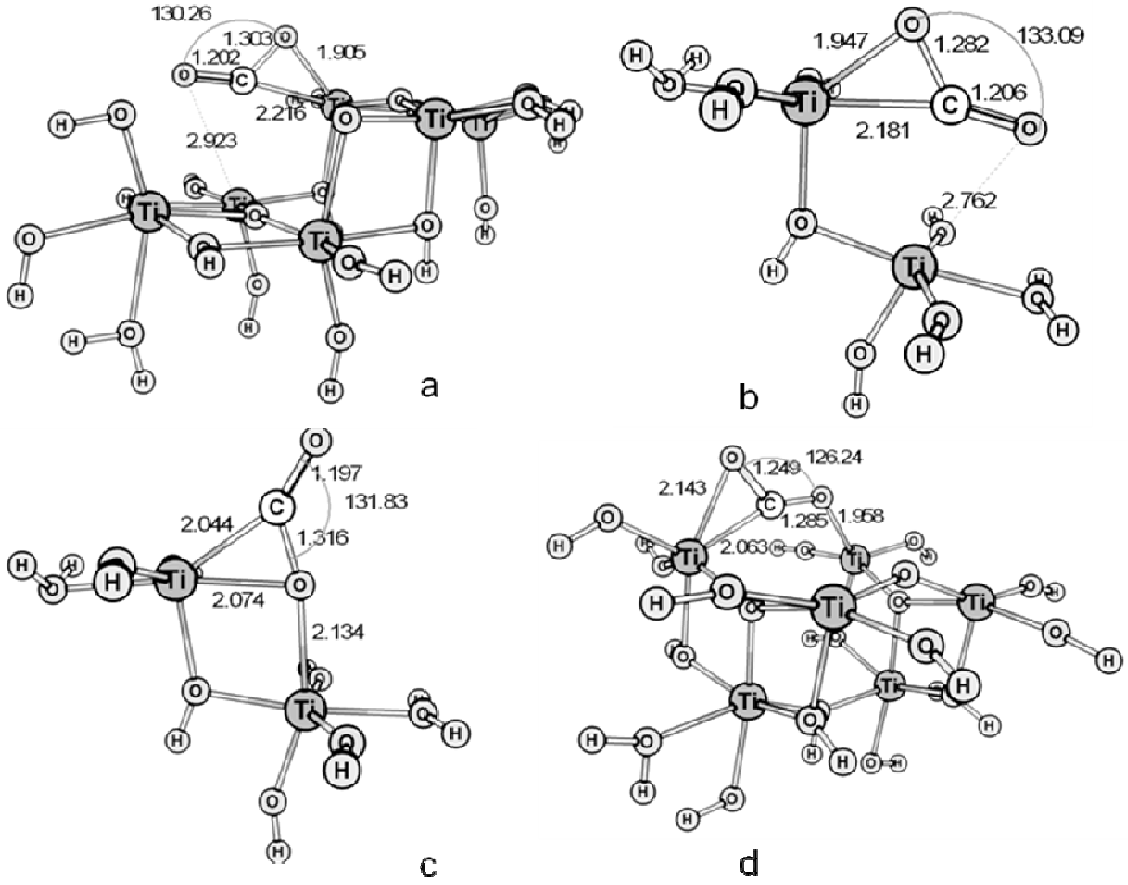

Figure **4-3**: Partially relaxed geometries of bent-CO_2 species from anatase surfaces from B3LYP/def2-SV(P) calculations. (a) (010) surface, 6 Ti atom cluster (Ti6Vo_010_CO2_a), (b) (010) surface, 2 Ti atom cluster: (Ti2Vo_010_CO2_1), (c) (010) surface, 2 Ti atom cluster (Ti2Vo_010_CO2_2), (d): (001) surface, 6 Ti atom cluster (Ti6Vo_001_CO2). Species (a) and (b) converted to bridged (μ_2-η^4) bent-CO_2 species similar to Ti2Vo_110_CO2_c (from Figure **4-2**) upon relaxing all cluster atoms. Similar to the rutile (110) surface, two kinds of bent-CO_2 species are observed on the anatase (010) surface. The bond distances are in Å, the angles are in degrees.

4.4.3 Vibrational frequencies of relaxed bent-CO_2 species

To compare the IR frequencies of bent-CO_2 species with experimental results, we fully relaxed the bent-CO_2 clusters from anatase and rutile surfaces, and calculated the scaled harmonic vibrational frequencies. Previous studies by Ramis et al.[27], Raskó and Solymosi[7] and Papai et al.[29] were used to provide data for comparisons. These frequencies, along with similar results from anatase (010) and (001) surface planes, are shown in Figure **4-4**. The experimental data used for comparisons are shown in Table **4-3**. The assignments of the side-on bonded and C-end bonded bent $CO_2^{\delta\bullet-}$ species by Ramis et al.[27], and Raskó and Solymosi[7] are inconsistent with earlier observations of CO_2 chemisorption on metal oxides by Busca and Lorenzelli[30]. Busca and Lorenzelli attributed species exhibiting high values of $\Delta\nu_3$ splittings (such as 1750, 1150 cm^{-1}) and low thermal stabilities to "side-on" bent-CO_2 species exhibiting a η^2_{CO} coordination, whereas Ramis et al.[27] assigned these frequencies to C-bonded bent-CO_2 species having a η^1_C coordination to the Ti^{3+} electron centers. Our previous work[31] on CO_2 adsorption as carbonate on various anatase surface planes also revealed evidence for carbonate-like species with high $\Delta\nu_3$ splittings. Therefore, high $\Delta\nu_3$ splittings measured experimentally might not always be indicative of negatively charged $CO_2^{\delta\bullet-}$ species. Papai et al.[29] calculated vibrational frequencies at 1800 cm^{-1} and 1000 cm^{-1} through DFT studies of η^2_{CO} (side-on) $CO_2^{\delta\bullet-}$ species. Compared to η^2_{CO} species, the μ_2-η^3 species would be bound more strongly to the surface, resulting in higher frequencies.

Our modeling did not reveal C-bound CO_2 species having a η^1_C coordination to the surface Ti^{3+} to be a stable species at 0 K. Therefore, the assignment of bent-CO_2 species

to C-bound CO_2 species is in question. Nevertheless, from Figure **4-4**, and Figure **4-5** it is clear that the vibrational frequencies for $CO_2^{\delta\bullet-}$ species adsorbed on reduced rutile (110) surface are more consistent with the experimental values than corresponding values for $CO_2^{\delta\bullet-}$ species on anatase surfaces.

Table **4-3**: Experimental IR frequencies attributed to bent-CO_2 species on TiO_2 (from literature).

	Side-on bonded CO_2		C-end bonded CO_2	
	ν_1, cm^{-1}	ν_2, cm^{-1}	ν_1, cm^{-1}	ν_2, cm^{-1}
Raskó & Solymosi[7]	1674	1310	1630-1640	1219
Ramis et al.[27]	1668	1315	1713, 1750	1150

From Figure **4-4** and Figure **4-3**, the larger (010) anatase Ti6- cluster gives results similar to the (010) anatase Ti2-cluster. Therefore, CO_2 adsorption on reduced TiO_2 surfaces is governed mostly by local interactions with the surface.

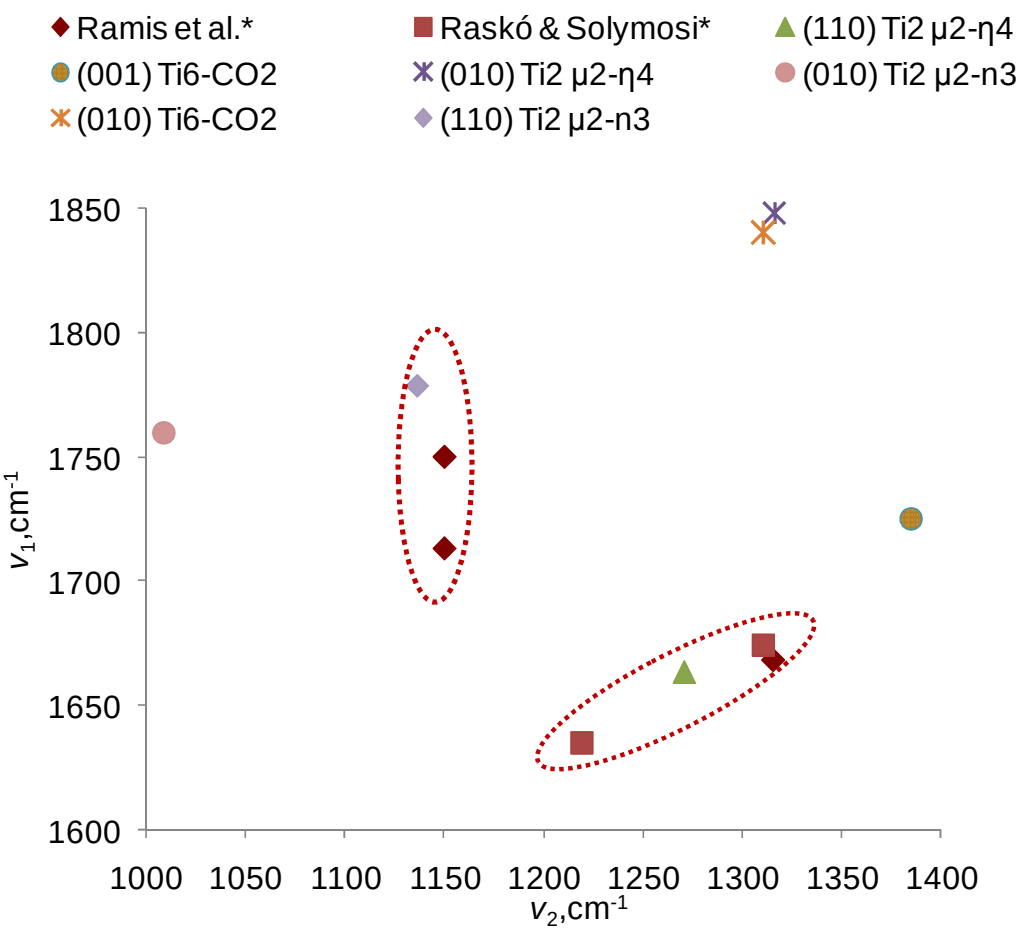

Figure **4-4**: Comparison of vibrational frequencies of fully relaxed bent-CO_2 clusters from anatase (001) , (010) and rutile (110) surfaces from B3LYP/def2-SV(P) calculations with experimental IR frequencies[7, 27] of $CO_2^{\delta\bullet-}$ species on reduced TiO_2. (110) Ti2 μ2-η3: Ti2Vo_110_CO2d, (110) Ti2 μ2-η4: Ti2Vo_110_CO2c, (010) Ti2 μ2-η4: Ti2Vo_010_CO2_1, (010) Ti2 μ2-η3: Ti2Vo_010_CO2_2, (010) Ti6 μ2-η4: Ti6Vo_010_CO2_a, (001) Ti6 μ2-η3: Ti6Vo_001_CO2. CO_2 adsorption on TiO_2 surfaces is structure-sensitive. The experimental results are more consistent with the vibrational frequencies of bent-CO_2 species on the rutile (110) surface, compared to the anatase (001) and (010) surface.

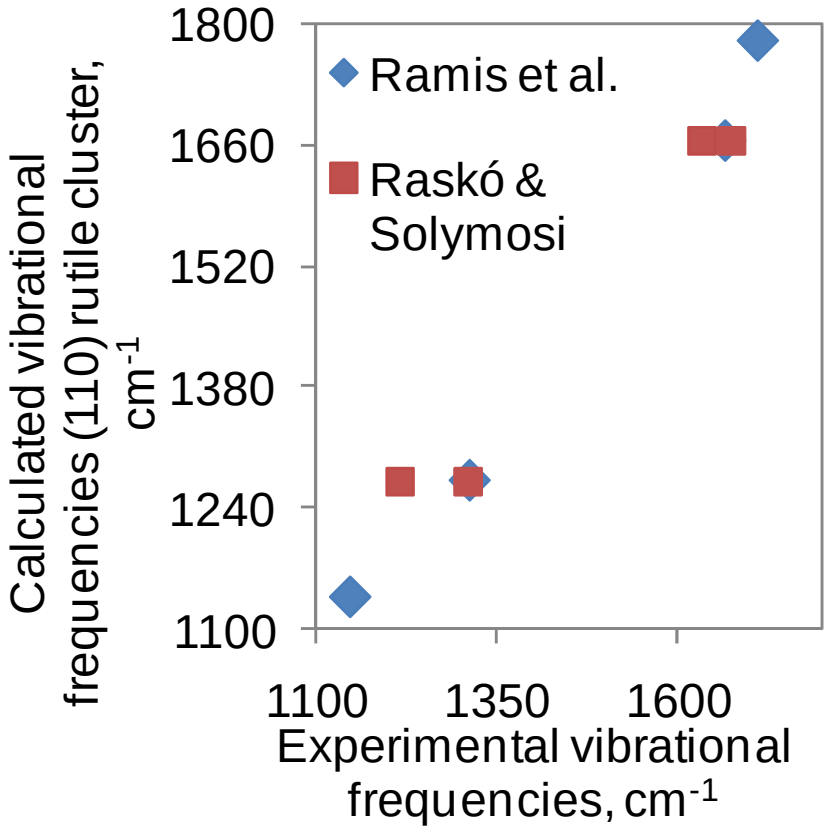

Figure **4-5**: C-O IR frequencies from the 2-Ti atom clusters from the rutile (110) surface (Ti2Vo_110_CO2c, Ti2Vo_110_CO2d) are consistent with those obtained from in situ FTIR spectroscopic studies of CO_2 adsorption on TiO_2

4.4.4 Fate of various bent-CO_2 species on rutile and anatase surface planes.

Ground state DFT calculations indicate that bent, negatively charged CO_2 species are formed upon CO_2 adsorption at surface two-coordinate oxygen vacancies on anatase and rutile TiO_2 surfaces. Subsequently, we studied further photoreactions of these species. The bent-CO_2 species could undergo thermal or photoreactions at the surface, forming CO, carbonates or desorbed CO_2. Excited states of the chemisorbed $CO_2^{\bullet\delta-}$

species are likely to be multi-configurational. However, to simplify the analysis, we used frontier orbital analyses and TD-DFT excitation energies to analyze the potential for further charge transfer to CO_2 in the excited state.

Frontier orbitals of the Ti6Vo_010_CO2 μ_2-η^3 cluster are shown in Figure **4-6**. They indicate that CO_2 does not constitute the lowest unoccupied molecular orbital (LUMO) or (LUMO+1) orbitals of the Ti6Vo_010_CO2 complex. Therefore, electron transfer to CO_2 in the excited state is not possible. Moreover, because CO_2 contributes to the HOMO of the cluster, and given the fact that CO_2 does not contribute to the LUMO of the cluster strongly, light irradiation will likely result in the photodesorption of neutral CO_2 species from the reduced (010) surface.

Emeline et al.[32] showed that the adsorption of CO_2 on Zr^{3+} centers resulted in the formation of $CO_2^{\delta\bullet-}$ species. Upon irradiation, these species photodesorbed from the surface, resulting in the regeneration of Zr^{3+} centers. The frontier orbital analysis of the Ti6Vo_010_CO2 cluster is consistent with this result. CO_2 forms a negatively charged species upon adsorption at Ti^{3+} centers, formed due to the oxygen vacancies. Upon irradiation with light, these species are photooxidized and the resulting CO_2 desorbs from the surface. Similar photoreactions occur on n-type semiconductor surfaces as well (increasing the concentration of oxygen vacancies would make TiO_2 n-type). The orbital analysis presented in this study therefore does not support the findings of Raskó and Solymosi[7], where further electron transfer to the negatively charged CO_2 species occurred upon irradiation.

CO formation via decomposition of the bent-CO_2 species, thus replenishing the oxygen vacancy, is energetically favorable. For example, the change in the electronic

interaction energy for the reaction (Ti2Vo_010_CO2_1) → Ti2_010 + CO (calculated at the B3LYP/def2-SV(P) level of theory) is -0.316 eV (-30 kJ/mol). Since CO_2 adsorption on the Ti2Vo_010_CO2_1 cluster is also energetically feasible, it follows that the formation of CO from gas phase CO_2 on reduced anatase (010) surfaces is feasible. Wilson et al.[33] found that CO_2 underwent C-C coupling reactions on reduced TiO_2 surfaces prepared by sputtering. However, this and similar reactions on other surfaces lead to the consumption of the oxygen vacancy.

Possible *photocatalytic* cycles either involve a means to regenerate this oxygen vacancy or could involve a transformation of the bent-CO_2 species to a more electron-accepting species that undergoes further reactions under band-gap illumination. We have examined the energetics of such reactions involving CO_2 and H_2O adsorbed on the Ti6Vo_010 cluster, and the results are summarized in Figure **4-7**. The results indicate that whereas C_1 species-forming reactions which consume oxygen vacancies are thermodynamically feasible, reactions which involve regeneration of the oxygen vacancies, thus completing the photocatalytic cycle are thermodynamically uphill, likely consuming more than one UV photon. Moreover, experimental evidence in the literature suggests that interaction of low-intensity UV/solar radiation with TiO_2 surfaces is not likely to create oxygen vacancies, as opposed to the original arguments for photoinduced hydrophilicity[34]. Therefore, CO_2 photoreduction on reduced-TiO_2 surfaces is likely to involve multiple photons or is a non-catalytic process, resulting in the consumption of the oxygen vacancy.

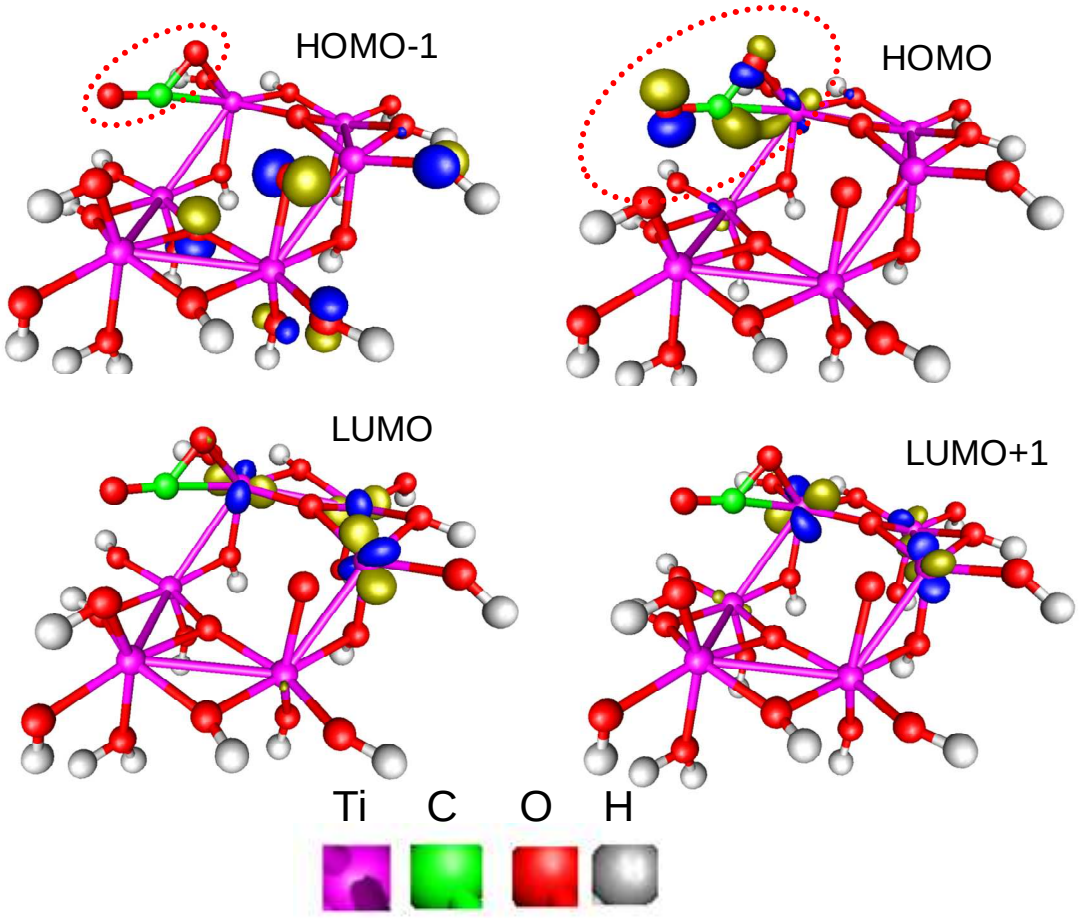

Figure **4-6**: Frontier molecular orbitals of the ground state singlet, neutral Ti6Vo_010_CO2 μ_1-η^2 cluster, from B3LYP/def2-SV(P) calculations, shown at an isocontour value of 0.03 $e^{1/2}/Å^{3/2}$. CO_2 does not form acceptor states, as shown by the LUMO and LUMO+1 orbitals. Therefore, band gap illumination of the surface would likely result in the desorption of bent CO_2 as neutral species. (Plotted with the gOpenMol visualization program[25, 26])

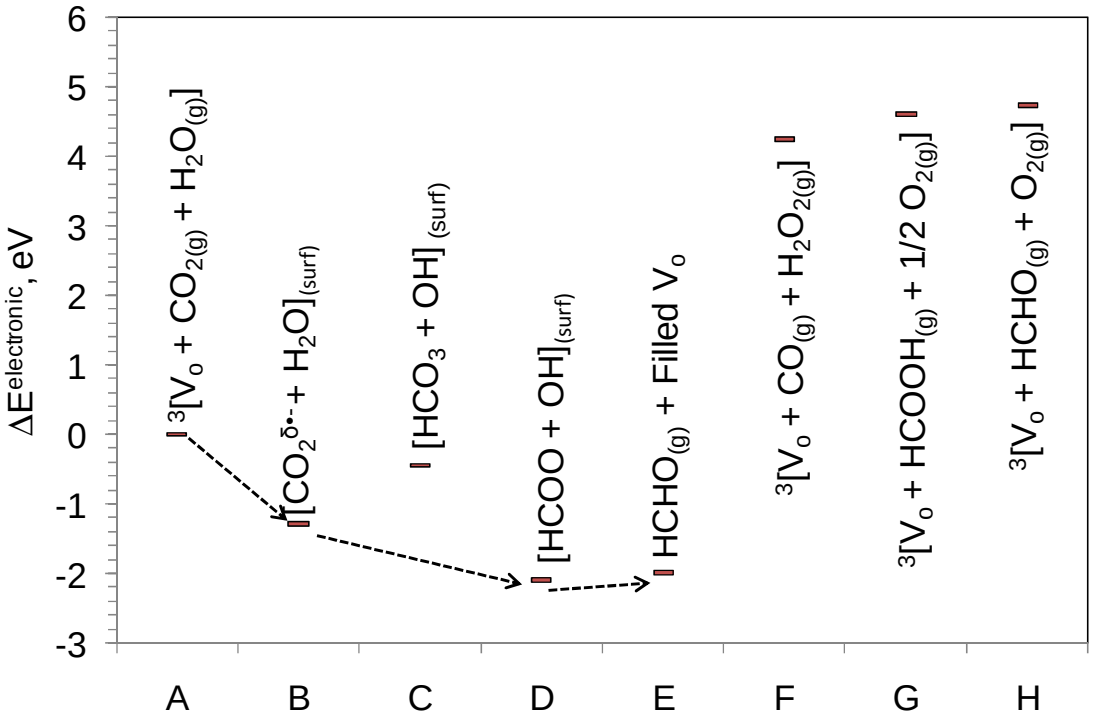

Figure **4-7**: Relative energetics of reactions involving the formation of reduced C_1 species from gas phase CO_2 and water molecules on model cluster from the (010) anatase surface (Ti6_Vo_010). (A), calculated from B3LYP/def2-SV(P) calculations: Gas phase CO_2 and H_2O (located 7 Å from the surface) of a triplet Ti6_Vo_010 cluster, (B): Singlet negatively charged $CO_2^{\delta\bullet-}$ species along with coadsorbed water molecule on a singlet Ti6_Vo_010 cluster, (C): Bicarbonate species coadsorbed with $O^{surf}H$ species, (D): Formate and hydroxyl groups on the surface, (E): Desorption of formaldehyde and the refilling of the oxygen vacancy, (F): Desorbed gas phase CO, H_2O_2 and triplet state Ti6_Vo_010 cluster, (G): HCOOH and O desorbed from a triplet Ti6_Vo_010 cluster, (H): HCHO and O_2 desorbed from a triplet Ti6_Vo_010 cluster. Both singlet and triplet states were modeled, the state with the lowest energy is shown in the figure. The dotted arrows represent potential intermediates involved in the refilling of the oxygen vacancy. The energy required to desorb reduced C_1 species indicates that the reduction of CO_2 possibly consumes more than one photon.

4.5 Conclusions

CO_2 adsorption and further reaction has been modeled using DFT calculations on the anatase (010), (001) and rutile (110) surfaces. CO_2 forms negatively charged, bent $CO_2^{\delta\bullet-}$ species on surface oxygen vacancies on these surfaces. The bent-CO_2 species were more strongly held than the linear species (at 0 K). The "two-step desorption" of CO_2 observed during TDS studies on rutile (110) surfaces may be applicable to anatase (010), (001) surfaces as well. CO_2 adsorption is primarily local in nature. Two kinds of bent CO_2 species were observed upon full relaxation of the cluster, having three (μ_2-η^3) or four bonds (μ_2-η^4) with the adjacent Ti atoms. The (μ_2-η^3) species on rutile (110) surface are more stable than the (μ_2-η^4) species. On all surfaces studied, the OCO bond angles of the (μ_2-η^3) species are lower than those of the (μ_2-η^4) species. CO_2 does not gain additional charge from the surface upon band-gap illumination, and likely desorbs as neutral CO_2 species. On the other hand, in presence of coadsorbed water, the formation of C_1 species is thermodynamically feasible, resulting in the consumption of the oxygen vacancy. Re-creation of the oxygen vacancy is a key step in the photocatalytic reduction of CO_2 on reduced TiO_2 surfaces. The data from the anatase (010) TiO_2 cluster indicate that the energy required to reform the oxygen vacancy on TiO_2 surfaces exceeds that of a band gap energy-equivalent single UV photon. Therefore, photoreduction on reduced TiO_2 surfaces either is stoichiometric or consumes more than a single UV photon.

4.6 References

1. Ganduglia-Pirovano, M. V.; Hofmann, A.; Sauer, J., Oxygen vacancies in transition metal and rare earth oxides: Current state of understanding and remaining challenges. *Surface Science Reports* **2007,** 62, (6), 219.
2. Haber, J., In *Perspectives in Catalysis*, Thomas, J. M.; Zamaraev, K. I., Eds. Blackwell Scientific Publications: London, 1992; pp 371-386.
3. Greenwood, N. N.; Earnshaw, A., *Chemistry of the Elements*. Pergamon Press: Oxford, 1984; p 954-975.
4. Wiberg, N., *Inorganic Chemistry*. Academic Press: San Diego, 2001; p 1325-1344.
5. Masel, R. I., *Principles of Adsorption and Reaction on Solid Surfaces*. Wiley: New York, 1996; p 108-234, and references cited therein.
6. Indrakanti, V. P.; Schobert, H.; Kubicki, J. D., Quantum mechanical modeling of CO2 interactions with irradiated stoichiometric and oxygen-deficient anatase TiO2 surfaces: Implications for the photocatalytic reduction of CO2. *submitted to Energy & Fuels*.
7. Rasko, J.; Solymosi, F., Infrared spectroscopic study of the photoinduced activation of CO2 on TiO2 and Rh/TiO2 catalysts. *Journal of Physical Chemistry* **1994,** 98, (29), 7147-7152.
8. Chen, L.; Graham, M. E.; Li, G.; Gray, K. A., Photoreduction of CO2 over reactive DC magnetron sputtered TiO2 thin films. *Abstracts of Papers, 234th ACS National Meeting, Boston, MA, United States, August 19-23, 2007* **2007**, CATL-032.
9. Samuel A. French; Alexey A. Sokol; Stefan T. Bromley; C. Richard A. Catlow; Stephen C. Rogers; Frank King; Sherwood, P., From CO2 to Methanol by Hybrid QM/MM Embedding. *Angewandte Chemie* **2001,** 113, (23), 4569-4572.
10. Wu, X.; Selloni, A.; Nayak, S. K., First principles study of CO oxidation on TiO2(110). The role of surface oxygen vacancies. *Journal of Chemical Physics* **2004,** 120, (9), 4512-4516.
11. Bonapasta, A. A.; Filippone, F., Photocatalytic reduction of oxygen molecules at the (100) TiO2 anatase surface. *Surface Science* **2005,** 577, (1), 59-68.
12. Florez, E.; Fuentealba, P.; Mondragon, F., Chemical reactivity of oxygen vacancies on the MgO surface: Reactions with CO2, NO2 and metals. *Catalysis Today* **2008,** 133-135, 216-222.
13. Cotton, F. A.; Wilkinson, G.; Murillo, C. A.; Bochman, M., *Advanced Inorganic Chemistry*. 6th ed.; Wiley: New York, 1999; p 444-495.
14. Bredow, T., Effect of embedding and cluster size on the ab initio study of potassium adsorption at rutile(110). *International Journal of Quantum Chemistry* **1999,** 75, (2), 127-132.
15. de Lara-Castells, M. P.; Krause, J. L., Theoretical study of the UV-induced desorption of molecular oxygen from the reduced TiO2 (110) surface. *Journal of Chemical Physics* **2003,** 118, (11), 5098-5105.

16. Henderson, M. A., Evidence for bicarbonate formation on vacuum annealed TiO2(110) resulting from a precursor-mediated interaction between CO2 and H2O. *Surface Science* **1998,** 400, (1-3), 203.
17. Funk, S.; Burghaus, U., Adsorption of CO2 on oxidized, defected, hydrogen and oxygen covered rutile (1 * 1)-TiO2(110). *Physical Chemistry Chemical Physics* **2006,** 8, (41), 4805-4813.
18. Serpone, N.; Salinaro, A.; Emeline, A.; Ryabchuk, V., Turnovers and photocatalysis: A mathematical description. *Journal of Photochemistry and Photobiology A: Chemistry* **2000,** 130, (2-3), 83.
19. Raupp, G. B.; Dumesic, J. A., Adsorption of carbon monoxide, carbon dioxide, hydrogen, and water on titania surfaces with different oxidation states. *Journal of Physical Chemistry* **1985,** 89, (24), 5240-6.
20. Gibson, D. H., Carbon dioxide coordination chemistry: metal complexes and surface-bound species. What relationships? *Coordination Chemistry Reviews* **1999,** 185-186, 335-355.
21. Indrakanti, V. P.; Schobert, H.; Kubicki, J. D., Quantum mechanical modeling of CO2 interactions with irradiated stoichiometric and oxygen-deficient anatase TiO2 surfaces: Implications for the photocatalytic reduction of CO2. *to be submitted to Energy & Fuels* **expected publication in 2009**.
22. Ahlrichs, R.; Bär, M.; Häser, M.; Horn, H.; Kölmel, C., Electronic structure calculations on workstation computers: The program system Turbomole. *Chemical Physics Letters* **1989,** 162, (3), 165.
23. Glendening, E. D.; Reed, A. E.; Carpenter, J. E.; Weinhold, F. NBO Version 3.1.
24. Scott, A. P.; Radom, L., Harmonic Vibrational Frequencies: An Evaluation of Hartree-Fock, Moller-Plesset, Quadratic Configuration Interaction, Density Functional Theory, and Semiempirical Scale Factors. *The Journal of Physical Chemistry* **1996,** 100, (41), 16502-16513.
25. Laaksonen, L., A Graphics Program For The Analysis And Display Of Molecular-Dynamics Trajectories. *Journal of Molecular Graphics* **1992,** 10, (1), 33-&.
26. Bergman, D. L.; Laaksonen, L.; Laaksonen, A., Visualization of solvation structures in liquid mixtures. *Journal of Molecular Graphics & Modelling* **1997,** 15, (5), 301-306.
27. Ramis, G.; Busca, G.; Lorenzelli, V., Low-temperature carbon dioxide adsorption on metal oxides: spectroscopic characterization of some weakly adsorbed species. *Materials Chemistry and Physics* **1991,** 29, (1-4), 425-35.
28. de la Peña O'Shea, V. A.; González, S.; Illas, F.; Fierro, J. L. G., Evidence for spontaneous CO2 activation on cobalt surfaces. *Chemical Physics Letters* **2008,** 454, (4-6), 262.
29. Papai, I.; Mascetti, J.; Fournier, R., Theoretical Study of the Interaction of the Ti Atom with CO2: Cleavage of the C-O Bond. *J. Phys. Chem. A* **1997,** 101, (24), 4465-4471.
30. Busca, G.; Lorenzelli, V., Infrared spectroscopic identification of species arising from reactive adsorption of carbon oxides on metal oxide surfaces. *Materials Chemistry* **1982,** 7, (1), 89-126.

31. Indrakanti, V. P.; Schobert, H. H.; Kubicki, J. D., Quantum Chemical Modeling of Ground States of CO2 Chemisorbed on Anatase (001), (101), and (010) TiO2 Surfaces. *Energy & Fuels* **2008,** 22, (4), 2611-2618.
32. Emeline, A. V.; Kataeva, G. V.; Panasuk, A. V.; Ryabchuk, V. K.; Sheremetyeva, N. V.; Serpone, N., Effect of surface photoreactions on the photocoloration of a wide band gap metal oxide: Probing whether surface reactions are photocatalytic. *Journal of Physical Chemistry B* **2005,** 109, (11), 5175-5185.
33. Wilson, J. N.; Senanayake, S. D.; Idriss, H., Carbon coupling on titanium oxide with surface defects. *Surface Science* **2004,** 562, (1-3), L231-L237.
34. Wang, R.; Hashimoto, K.; Fujishima, A.; Chikuni, M.; Kojima, E.; Kitamura, A.; Shimohigoshi, M.; Watanabe, T., Light-induced amphiphilic surfaces. *Nature* **1997,** 388, (6641), 431.

Chapter 5

Experimental studies of CO_2 photoreduction : Catalyst syntheses and EPR studies

5.1 Abstract

This chapter describes experimental studies of CO_2 photoreduction comprising catalyst syntheses, photoreduction experiments and in situ electron paramagnetic resonance (EPR) studies of TiO_2 catalysts. Because the primary controlling factor in any photocatalytic process is the electron-hole recombination, studies using lanthanide (Ln)-doped TiO_2 would indicate the role of the dopants in affecting activity towards CO_2 photoreduction. In situ pulsed-EPR experiments on calcined TiO_2 samples provide evidence for surface electron and hole-centers on TiO_2. However, contrary to expectations, no additional paramagnetic centers created due to lanthanide doping of TiO_2 could be detected in the EPR experiments. Additionally, irradiating TiO_2 in the presence of CO_2 did not create paramagnetic signals corresponding to the $CO_2^{\bullet\delta-}$ radical anion.

5.2 Introduction

The previous chapters of this thesis addressed computational studies to understand the initial steps of the photoinduced conversion of CO_2 to fuels. In addition to understanding the first steps of CO_2 photoreduction, current research on TiO_2 photocatalysis has also been focused on improving the efficiency of the photogenerated

electron hole pair separation. Because a majority of the photogenerated-charge carriers recombine in a very short time period, any photocatalytic process that uses either of these species to do useful chemical work would greatly benefit from their effective trapping and separation. Direct recombination of free carriers occurs on a time scale (ps) much faster than interfacial electron transfer processes[1]. The free carriers left over from this reaction are trapped by the surface and bulk of the semiconductor. These trapped carriers can diffuse thermally from the traps and recombine with the opposite charges.

Recent photoluminescence studies [2] have shown that oxygen vacancies created by lanthanide doping contribute to the photocatalytic activity of doped titania. Lanthanide doping was also shown to result in a red-shift of the TiO_2 band gap and therefore, has the potential to absorb a greater portion of the visible light. Additionally, lanthanide species also have been proposed to act as Lewis acids and aid in the enhanced adsorption of organic species on the TiO_2 surface. The role of lanthanide doping in creating such active sites/states mediating CO_2 photoreduction is unknown.

Electron paramagnetic resonance (EPR) is defined as the form of spectroscopy concerned with transitions between magnetic energy levels of electrons having a net spin and orbital angular momentum[3]. Essentially, an unpaired electron placed in a magnetic field can align itself parallel or anti-parallel to the field. This results in two energy states which the electron can access, and when the field is varied, the electron can undergo transitions between the two energy levels. The energy associated with this transition is given as $\Delta E = h\nu = g\mu_B B_o$, where h represents the Planck constant, ν the frequency of the microwave cavity, g the Landé *g*-factor, μ_B the Bohr magneton, and B_o represents the magnetic field strength. In practice, the *g*-factor characterizes the local environment

around the unpaired electron. A rigorous discussion of the quantum physics involved electron spin (paramagnetic) resonance is provided by Jen[4].

Through EPR spectroscopy[5] and semi empirical calculations[6], it has been shown that a majority of the photogenerated electrons on undoped anatase surfaces are trapped deep in the bulk solid, whereas the holes are available for oxidative surface reactions. In most photocatalytic syntheses of interest, both the charge carriers should be available at the surface. Therefore, the surface should trap electrons as well as holes effectively, but at different sites. Doping TiO_2 creates defect states, which, along with the new surface sites, can affect the photocatalytic activity[7]. Photoelectrochemical studies[8] have shown that the incident photon to current conversion efficiency of rare earth doped TiO_2 is higher than that for the undoped TiO_2, due to efficient electron hole pair separation. It has been proposed [9, 10] that metal ion dopants having half filled electronic shells enhance charge carrier lifetimes in doped TiO_2. Among the lanthanides, La^{3+}, Sm^{3+} and Gd^{3+} have unfilled, partially filled and half-filled f-orbitals respectively. It is not known whether this variation in charge carrier trapping affects the activity towards CO_2 photoreduction.

In preliminary experiments, UV irradiation of La-doped TiO_2 resulted in an EPR signal corresponding to $CO_2^{\bullet-}$ and that for the electron capture by a La^{3+} atom. The use of EPR spectroscopy in understanding the first steps of CO_2 photoreduction can not only identify intermediate species but also provide quantitative information about the dopant-induced charge carrier trapping in lanthanide-doped titania.

5.3 Experimental Methods

5.3.1 Catalyst Synthesis

Sol-gel lanthanide-doped TiO_2 catalysts were synthesized according to Xu et al.[7] The step-wise procedure is shown in Figure **5-1**. All reagents used were analytical grade. Briefly, tetrabutyl orthotitanate ($Ti(OBu)_4$) was hydrolyzed with ethanol (EtOH) in the presence of an acid catalyst (HNO_3). Water was added to the solution to promote the condensation reactions leading to the sol formation. A measured quantity of the lanthanide nitrate salt was added with the water, and the sol was aged for 48 hours, followed by subsequent drying and calcinations steps. 0-1.5 % w/w La^{3+}-doped TiO_2, 0.5 % w/w Gd^{3+}- and Sm^{3+}-doped TiO_2 were synthesized in this manner. Both supported and powder catalysts were tested. Glass plate-supported catalysts were prepared by the evaporation of a slurry containing 60-70 mg of the catalyst in 10 ml ethanol, followed by 3 h calcination at 773 K.

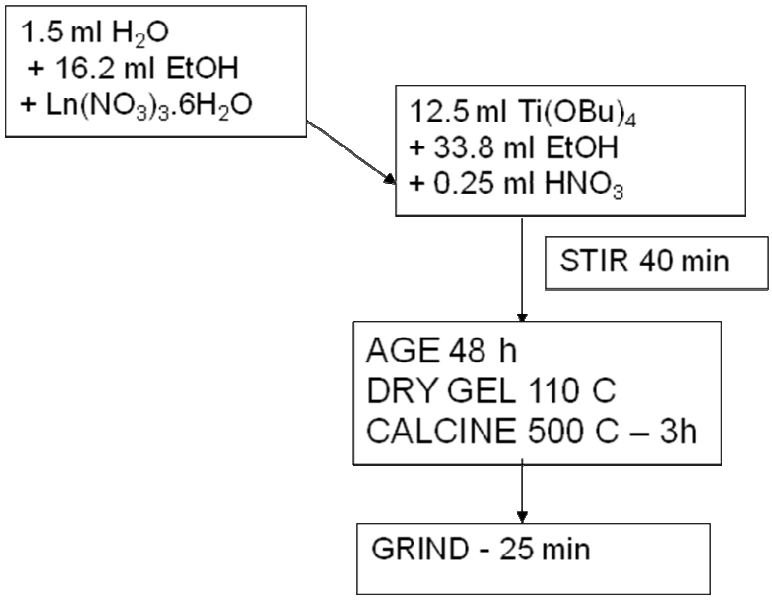

Figure **5-1**: Procedure for the preparation of rare earth-doped TiO_2

5.3.2 X-ray diffraction (XRD) Characterization and Photoreactions

XRD spectra of La-doped TiO_2 were obtained using a 1050 XRD (Philips Analytical, Netherlands) attached to a x-ray generator (Hilton Brooks, UK) producing copper Kα radiation at a wavelength of 0.15418 nm.

Preliminary photoreactions were performed at the University of Nottingham on a continuous flow photoreactor with five 8 W mercury lamps shown in Figure **5-2**. The inlet gases were controlled with flow controllers to estimate the CO_2:H_2O ratios. Experiments at Penn State were performed in a stainless steel vessel having a Teflon sleeve and quartz windows shown in Figure **5-3**. An Oriel 200 W mercury-xenon (Hg-Xe) lamp was used as the light source. The outlet products were analyzed in a gas chromatograph with a flame ionization detector (GC-FID).

5.3.3 EPR Experiments

X-band continuous wave (CW) and pulsed-EPR experiments were acquired with an ESP580 Bruker X-band (~9.5 GHz) spectrometer, at the Regional Center for Pulsed EPR, Binghamton University, State University of New York. Field sweeps 2000–3500 G were acquired at 1024 points with 100 kHz field modulation. Spectra were acquired at 20 K employing an Oxford CF935 liquid helium cryostat and ITC temperature controller (to 1% of the desired temperature). Sol-gel precalcined (773 K, 1h) TiO_2 samples (60-80 mg, both undoped and lanthanide doped) were degassed at 17 mTorr for ca. 20 minutes and flame-sealed in quartz vials. These vials were irradiated both in situ (during the EPR experiments at 20 K) and ex situ (1 h irradiation at at room temperature) by an Oriel 200 W Hg-Xe ultraviolet (UV) lamp using a light guide. Samples with CO_2 sealed over the catalyst were also studied. The following samples were studied: (a) Undoped TiO_2 (T1), (b) 0.5 % w/w La-doped TiO_2 (L1), (c) 0.5 % w/w Sm-doped TiO_2 (S1), (d) calcined undoped TiO_2 (T2).

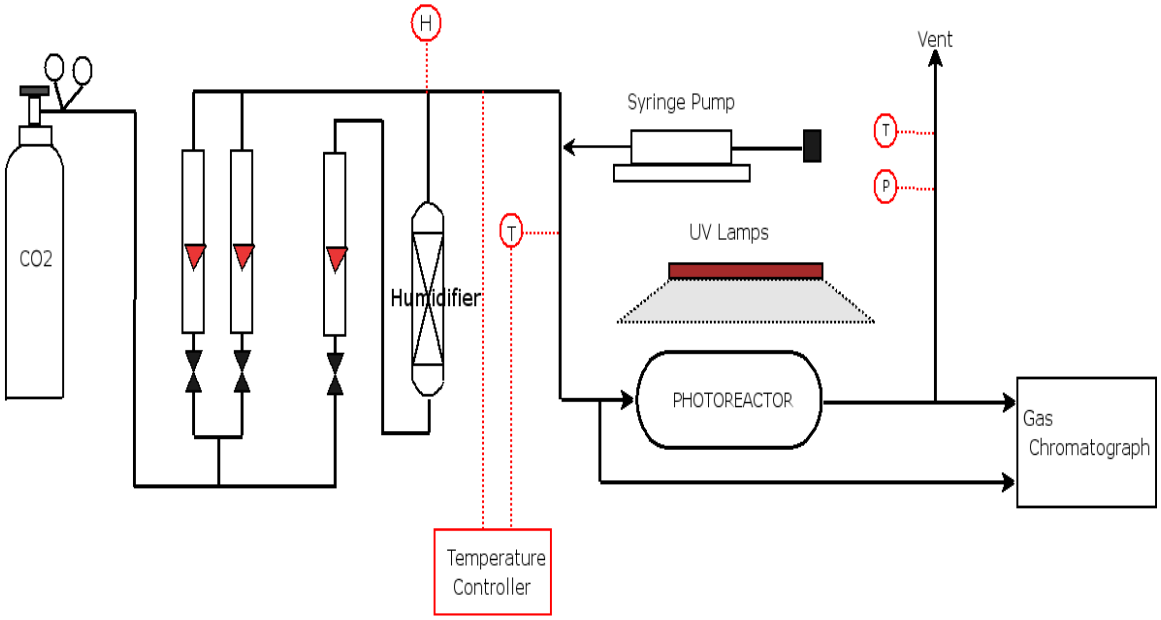

Figure 5-2: Experimental setup used for photoreactions at the University of Nottingham

Figure 5-3: Experimental setup for photoreactions at Penn State.

5.4 Results

5.4.1 XRD characterization and Photoreactions

X-ray diffraction patterns of sol-gel La-doped and undoped TiO_2 shown in Figure 5-4 indicate that anatase constitutes the dominant phase, consistent with that observed by other workers[11]. Photoreduction experiments were performed in a continuous gas-solid photoreactor (CO_2 flow rate: 600 ml/min) at room temperature (operating at an inlet temperature of 373 K), at near atmospheric pressure (111 kPa) and with 600 ml/min flow of CO_2. Methane was identified as a photoproduct. Blank tests with nitrogen, light and without catalyst showed that the reaction was indeed photoinitiated. As shown in Figure 5-5, the ordinate (GC peak areas per mg of catalyst weight) indicates the concentration of methane produced in the outlet. The abscissa is labeled with sample conditions at various times. Increasing the water to CO_2 ratio leads to a monotonic decrease of the amount of CH_4 formed, which indicates that water likely competes with CO_2 for the active sites.

However, further tests at Penn State revealed that the use of ethanol for coating TiO_2 powder on the glass plates led to the CH_4 being detected in the flame ionization detector. Experiments in 2 ml vials sealed with CO_2 and water did not produce methane. Likely pathways for the formation of methane include the photooxidation of residual acetate groups formed by the oxidation of ethanol, as shown Scheme 5.1.

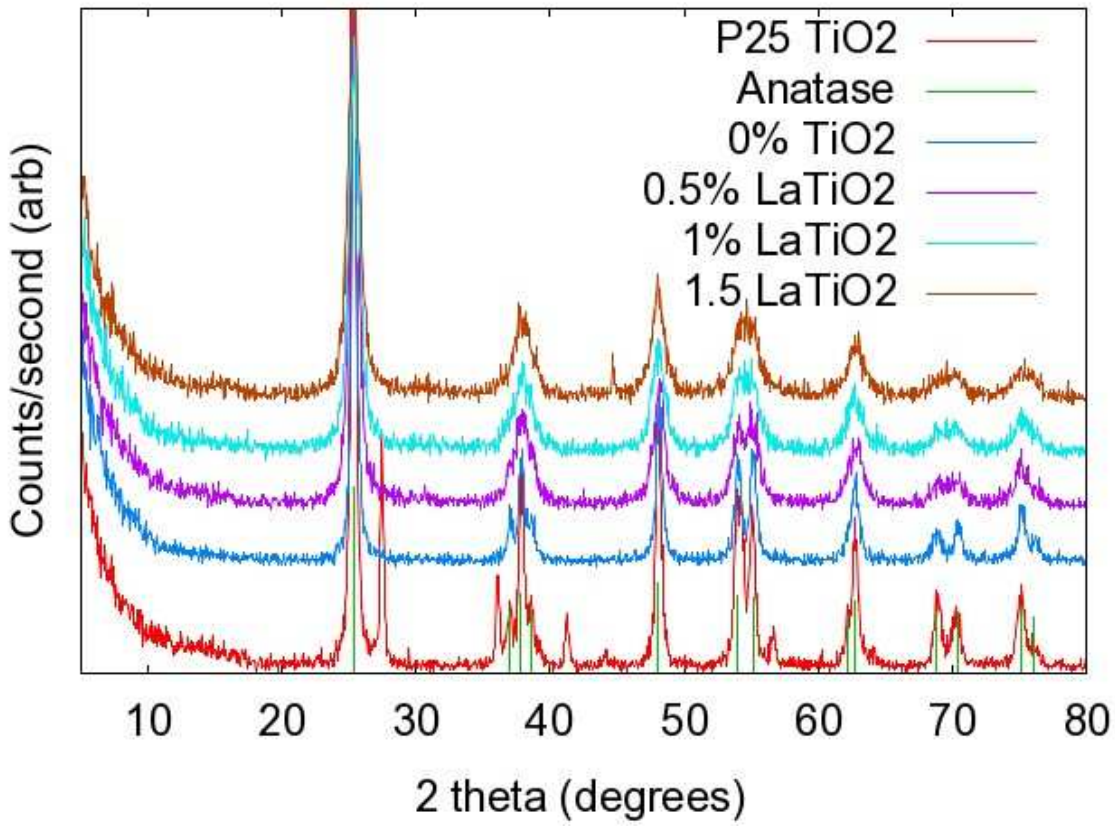

Figure **5-4**: XRD spectra of La-doped TiO_2 compared with anatase and P25 TiO_2

Reactions involving CO_2 reduction are highly endergonic. On the other hand, acetic acid oxidation to produce CH_4 and CO_2 is exergonic. Photodecomposition of acetic acid to CH_4 and CO_2 is well studied in the literature[12]. Further tests are therefore required to estimate the catalytic activity of these materials.

The lanthanide-doped catalyst became slightly yellow at the end of each run; this coloration is lost after exposure to laboratory conditions for ~ 1-2 h. This photocoloration was subsequently investigated in using EPR spectroscopy.

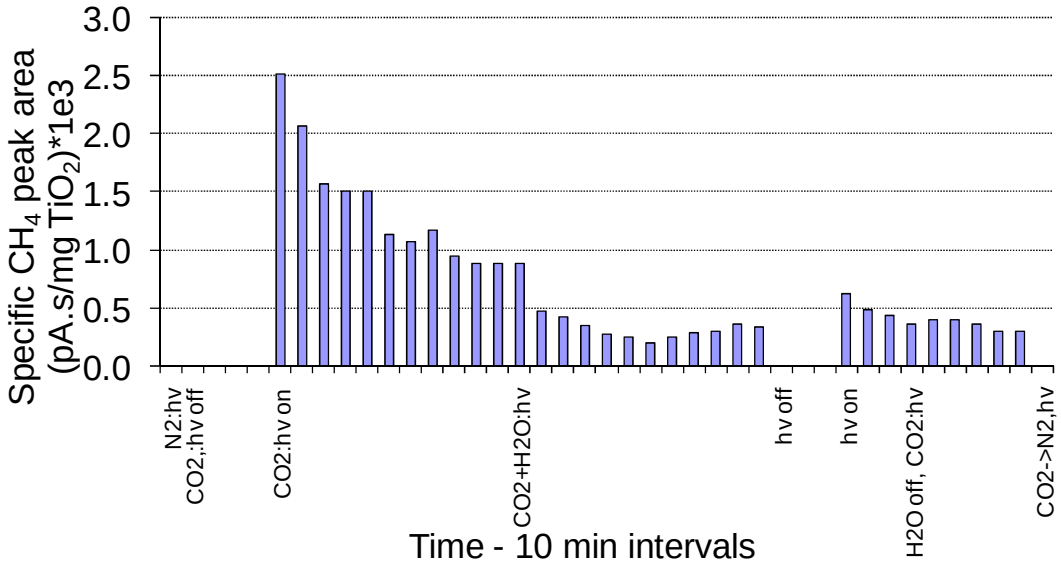

Figure **5-5**: Results using 2.5% w/w La-TiO_2-coated glass plates in the continuous flow reactor. Although methane is evolved as a photoproduct, further tests show that this is likely due to contamination by the ethanol used in catalyst synthesis and coating.

		ΔG_r^0, kJ/mol	**5.1**
$CH_3COOH + CO_2 + H_2O$	$\longrightarrow$ $3\ CO + 3\ H_2 + O_2$	609.88	
CO_2	$\longrightarrow$ $CO + 1/2\ O_2$	257.19	
CH_3COOH	$\longrightarrow$ $CH_4 + CO + 1/2\ O_2$	202.01	
$CH_3COOH + CO_2$	$\longrightarrow$ $CH_4 + 3\ CO$	559.16	
$C_2H_5OH + CO_2$	$\longrightarrow$ $3/2\ CO + 3/2\ CH_4 + 3/4\ O_2$	447.74	
$CH_3COOH + CO_2 + H_2O$	$\longrightarrow$ $3\ CO + 3\ H_2 + O_2$	609.88	
CH_3COOH	$\longrightarrow$ $CH_4 + CO_2$	-55.18	

5.4.2 EPR Experiments

As-synthesized, uncalcined, flame-sealed undoped TiO_2 samples (T1) exhibited photocoloration lasting 1-2 days at room temperature subsequent to room temperature irradiation. Pulsed-EPR experiments on these uncalcined samples indicated an EPR signal at $g \approx 1.93$. However, upon calcination in air at 773 K for 1h and subsequent flame-sealing, photocoloration was not visible upon room temperature irradiation. On the other hand, as shown in Figure **5-6**, X-band pulsed-EPR spectra of such calcined TiO_2 catalysts (T2) measured at 20 K presented in show signals at $g \approx 1.93$, although at a largely decreased level compared to the uncalcined samples. Further in situ irradiation of the sample at 20 K resulted in the growth of an additional signal at $g \approx 2.01$, increasing with the time of irradiation. Upon switching the lamp off, the signal at $g \approx 2.01$ decreased and quickly reached a steady state value, as shown in Figure **5-6**.

In the next phase of this study, in situ pulsed-EPR experiments were performed on calcined TiO_2 in the presence of 3 Torr CO_2. The results shown in Figure **5-7**, indicate that the EPR signals obtained are similar to those without CO_2. The lack of additional EPR signals indicates that CO_2 does not undergo electron transfer from calcined TiO_2 surfaces at 20 K or that the intermediates generated are diamagnetic. Pulsed-EPR experiments with uncalcined 0.5% w/w La-doped TiO_2 (L1) and 0.5% w/w Sm-TiO_2 (T1) also exhibited a signal at $g \approx 1.93$, but no additional signals after 20 minutes of room temperature irradiation.

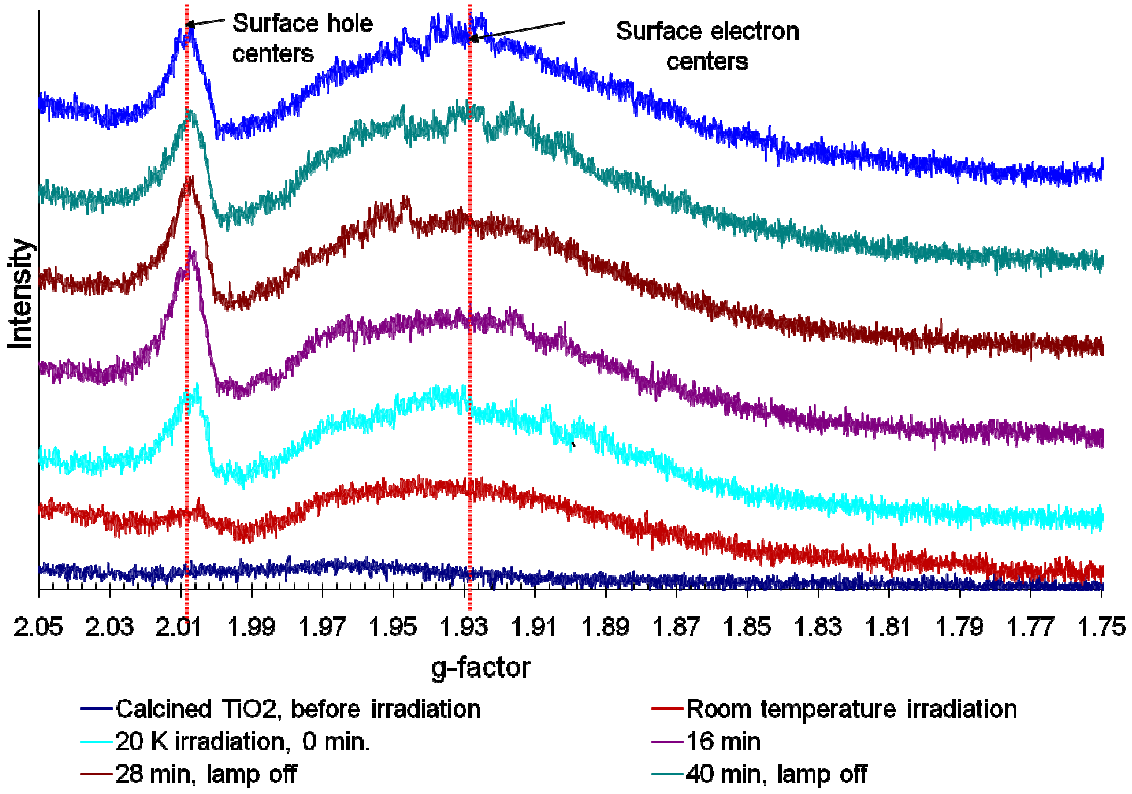

Figure **5-6**: X-band pulsed-EPR spectra of calcined sol-gel TiO_2 at 20 K.

What inferences can be drawn from the EPR data? Hurum et al.[5] assigned the EPR signal corresponding to $g \approx 1.93$ to anatase surface trapping sites. This is consistent with the anatase bulk structure observed across La-doped and undoped TiO_2 samples shown in Figure **5-4**. Additionally, the signal corresponding to $g \approx 2.01$ was assigned to surface hole-trapping sites on titania[5, 13].Together, these enable us to put together a picture of electron and hole-trapping in TiO_2.

Firstly, most of the electrons and holes formed upon irradiation were trapped at various surface trapping sites. Degassed TiO_2 samples, as well as samples exposed to CO_2 exhibit similar signals in pulsed-EPR spectroscopy. Only surface electron and hole-trapping centers were observed in the EPR experiments. The signals corresponding to

lattice or bulk trapping centers[5] were not observed. Additionally, under the experimental conditions, paramagnetic C-species (ex: $CO_2^{\bullet\delta-}$) formed by electron transfer to CO_2 from the TiO_2 surface were not detected. This leads us to conclude that either electron transfer to CO_2 did not occur, or that the intermediate species formed are diamagnetic.

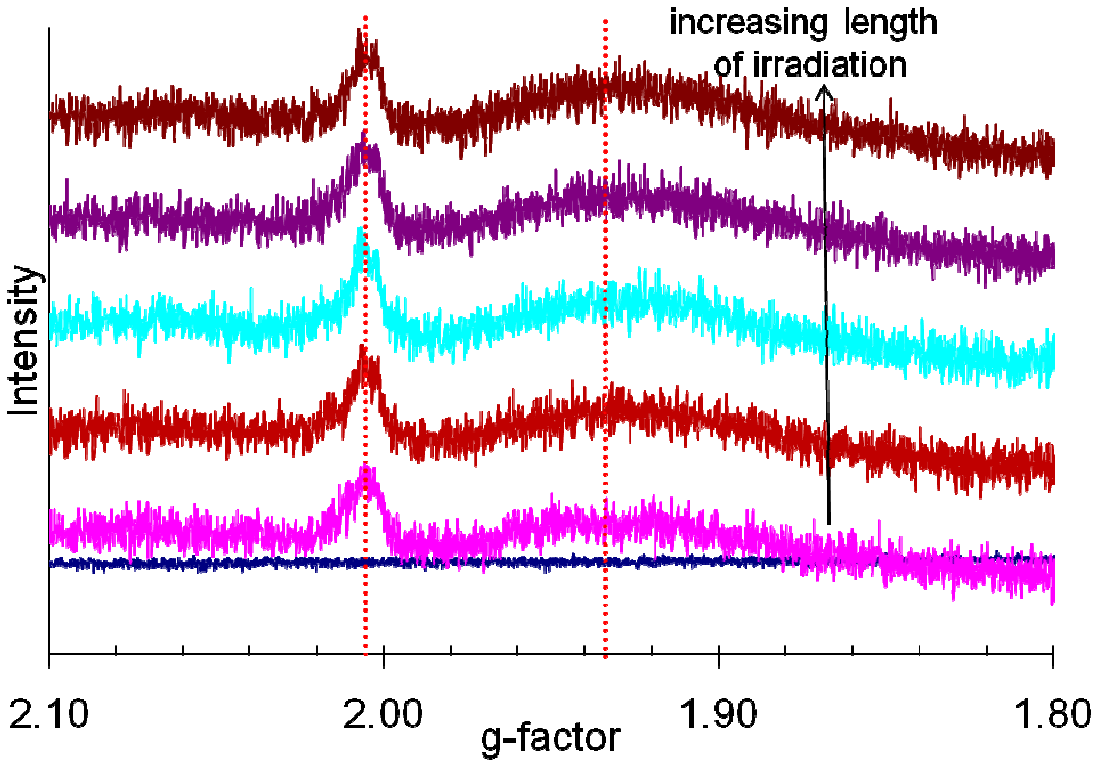

Figure 5-7: X-band pulsed-EPR spectra of calcined sol-gel TiO_2 and 3 Torr CO_2 at 20 K. The EPR signals at $g \approx 1.93$ and $g \approx 2.01$ are similar to those shown in Figure 5-6.

Secondly, because both lanthanide-doped (L1, S1) and undoped-TiO_2 (T1, T2) samples exhibit similar signals, it is likely that electron-trapping centers created due to lanthanide doping were not probed by EPR spectroscopy under the experimental conditions chosen.

5.5 Conclusions and Future Work

La, Gd- and Sm-doped TiO_2 were prepared using a sol-gel synthesis. The sol-gel TiO_2 consisted primarily of anatase. Evidence for photoreduction of CO_2 during preliminary photoreduction studies was not found. Contrary to expectations, lanthanide-doping of TiO_2 did not create additional paramagnetic centers which could be probed by EPR spectroscopy. On the other hand, surface electron and hole-trapping sites on undoped and doped TiO_2 could be observed using pulsed-EPR spectroscopy. The presence of CO_2 did not result in the generation of additional paramagnetic centers on the undoped TiO_2 catalyst. Therefore, electron transfer from calcined TiO_2 to CO_2 likely does not occur under experimental conditions chosen (20 K, 3 Torr CO_2).

Further CO_2 photoreduction studies as well as EPR experiments on TiO_2 calcined at various temperatures will not only enable a better understanding of the photoactivity of lanthanide-doped TiO_2 but also provide insights into the nature of oxygen vacancies in activating CO_2.

5.6 References

1. Colombo, D. P., Jr.; Bowman, R. M., Does Interfacial Charge Transfer Compete with Charge Carrier Recombination? A Femtosecond Diffuse Reflectance Investigation of TiO2 Nanoparticles. *Journal of Physical Chemistry* **1996,** 100, (47), 18445-18449.
2. Jing, L. Q.; Sun, X. J.; Xin, B. F.; Wang, B. Q.; Cai, W. M.; Fu, H. G., The preparation and characterization of La doped TiO2 nanoparticles and their photocatalytic activity. *Journal of Solid State Chemistry* **2004,** 177, (10), 3375-3382.
3. McNaught, A. D.; Wilkinson, A.; Nic, M.; Jirat, J.; Koskata, B. IUPAC Compendium of Chemical Terminology. http://dx.doi.org/10.1351/goldbook.E02005 (3/12/2009).

4. Jen, C. K., Electron spin resonance studies of trapped radicals. In *Formation and Trapping of Free Radicals*, Bass, A. M.; Broida, H. P., Eds. Academic Press: New York, London, 1960; pp 213-225.
5. Hurum, D. C.; Gray, K. A.; Rajh, T.; Thurnauer, M. C., Recombination Pathways in the Degussa P25 Formulation of TiO2: Surface versus Lattice Mechanisms. *Journal of Physical Chemistry B* **2005,** 109, (2), 977-980.
6. Bredow, T.; Jug, K., SINDO1 Study of Photocatalytic Formation and Reactions of OH Radicals at Anatase Particles. *Journal of Physical Chemistry* **1995,** 99, (1), 285-91.
7. Diebold, U., The surface science of titanium dioxide. *Surface Science Reports* **2003,** 48, (5-8), 53-229.
8. Wang, Y.; Cheng, H.; Zhang, L.; Hao, Y.; Ma, J.; Xu, B.; Li, W., The preparation, characterization, photoelectrochemical and photocatalytic properties of lanthanide metal-ion-doped TiO2 nanoparticles. *Journal of Molecular Catalysis A: Chemical* **2000,** 151, (1-2), 205.
9. Choi, W. Y.; Termin, A.; Hoffmann, M. R., The Role Of Metal-Ion Dopants In Quantum-Sized Tio2 - Correlation Between Photoreactivity And Charge-Carrier Recombination Dynamics. *Journal of Physical Chemistry* **1994,** 98, (51), 13669-13679.
10. Xu, A.; Gao, Y.; Liu, H., The preparation, characterization, and their photocatalytic activities of rare-earth-doped TiO2 nanoparticles. *Journal of Catalysis* **2002,** 207, (2), 151-157.
11. Ranjit, K. T.; Willner, I.; Bossmann, S. H.; Braun, A. M., Lanthanide Oxide Doped Titanium Dioxide Photocatalysts: Effective Photocatalysts for the Enhanced Degradation of Salicylic Acid and t-Cinnamic Acid. *Journal of Catalysis* **2001,** 204, (2), 305-313.
12. Muggli, D.; Keyser, S.; Falconer, J., Photocatalytic decomposition of acetic acid on TiO2. *Catalysis Letters* **1998,** 55, (3), 129.
13. Micic, O. I.; Zhang, Y.; Cromack, K. R.; Trifunac, A. D.; Thurnauer, M. C., Trapped holes on titania colloids studied by electron paramagnetic resonance. *The Journal of Physical Chemistry* **1993,** 97, (28), 7277-7283.

Chapter 6

Summary and Future Work

6.1 Summary

CO_2 utilization has a significant role in mitigating CO_2 emissions, especially in comparison to other means of CO_2 abatement. The conversion of CO_2 to fuels using solar energy is one of the "grand challenges" for a variety of scientific disciplines. Significantly increased specific rates (~tens of millimoles CO_2 converted/g-TiO_2/h) under visible light irradiation are required to make this process economically feasible. To achieve this goal, we need to understand how CO_2 reacts on irradiated TiO_2 surfaces. Knowledge of both collective and local factors is required to understand surface photocatalytic mechanisms and develop efficient and selective photocatalysts.

Using DFT calculations, we have modeled the ground states of CO_2 on $Ti_2O_9H_{10}$ clusters from the anatase (010), (101) and (001) surface planes. The results indicate that the dominant control over surface reactivities is local in nature to a first approximation. Additionally, the fact that pairs of vibrational frequencies of CO_2 species modeled using small (two Ti-atom) clusters agree with experimental FT-IR (C-O) stretch frequencies indicates that the cluster approximation is a useful tool to study localized phenomena on TiO_2 surfaces. Existing mechanisms proposed for CO_2 photoreduction do not indicate the state of CO_2 adsorbed on TiO_2. This is important, because if the interaction between the surface atoms and CO_2 is very strong, CO_2 becomes irreversibly chemisorbed on the

surface, whereas weak interactions at large inter-atomic distances will not result in efficient charge transfer from the photo-excited surface.

The work presented in this thesis points that CO_2 likely does not gain electrons from defect-free, stoichiometric anatase TiO_2. CO_2 photoreduction mechanisms in the literature assume that CO_2 gains electrons from the conduction band of TiO_2. Therefore, the primary interfacial charge transfer event in the photoreduction of CO_2 is not the transfer of electrons from the conduction band of TiO_2. However, our results show that such electron transfer may only be mediated by surface defects. This work therefore underscores the significance of defects such as steps, kinks and vacancies on anatase TiO_2 surfaces in promoting electron transfer to CO_2 in the excited state. CO_2 adsorption on oxygen-deficient rutile and anatase surfaces leads to the formation of negatively charged, bent-CO_2 species which likely desorb as neutral CO_2 under irradiation. In the presence of coadsorbed water, the formation of reduced C_1 species concomitant with the consumption of the oxygen vacancy is feasible on the anatase (010) surface. Re-creation of the oxygen vacancy, however consumes greater energy than that available through the energy of a single near-UV photon. These results therefore point that the photoinduced reactions of CO_2 on reduced anatase TiO_2 surfaces likely involve multiple photons, or are stoichiometric.

Surface electron and hole-trapping sites on undoped and doped TiO_2 were characterized using pulsed-EPR spectroscopy. Contrary to expectations, lanthanide-doping (0.5% w/w) of TiO_2 did not create additional paramagnetic centers which could be probed by EPR spectroscopy to test the hypothesis that lanthanide doping of TiO_2 creates electron traps which enhance photocatalytic activity. The presence of CO_2 did not

result in the generation of additional paramagnetic centers on the undoped TiO_2 catalyst. Therefore, electron transfer from calcined TiO_2 to CO_2 likely does not occur under experimental conditions chosen (20 K, 3 Torr CO_2). Evidence for photoreduction of CO_2 during preliminary photoreduction studies was not found.

6.2 Implications for Future Work

Possible improvements in semiconductor-assisted photocatalytic reduction of CO_2 could be grouped as:

1. Physico-chemical modification of TiO_2: TiO_2 is widely employed as a photocatalyst because it is non-toxic, comparatively cheap and abundant in the Earth's crust. The results presented in this thesis indicate that stoichiometric TiO_2 surfaces likely do not promote electron transfer to CO_2. Oxygen vacancies, created either by modifications[1] such as thermal treatment, cation/anion doping or metal impregnation serve as the sites for CO_2 activation, but this reactivity is likely to be stoichiometric. Any chemical modification of TiO_2 that decreases the energy for the formation of oxygen vacancies could enable the reduction of CO_2 on oxygen vacancies to be catalytic.
2. Choice of semiconductors other than TiO_2: Because the conduction band of TiO_2 is lower in energy compared to the lowest unoccupied molecular orbital (LUMO) of CO_2, other semiconductors such as zinc oxide (ZnO),zinc sulfide (ZnS)[2], silicon carbide (SiC)[3] having conduction band electrons of higher energy could promote electron transfer to CO_2.

3. Physico-chemical modification of CO_2: Instead of modifying TiO_2 by creating oxygen vacancies, as outlined before, an alternate approach would be to modify CO_2, lowering its LUMO compared to the TiO_2 conduction band, or by modifying CO_2 to make it more feasible to gain electrons. Whereas gaseous CO_2 has a negative adiabatic electron affinity, high-level quantum calculations indicate that $(CO_2)_n^{\bullet-}$ clusters have positive electron affinities for $n \geq 4$[4]. Interestingly, Shkrob and Sauer[5] noted that the electron photodetachment spectrum of anions in supercritical CO_2 resembled photoelectron spectra of n=6-9 gas-phase anion clusters $(CO_2)_n^{\bullet-}$. However, this enhanced thermodynamic feasibility of electron transfer to CO_2 is attributed to long-range dispersive effects[4], and not to the overlap of orbitals belonging to various CO_2 molecules. Indeed, Fock et al.[6] note that the overlap of orbitals belonging to neighboring molecules in a molecular crystal such as solid CO_2 is small. Future research should aim at utilizing the knowledge from spectroscopic and computational studies of CO_2 clusters in the gaseous and supercritical state, to design high-rate catalytic systems for CO_2 photoreduction.

The challenges involved in understanding the initial steps of CO_2 photoreduction on TiO_2 are many-fold. From a surface science and catalysis perspective, the fact that electrons from the conduction band of stoichiometric TiO_2 are not likely transferred to CO_2 indicates that future modeling efforts should be focused on examining the reactivity of various defect structures such as kinks, steps and crystallographic shear planes. These studies would greatly benefit by using realistic surface models of such features obtained from single crystal anatase surface studies using techniques such as scanning tunneling microscopy (STM)[7]. Additionally, experimental techniques such as in situ laser flash

photolysis studies using powdered TiO_2 or anatase single crystals (refer to the work of Frei and coworkers[8-10] using isolated-Ti species for examples) are required to provide spectroscopic data to build, and validate the computational models. As indicated in Chapter 4 and Chapter 1, spectroscopic data of CO_2 adsorption on TiO_2 surfaces do not differentiate between anatase and rutile surfaces or various single crystal surfaces. The fact that similar IR frequencies can be obtained for the carbonate groups of the (010) anatase $Ti_2O_9H_{10}CO_2$ cluster (Figure **2-6**) and the bent-CO_2 species (110) rutile Ti2Vo_110_CO2 clusters (Figure **4-5**) indicates that further experimental studies on well-defined surfaces are needed to develop and validate better models.

Secondly, although the primary control on photoinduced reactivity towards CO_2 seems to be local in nature, periodic calculations of CO_2 surface states on TiO_2 surfaces is required to fully account for the long-range electrostatic interactions between negatively charged CO_2 species and the surface. Thirdly, because large basis sets and high levels of electron correlation are required to model the electron affinity of the carbon dioxide radical anion, the development of computationally inexpensive electronic structure methods capable of treating excited states (such as CAS-DFT[11]) will enable developing better computational models. Therefore, developments in computational chemistry (some of which are outlined in the computational chemistry technology roadmap[12]) are required to enhance our ability to model such surface photoreactions.

Thirdly, the presence of water on the surface significantly affects the reactivity towards CO_2, both on stoichiometric and oxygen-deficient surfaces. For example: A theoretical study by Markovits et al.[13] found that while CO_2 interacted weakly with the pristine rutile surface, the presence of hydroxyl groups on the hydrated surface promotes

the formation of adsorbed bicarbonate species. However, in sequentially dosed experiments on an oxygen-deficient rutile (110) surface, preadsorbed CO_2 is displaced by postdosed water, and preadsorbed water blocked subsequent postdosed CO_2 adsorption[14]. Bicarbonate species were formed only in the case of simultaneous dosing of CO_2 and H_2O onto the surface. Therefore, the presence of excess water could inhibit activity towards CO_2 photoreduction. On the other hand, in the presence of noble metal catalysts, hydrogenation of the bicarbonate species could result in potentially more facile means of activating CO_2. Future work therefore needs to address the role of water in influencing activity towards CO_2.

From the previous discussion and Chapter 1, the main factors affecting photocatalytic CO_2 reduction are the electron-hole recombination in semiconductor photocatalysts, and the need for UV radiation, resulting in ineffective utilization of sunlight. However, under limiting intensity conditions, Mitra and Melis[15] note that microalgae could convert 82% of the absorbed solar energy into chemical energy, which is a significant improvement in solar energy utilization compared to semiconductor photocatalysis. Other show-stoppers for photocatalysis include electron transfer to CO_2, and water inhibition of activity. Any improvements in modifying TiO_2 via doping are likely only to be incremental in nature. As outlined in Chapter 1, significant improvements are necessary for a Ti-based CO_2 photoreduction system to be economically feasible. On the other hand, indirect CO_2 utilization technologies which have potential for large scale emission reductions, such as algal biofuels production[16], enzymatic processes for activating CO_2[17], and electrochemical reduction of CO_2 with renewable or carbon-neutral[18] electricity, could be feasible in a shorter time span. Of

these, microalgal biodiesel production using open ponds or photoreactors[19, 20] is being commercialized currently[16]. The production of carbon-neutral fuels from hydrogenation of atmospheric CO_2 and related schemes were discussed by Zeman and Keith[18]. The current state of development of various technologies converting CO_2 to fuels is shown in Figure **6-1**. We note that this is an approximate representation of developments in large-scale CO2 conversion to fuels, and that significant advances in any of these technologies have the potential to alter our energy consumption and production patterns.

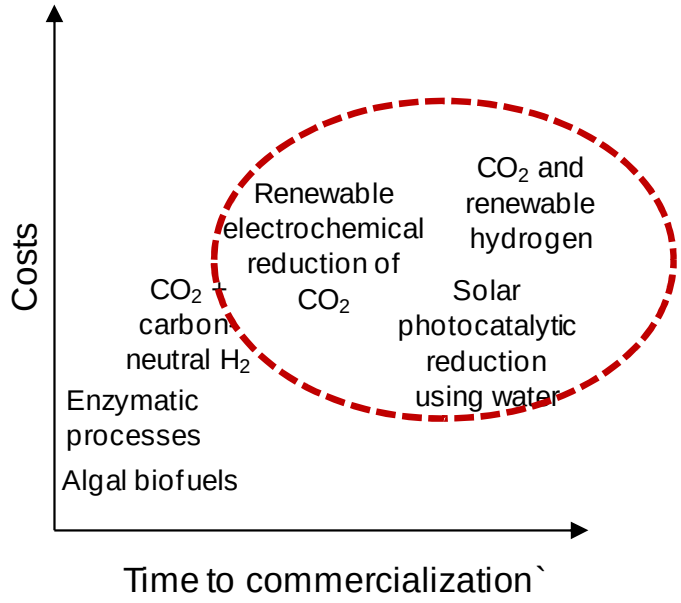

Figure **6-1**: A comparison of the stages of development of various technologies converting solar energy into chemical energy of C_1 compounds.

In conclusion, CO_2 photoreduction to produce fuels is a tantalizing research problem. Significant improvements in the specific rates, drastically lowered electron-hole recombination rates and visible light absorbing photosensitizers are required to make solar conversion of CO_2 to fuels commercially viable. Additionally developments in related fields such as solar PV technologies, semiconductor photocatalysis and

heterogeneous catalysis would also contribute to develop more effective and selective materials that could use solar energy and produce fuels and value-added chemicals from CO_2.

6.3 References

1. Carrettin, S.; Hao, Y.; Aguilar-Guerrero, V.; Gates, B. C.; Trasobares, S.; Calvino, J. J.; Corma, A., Increasing the number of oxygen vacancies on TiO2 by doping with iron increases the activity of supported gold for CO oxidation. *Chemistry-A European Journal* **2007,** 13, (27), 7771-7779.
2. Xu, Y.; Schoonen, M. A. A., The absolute energy positions of conduction and valence bands of selected semiconducting minerals. *American Mineralogist* **2000,** 85, (3-4), 543-556.
3. Inoue, T.; Fujishima, A.; Konishi, S.; Honda, K., Photoelectrocatalytic reduction of carbon dioxide in aqueous suspensions of semiconductor powders. *Nature (London, United Kingdom)* **1979,** 277, (5698), 637-8.
4. Sommerfeld, T.; Posset, T., Electron attachment to CO2 clusters. *Journal of Chemical Physics* **2003,** 119, (15), 7714-7724.
5. Shkrob, I. A.; Sauer, M. C., Jr., Metastable Electrons, High-Mobility Solvent Anions, and Charge Transfer Reactions in Supercritical Carbon Dioxide. *Journal of Physical Chemistry B* **2001,** 105, (19), 4520-4530.
6. Fock, J. H.; Lau, H. J.; Koch, E. E., Electronic band structure of solid CO2 as determined from the hv-dependence of photoelectron emission. *Chemical Physics* **1984,** 83, (3), 377.
7. Gong, X.-Q.; Selloni, A.; Batzill, M.; Diebold, U., Steps on anatase TiO2(101). *Nature Materials* **2006,** 5, (8), 665.
8. Lin, W. Y.; Han, H. X.; Frei, H., CO2 splitting by H2O to CO and O-2 under UV light in TiMCM-41 silicate sieve. *Journal of Physical Chemistry B* **2004,** 108, (47), 18269-18273.
9. Ulagappan, N.; Frei, H., Mechanistic Study of CO2 Photoreduction in Ti Silicalite Molecular Sieve by FT-IR Spectroscopy. *Journal of Physical Chemistry A* **2000,** 104, (33), 7834-7839.
10. Lin, W. Y.; Frei, H., Photochemical CO2 splitting by metal-to-metal charge-transfer excitation in mesoporous ZrCu(I)-MCM-41 silicate sieve. *Journal of The American Chemical Society* **2005,** 127, (6), 1610-1611.
11. Takeda, R.; Yamanaka, S.; Yamaguchi, K., CAS-DFT based on odd-electron density and radical density. *Chemical Physics Letters* **2002,** 366, (3-4), 321.
12. Cochran Jr., H. D.; Cummings, P. T.; Dixon, D. A.; Golab, J. T.; Heffelfinger, G. S.; Peterson, B. K.; Redondo, A.; Thompson, T. B.; Westmoreland, P. R. *Chemical Industry of the Future. Technology Roadmap for Computational Chemistry*; 1998.

13. Markovits, A.; Fahmi, A.; Minot, C., A theoretical study of CO2 adsorption on TiO2. *Theochem-Journal of Molecular Structure* **1996,** 371, 219-235.
14. Henderson, M. A., Evidence for bicarbonate formation on vacuum annealed TiO2(110) resulting from a precursor-mediated interaction between CO2 and H2O. *Surface Science* **1998,** 400, (1-3), 203.
15. Mitra, M.; Melis, A., Optical properties of microalgae for enhanced biofuels production. *Opt. Express* **2008,** 16, (26), 21807.
16. GreenFuel Algae CO2 Recycling Project with Aurantia Enters Second Phase at Spanish Cement Plant. *Global Warming Focus* November 2008, 2008.
17. Peckham, J., Carbon Sciences Unveils Low-Cost CO2-to-Fuel Scheme. *Diesel Fuel* 03/02/2009, 2009.
18. Zeman, F. S.; Keith, D. W., Carbon neutral hydrocarbons. *Philosophical Transactions of the Royal Society A: Mathematical, Physical and Engineering Sciences* **2008**.
19. Chisti, Y., Biodiesel from microalgae. *Biotechnology Advances* **2007,** 25, (3), 294-306.
20. Demirbas, A., Production of Biodiesel from Algae Oils. *Energy Sources Part A-Recovery Utilization And Environmental Effects* **2009,** 31, (2), 163-168.

Appendix A

Supplementary Information for Chapter 2

A.1 Cartesian coordinates for (010), (101) and (001) $Ti_2O_9H_{10}CO_2$ clusters

1. (010) $Ti_2O_9H_{10}CO_2$ B3LYP/6-31+G(d), C_2 symmetry

C	0.000000	0.000000	1.459117
O	0.000000	0.000000	0.103338
Ti	0.000000	2.086187	-0.083187
Ti	0.000000	-2.086187	-0.083187
O	-1.593457	2.691148	0.521129
O	1.593457	-2.691148	0.521129
O	1.714404	2.569436	0.399835
O	-1.714404	-2.569436	0.399835
O	0.317336	4.100836	-1.078930
O	-0.317336	-4.100836	-1.078930
O	-0.217371	1.728734	-1.887242
O	0.217371	-1.728734	-1.887242
O	0.056929	1.150513	1.969115
O	-0.056929	-1.150513	1.969115
H	-1.760594	2.775708	1.474407
H	1.760594	-2.775708	1.474407
H	1.989717	2.355053	1.306674
H	-1.989717	-2.355053	1.306674
H	-1.274068	-4.246561	-0.972406
H	1.274068	4.246561	-0.972406
H	-0.153004	-3.913025	-2.020463
H	0.153004	3.913025	-2.020463
H	0.745393	-0.952823	-2.140065
H	-0.745393	0.952823	-2.140065

2. (101) $Ti_2O_9H_{10}CO_2$ cluster, B3LYP/6-31+G(d) C_1 symmetry

Ti	-0.003660	1.595738	-0.054320
Ti	0.835682	-1.686749	-0.074468
O	1.451952	0.256014	0.050015
O	-0.711555	-0.221300	-0.526086
O	0.274295	-2.195744	1.624602
O	0.899307	-2.426200	-1.740238
O	-1.238983	-2.923479	-0.259049
O	1.930031	2.895813	0.101981
O	-0.122808	2.440391	1.574364

O	-0.037178	2.643864	-1.554477
O	2.592870	-2.093361	0.287666
H	-0.965541	2.380379	2.054087
H	-0.847448	2.703964	-2.086606
H	1.716649	3.408550	0.903029
H	1.821998	3.499480	-0.654761
H	2.381209	0.475271	0.220997
H	3.065306	-2.550933	-0.426502
H	0.178012	-3.013842	-2.018526
H	0.992949	-2.247205	2.276872
H	-1.285734	-3.214600	0.669100
H	-1.987241	-2.285636	-0.368506
C	-2.005248	0.106951	-0.255447
O	-2.011478	1.385518	0.038994
O	-2.923785	-0.692476	-0.292747

3. (001) $Ti_2O_9H_{10}CO_2$ cluster C_2 symmetry

Ti	-0.266557000	-2.211130000	0.113662000
O	0.000000000	0.000000000	0.215391000
Ti	0.266557000	2.211130000	0.113662000
O	0.000000000	2.265462000	1.927734000
O	-0.267456000	3.860682000	-0.500923000
O	2.069324000	2.295510000	0.008126000
O	-2.038957000	2.043448000	0.028662000
O	-2.069324000	-2.295510000	0.008126000
O	0.267456000	-3.860682000	-0.500923000
O	0.000000000	-2.265462000	1.927734000
O	2.038957000	-2.043448000	0.028662000
H	0.415427000	1.604391000	2.503584000
H	2.563944000	2.085929000	-0.800324000
H	0.386699000	4.513988000	-0.793513000
H	-2.303173000	2.059097000	0.964240000
H	-2.255251000	2.923051000	-0.331179000
H	-2.563944000	-2.085929000	-0.800324000
H	-0.386699000	-4.513988000	-0.793513000
H	-0.415427000	-1.604391000	2.503584000
H	2.303173000	-2.059097000	0.964240000
H	2.255251000	-2.923051000	-0.331179000
C	0.000000000	0.000000000	-1.103975000
O	-0.145531000	-1.136290000	-1.662727000
O	0.145531000	1.136290000	-1.662727000

A.2 Unscaled C-O stretch frequencies of the CO_3 group for the (010), (001) and (101) clusters

Table A-1: Unscaled C-O stretch frequencies (cm^{-1}) of the CO_3 group for the (001), (010) and (101) clusters

(001) cluster	711	734	762	830	1082	1428	1641
(010) cluster	693	788	825	1048	1371	1721	
(101) cluster	687	705	777	811	1041	1248	1788

A.3 CO_2 adsorption on the 4-c (110) $Ti_2O_7H_6CO_2$ cluster

The C-O harmonic frequencies of the 4-c (110) $Ti_2O_7H_6CO_2$ cluster (Figure A-1) are 681, 784, 816, 983, 1240, and 1797 cm^{-1}.

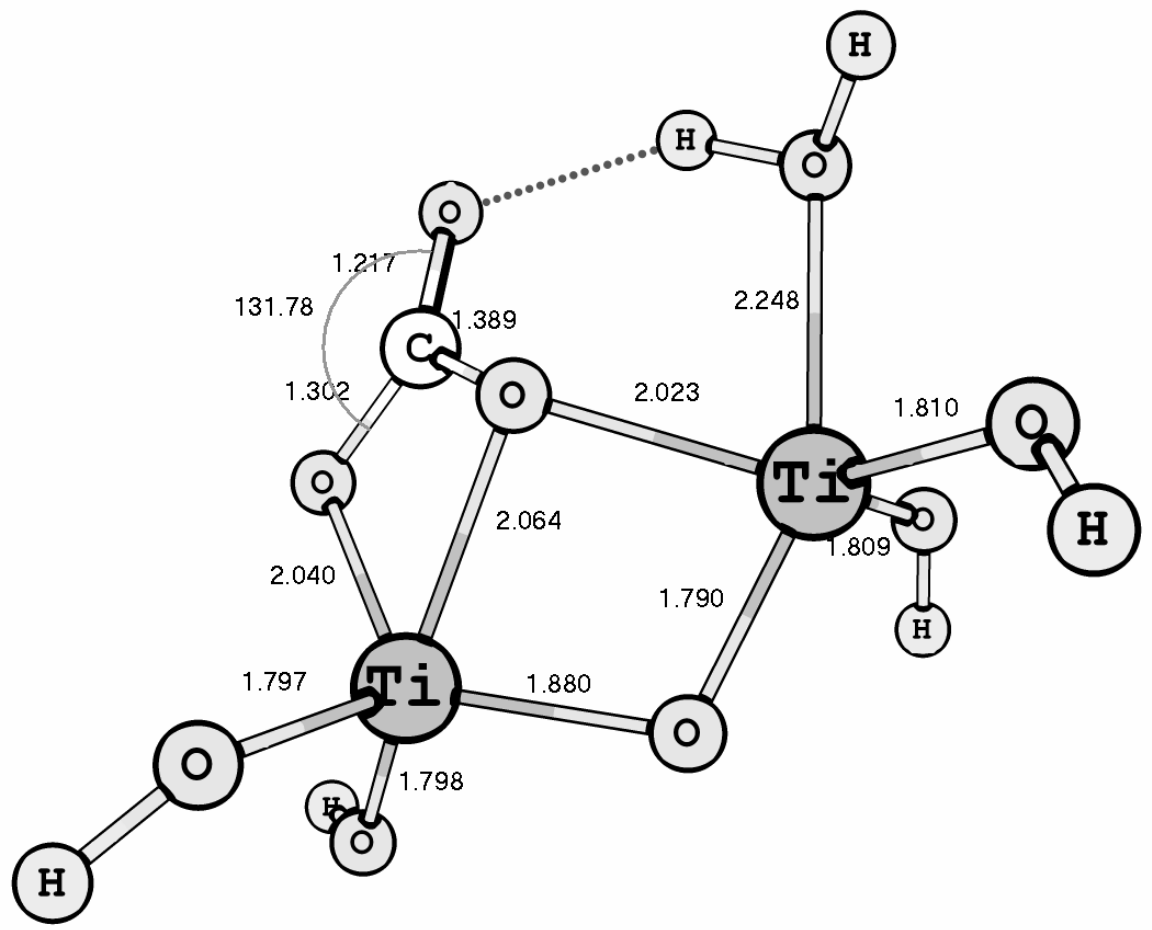

Figure **A-1**: Carbonate formation on the 4-c (110) $Ti_2O_7H_6$ cluster modeled using the B3LYP/6-31+G(d) model chemistry. The distances are in Å, the angles are in degrees.

A.4 Linear CO_2 species

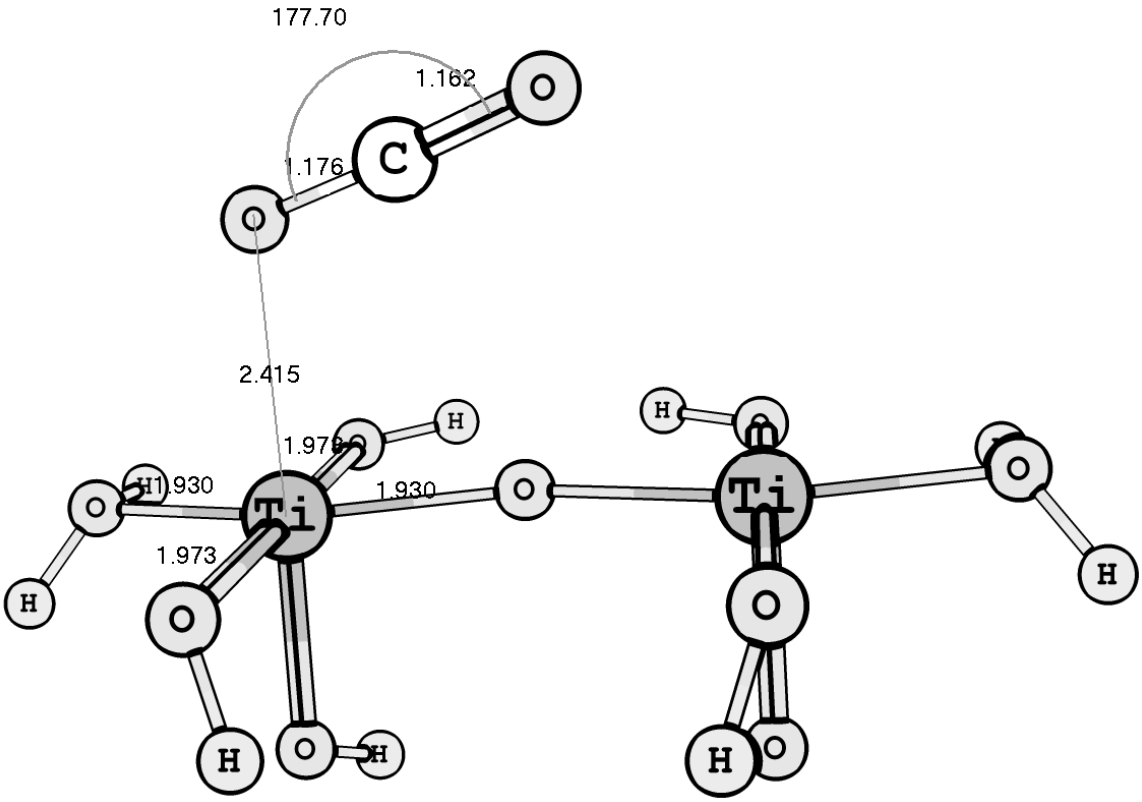

Figure A-2: Geometry of the (010) $Ti_2O_9H_{10}CO_2$: linearly adsorbed CO_2 on a constrained cluster (CO_2, Hs optimized, Ti, O fixed at their lattice positions) at B3LYP/6-31+G(d) with normal optimization criteria

Appendix B

Supplementary Information for Chapter 3

B.1 SAC-CI excitation energies, excited state configurations and canonical molecular orbitals for the (110) Ti-4cCO2 cluster

Occupied molecular orbitals: 36, 38, 39, 40
Virtual orbitals: 45, 46, 47, 48, 49, 51

```
###   1-st  ###          ---   1st state in this spin multiplicity ---
    This state is being used for optimizations.
    Total energy       in au =   -1338.230357
    Correlation energy in au =      -0.302114
    Excitation energy  in au =       0.156906    in eV =       4.269628
  *SINGLE EXCITATION
      40   46     0.59843        40   47    -0.52360
      40   45    -0.42739        40   49    -0.16945
      40   48    -0.15763        39   46    -0.07618
 ###   2-nd  ###          ---   2nd state in this spin multiplicity ---
    This state is being used for optimizations.
    Total energy       in au =   -1338.207997
    Correlation energy in au =      -0.279754
    Excitation energy  in au =       0.179266    in eV =       4.878067
  *SINGLE EXCITATION
      39   46     0.56619        39   47    -0.50828
      39   45    -0.45613        39   48    -0.22526
      39   49    -0.19682        39   42     0.07716
###   3-rd  ###          ---   3rd state in this spin multiplicity ---
    This state is being used for optimizations.
    Total energy       in au =   -1338.199643
    Correlation energy in au =      -0.271401
    Excitation energy  in au =       0.187620    in eV =       5.105389
  *SINGLE EXCITATION
      40   48     0.65227        40   49     0.29576
      38   48    -0.29460        40   46     0.24454
      38   45    -0.23186        40   47    -0.21016
      38   46     0.19203        38   49    -0.17190
      38   47    -0.17186        40   45     0.11474
###   4-th  ###          ---   4th state in this spin multiplicity ---
```

This state is being used for optimizations.
Total energy in au = -1338.192321
Correlation energy in au = -0.264079
Excitation energy in au = 0.194941 in eV = 5.304625
*SINGLE EXCITATION

38	48	0.70018	40	48	0.34024
38	49	0.32488	38	45	0.23637
38	51	-0.21695	40	49	0.16550
36	48	-0.12179	40	45	0.10339

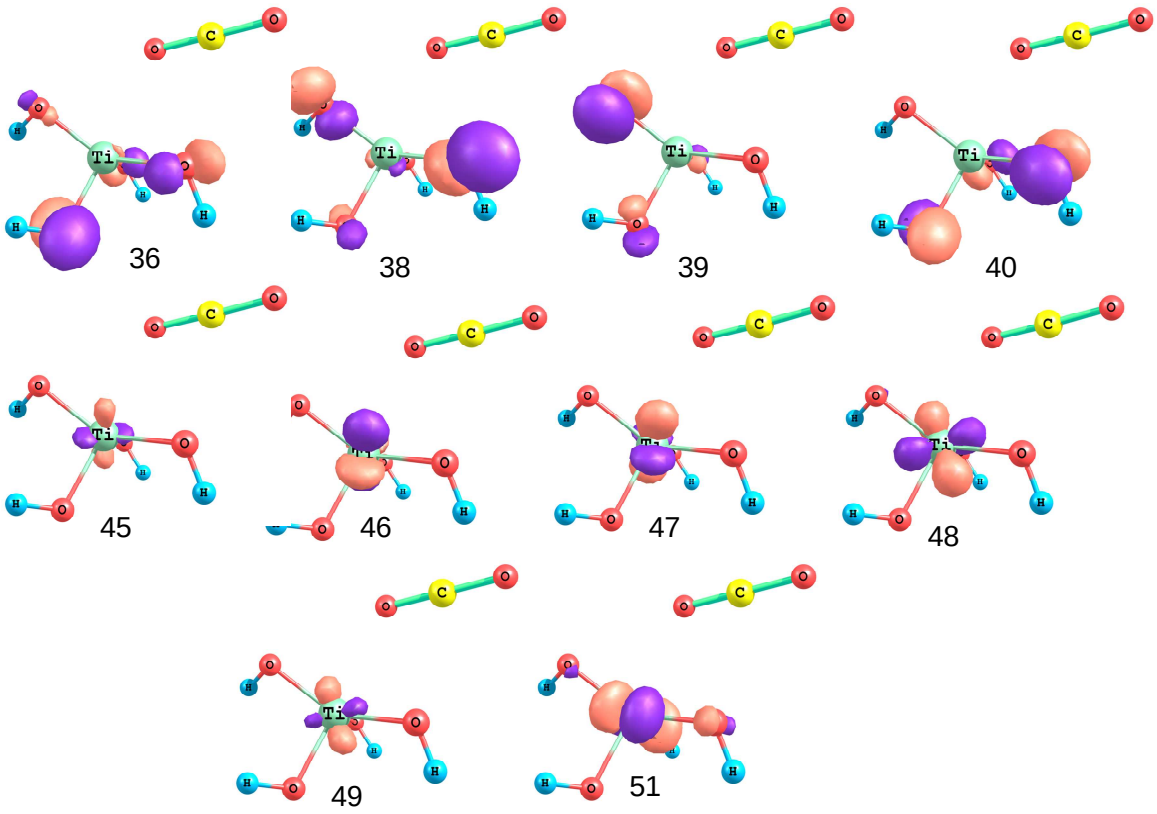

Figure **B-1**: Canonical molecular orbitals of the (110) Ti-4cCO2 cluster, plotted at an isocontour value of 0.1. The majority of the contribution to the unoccupied orbitals (45-51) comes from the Ti 3d atomic orbitals and not π^* C-O orbitals of CO_2.

B.2 SAC-CI excitation energies, excited state configurations and canonical molecular orbitals for the (001) Ti-watCO2 cluster

Occupied molecular orbitals: 39, 40, 42, 43, 44, 45.
Virtual molecular oribtals: 49, 50, 51, 52, 55,

1-st ### --- 1st state in this spin multiplicity ---
This state is being used for optimizations.
Total energy in au = -1414.346902
Correlation energy in au = -0.463357
Excitation energy in au = 0.080368 in eV = 2.186920
*SINGLE EXCITATION
45 50 0.92648 43 50 -0.15529
42 50 -0.13862 45 57 0.06381

2-nd ### --- 2nd state in this spin multiplicity ---
This state is being used for optimizations.
Total energy in au = -1414.335168
Correlation energy in au = -0.451624
Excitation energy in au = 0.092102 in eV = 2.506210
*SINGLE EXCITATION
45 51 0.83527 45 52 0.34076
45 49 -0.21936 43 51 -0.13186
42 51 -0.09760 45 55 0.08353

3-rd ### --- 3rd state in this spin multiplicity ---
This state is being used for optimizations.
Total energy in au = -1414.318595
Correlation energy in au = -0.435051
Excitation energy in au = 0.108674 in eV = 2.957172
*SINGLE EXCITATION
43 50 0.74649 42 50 -0.47262
44 50 -0.29195 41 50 -0.16183
40 50 -0.15325 43 66 0.04690

4-th ### --- 4th state in this spin multiplicity ---
This state is being used for optimizations.
Total energy in au = -1414.311118
Correlation energy in au = -0.427574
Excitation energy in au = 0.116151 in eV = 3.160639
*SINGLE EXCITATION
44 51 -0.66303 43 51 -0.50803
44 52 -0.27438 43 52 -0.19792
44 49 0.17541 39 51 -0.15456
43 49 0.13418 45 51 -0.09109

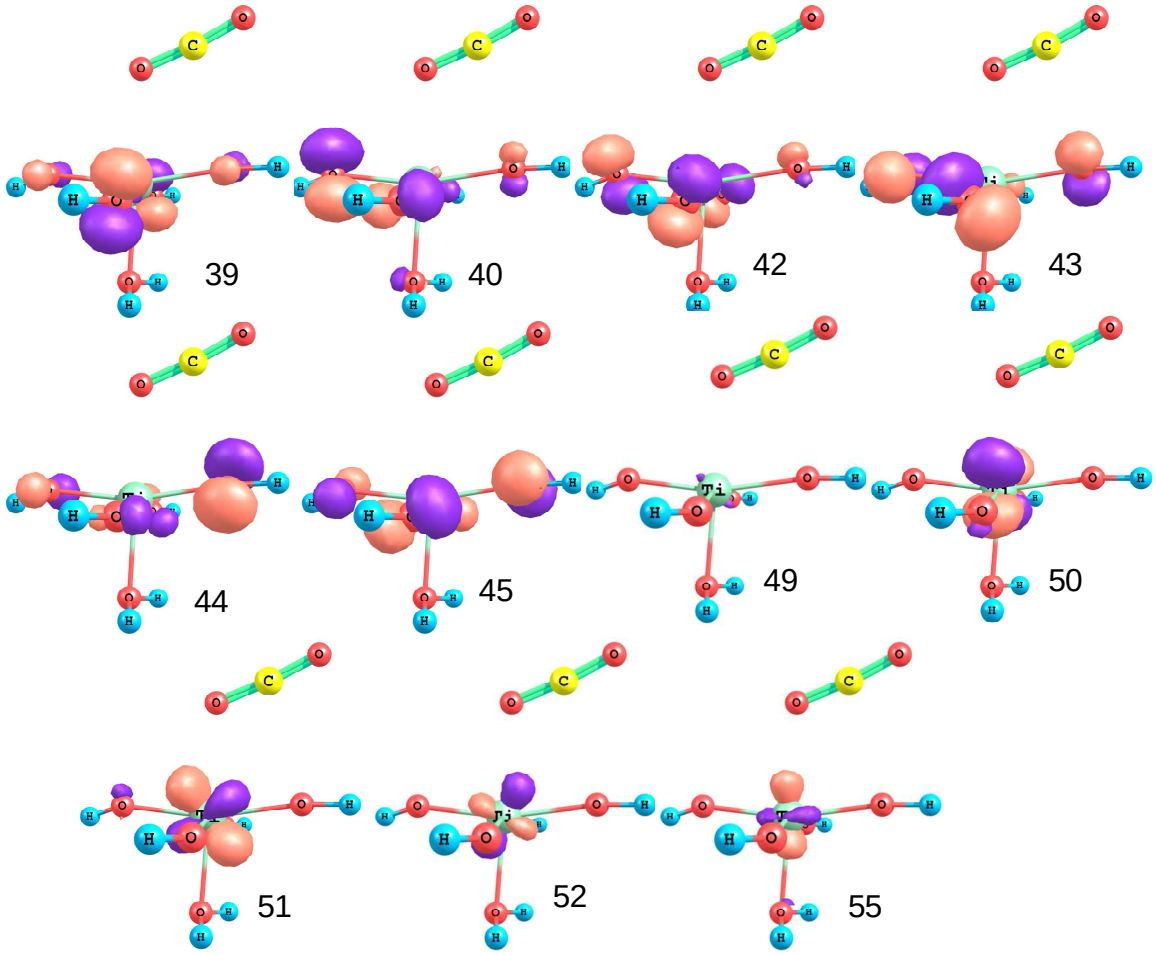

Figure **B-2**: Canonical molecular orbitals of the (001) Ti-watCO2 cluster, plotted at an isocontour value of 0.1. The majority of the contribution to the unoccupied orbitals (50-55) comes from the Ti 3d atomic orbitals and not π^* C-O orbitals of CO_2.

B.3 Cartesian coordinates

1. (110) Ti-4cCO2

Ti	0.835775000	-0.021610000	-0.021729000
O	-0.286638000	-1.280005000	-0.773309000
O	1.100408000	1.743167000	-0.417728000
O	0.828102000	-0.336900000	1.759899000

O	2.482168000	-0.634302000	-0.501411000
O	-1.661897000	0.959653000	0.100869000
C	-2.601018000	0.264187000	-0.010452000
O	-3.550335000	-0.402405000	-0.111941000
H	0.086840000	-2.167956000	-0.619092000
H	2.874208000	0.027539000	-1.092100000
H	0.996853000	-1.291589000	1.803709000
H	1.966689000	1.928636000	-0.002805000

2. (010) Ti6-5cCO2 triplet

O	-4.697765700	16.317841000	6.732270700
O	-5.092846000	13.700209200	5.995672000
Ti	-4.453270100	14.724124000	7.602590400
O	-4.619371800	15.410589900	9.410940100
O	-2.680203100	14.381436700	7.489868100
O	-5.249579600	11.145901200	5.006898300
Ti	-5.000274400	11.782041300	6.709311700
O	-5.151052300	13.134370500	8.479415000
Ti	-4.783427400	13.493594900	10.418245600
O	-5.201286500	14.688214900	11.838293000
O	-2.992117000	11.555497300	6.836587300
O	-2.925871300	13.350995800	10.699541800
O	-4.830287700	11.872585000	11.010022300
O	-4.857499400	10.056179800	7.840660100
Ti	-2.853441800	9.782926300	7.662341100
Ti	-2.894551900	11.388229800	11.306689100
O	-5.006716100	8.063184800	10.601697500
Ti	-3.279755300	8.417096100	10.413082400
C	-7.684983600	12.105097400	8.336026000
O	-8.105899000	12.451935000	9.355669500
O	-7.311665200	11.743363800	7.286913700
H	-4.876000100	13.591659200	5.045415100
H	-4.876000100	15.884339300	10.235802200
H	-3.926901100	16.907293300	6.682394100
H	-4.876000100	11.021983200	4.116497100
H	-4.875999100	14.840372300	12.760925200
H	-2.038902000	15.100472300	7.480498100
H	-2.038902000	11.805851200	6.871803100
H	-2.038902000	13.331558200	10.325842200
H	-4.886248100	7.207571100	11.055394200
O	-2.988000100	8.690498200	6.183920100
O	-2.988000100	10.216205200	9.637960200
O	-2.987999100	11.741913200	13.092000200
O	-1.100000000	11.707943200	11.043019200
O	-1.100000000	10.182234200	7.588980100
O	-2.988001100	8.012940100	8.547194200
O	-2.987999100	9.538648200	12.001235200
O	-1.099998000	8.046910100	10.596171200

O	-2.987998100	6.606499100	11.232428200
H	-2.988002100	7.446248100	7.759945100
H	-2.987998100	9.738930200	12.950333200
H	-0.150902000	11.524736200	11.123944200
H	-1.099998000	7.159617100	10.988103200
H	-0.150900000	8.230115200	10.515247200
H	-2.038899000	6.423294100	11.313352200
H	-0.150902000	9.999028200	7.669905100
H	-2.987999100	12.308606200	13.879249300
H	-2.988000100	8.490216200	5.234822100

3. (101) Ti6-5cCO2

O	-1.007432900	12.769358100	3.698065000
Ti	-1.883910100	11.137118300	3.704557600
O	-1.009807300	7.596801300	1.777471000
O	-0.912541200	7.906072200	5.512512200
Ti	-2.646855400	8.841770400	1.716140600
Ti	-2.707182100	8.840215500	5.647619700
Ti	-1.769163800	6.029985200	1.721396600
Ti	-1.694659200	5.938979400	5.664475900
O	-0.874459800	2.598091800	3.690358700
Ti	-2.347704100	3.619508900	3.700057400
O	-3.321450100	1.875266000	3.688000100
O	-2.444382000	4.078618100	5.576000100
O	-2.444383000	4.078618100	1.800000000
O	-4.493213100	4.036543100	3.688000100
O	-1.862009000	5.541645100	-0.088000000
O	-1.862009000	5.541645100	7.464000100
O	-3.321450100	6.980223100	1.800000000
O	-3.321450100	6.980223100	5.576001100
O	-2.444382000	9.183577200	7.464001100
O	-2.444383000	9.183577200	3.688001100
O	-2.444383000	9.183576200	-0.088001000
O	-4.493212100	9.141501200	5.576002100
O	-1.862010000	10.646602200	1.799999000
O	-1.862009000	10.646602200	5.576001100
O	-3.321450100	12.085182200	3.688000100
O	-4.493213100	9.141501200	1.799998000
O	-1.862009000	5.541645100	3.688000100
H	-1.343684000	1.738816000	3.687999100
H	-2.518454000	3.892537100	0.850902000
H	-2.518453000	3.892537100	6.525098100
H	-4.277326100	2.040196000	3.688000100
H	-1.787940000	5.727726100	-1.037098000
H	-1.787936000	5.727726100	8.413098200
H	-4.851954100	3.135320100	3.688001100
H	-5.300945100	4.573637100	3.688000100
H	-4.277326100	7.145153100	1.800000000

H	-4.277326100	7.145152100	5.576002100
H	-2.518454000	8.997494200	8.413099200
H	-2.518455000	8.997495200	-1.037099000
H	-1.787939000	10.832684200	0.850901000
H	-1.787938000	10.832684200	6.525099100
H	-5.300945100	9.678593200	1.799998000
H	-1.792675000	13.387049200	3.688001100
H	-4.277326100	12.250111200	3.688000100
H	-5.300944100	9.678592200	5.576002100
O	0.594596400	5.309882600	5.387064800
C	1.367285300	5.753779000	4.629333100
O	2.148771400	6.174714900	3.889206600

4. (001) Ti6-5cCO2

Ti	-0.539885700	9.565682000	5.720989400
O	-1.020197800	7.564778200	5.723012400
Ti	-0.408236200	5.478358800	5.497540100
O	0.270301600	5.711374800	7.952486400
Ti	-0.543007100	5.610407200	9.689897000
O	-1.013449900	7.525222800	9.376243800
Ti	-0.503415500	9.514348300	9.449219700
O	-0.048409900	9.466934000	7.494189700
O	-1.098604700	11.370783300	5.676916600
O	-0.543231200	11.328157300	9.461950300
O	-0.191305000	9.348340700	11.292069400
O	0.058448100	5.855137500	11.407809200
O	-0.628768600	3.775670900	9.640892100
O	-0.451466900	3.676885600	6.036461400
O	0.039019600	5.596407300	3.716812900
O	-0.107999600	9.434591000	3.795861900
O	-2.504036900	9.442733800	5.656748600
Ti	-2.840090900	7.515672500	5.793806200
O	-2.412378900	5.606638200	5.530815100
O	-2.468254500	5.624268400	9.576495100
Ti	-2.994393100	7.559165800	9.582812600
O	-2.426233800	9.481836100	9.398322000
O	1.979474300	8.690656600	5.311725700
C	2.136442800	8.491104100	4.167102700
O	2.427397900	8.259916400	3.068351200
H	-0.358871000	9.440001200	2.826902100
H	-0.755133000	12.277098200	5.664000100
H	-0.755131000	12.277098200	9.440000200
H	-0.358870000	9.440000200	12.277098200
H	-0.358871000	5.664000100	12.277098200
H	-0.755130000	2.826902100	9.439999200
H	-0.755130000	2.826902100	5.663999100
H	-0.358872000	5.664001100	2.826902100
O	-3.326913100	7.552000100	11.327999200

O	-4.901588100	7.552000100	9.439998200
O	-3.326912100	7.552000100	7.551999100
O	-3.326912100	7.552001100	3.776000100
O	-4.901588100	7.552001100	5.664000100
H	-2.730371000	10.389098200	9.440000200
H	-2.730372000	10.389098200	5.664000100
H	-2.730370000	4.714902100	5.664000100
H	-2.730371000	4.714902100	9.439998200
H	-4.296912100	7.552000100	7.551998100
H	-4.296912100	7.552001100	3.776000100
H	-3.126630100	7.552001100	2.826902100
H	-5.101871100	7.552000100	10.389097200
H	-5.101870100	7.552001100	4.714902100
H	-3.126631100	7.552000100	12.277097200

5. (010) Ti6(Vo)-5cCO2 –bent singlet

O	-5.115802300	16.182633800	7.108148100
O	-6.417073100	14.795049700	5.098693500
Ti	-5.154839700	14.420938600	6.617782300
O	-4.759258000	13.581046600	8.302711900
O	-3.521281700	14.159439600	5.908130700
O	-7.959378100	13.945552500	3.366954000
Ti	-7.022729000	12.922095900	4.623122000
O	-6.021261800	12.684150400	6.367461300
Ti	-4.861529400	11.532299500	7.683842800
O	-4.060486500	11.458016200	9.382803700
Ti	-5.844581900	10.641416000	2.862786100
Ti	-3.742891700	9.374735500	5.980233100
O	-5.309676900	9.949542700	7.214116400
O	-5.491499700	12.440726400	3.521734700
O	-3.317037800	11.246637700	6.651538700
O	-7.043908500	7.419897600	5.009554600
Ti	-5.609310200	7.789304300	4.052881500
C	-8.013019300	10.964811100	4.307192000
O	-8.479340200	11.823362000	5.169256300
O	-8.471878500	9.921786600	3.923113900
H	-4.288820100	16.584529300	6.786948100
H	-7.056168100	15.272562300	4.507817100
H	-4.018225100	13.441314200	8.936579200
H	-3.129237100	14.682231300	5.204944100
H	-8.457679200	14.012658300	2.529301000
H	-3.398079100	10.962771200	9.905266200
H	-4.687498100	12.672340200	3.023844100
H	-2.665842000	11.453703200	5.971046100
H	-7.137631100	6.506661100	4.677700100
O	-6.993842100	10.861699200	1.439719000
O	-4.981733100	9.657382200	4.399317100

O	-2.943005100	8.427261200	7.328697100
O	-6.349805100	8.769934200	2.559492000
O	-4.265286100	7.546419100	5.452575100
O	-4.267067100	10.903130200	2.011558000
O	-2.245963000	9.757564200	4.981690100
O	-5.784783100	5.911670100	3.382999100
O	-3.926151100	7.345828100	2.653047000
H	-7.453541100	11.353864200	0.741615000
H	-2.395247000	8.310490200	8.120674100
H	-3.540197100	10.658276200	1.417752000
H	-1.506259000	9.551404200	4.389038100
H	-6.901595100	8.883176200	1.769806000
H	-3.796756100	7.050582100	6.142159100
H	-5.064077100	5.695593100	2.770793100
H	-4.135070100	6.429463100	2.413197000
H	-3.119171100	7.508166100	2.139890000

6. (010) Ti6(Vo)-5cCO2 –linear singlet

O	-4.765910900	16.387397800	6.727365700
O	-6.059595800	14.985361300	4.718745300
Ti	-4.837491400	14.619518300	6.244978500
O	-4.329904800	13.867648500	8.013877900
O	-3.276104600	14.261095800	5.401644300
O	-8.016813200	13.806068300	3.174647900
Ti	-6.759706600	13.065317700	4.348682000
O	-5.767850300	12.921887500	6.201014200
Ti	-4.501485000	11.838327700	7.504697300
O	-3.785416300	11.727745800	9.237180100
O	-5.227173200	12.827404600	3.208820600
O	-2.926361300	11.557670700	6.518955500
O	-4.968009900	10.261340500	6.982143600
Ti	-5.503407800	11.015069300	2.686907300
Ti	-3.407803100	9.690994900	5.792268200
O	-6.757746000	7.777358700	4.724161400
Ti	-5.247855400	8.133924500	3.825426000
C	-8.797005000	10.357799300	4.663233300
O	-8.000428600	11.204916200	4.797904100
O	-9.597997100	9.537110200	4.523714100
H	-3.951238100	16.903987300	6.602599100
H	-6.718586100	15.592020300	4.323468100
H	-3.680643100	13.760772300	8.752230200
H	-8.120097100	14.332115300	2.344952000
H	-3.060496100	11.282229200	9.720917200
H	-2.791655100	15.001689300	5.020595100
H	-4.349916100	12.991798200	2.839495100
H	-2.328260000	11.773161200	5.786697100
O	-6.648735100	11.183995200	1.249944000

O	-4.627079100	9.965356200	4.197147100
O	-2.605422000	8.746719200	7.144348100
O	-5.949360100	9.084515200	2.321025000
O	-3.927703100	7.865877100	5.268226100
O	-1.908381000	10.077022200	4.797341100
O	-3.545870100	7.688067100	2.513844000
O	-5.407589100	6.230979100	3.188417100
O	-3.930038100	11.295660200	1.850138000
H	-6.497118100	9.201287200	1.529049000
H	-3.459173100	7.370040100	5.957810100
H	-1.168677000	9.870862200	4.204689100
H	-3.190334100	11.089501200	1.257487000
H	-4.667883100	6.024820100	2.595765000
H	-3.737726100	6.770129100	2.265891000
H	-2.726937000	7.860974100	2.023587000
H	-6.800048100	6.826118100	4.493351100
H	-7.117265100	11.679831200	0.560361000
H	-2.057664000	8.629948200	7.936326100

7. (010) Ti6(Vo)-5cCO2-bent- triplet

O	-4.694511900	15.884226000	7.317435800
O	-6.540885500	14.862013800	5.255854100
Ti	-5.133522500	14.289631400	6.509258100
O	-4.685015800	13.424336500	8.234072500
O	-3.736652000	13.956443700	5.389759700
O	-7.951076200	14.110075400	3.359662500
Ti	-6.984737800	13.011114600	4.621030000
O	-5.998202300	12.583256800	6.452596300
Ti	-4.843467500	11.463689600	7.698434100
O	-4.215978400	11.182481500	9.419371500
Ti	-5.793210900	10.602202100	2.841726200
Ti	-3.736230000	9.381711000	6.010742100
O	-5.287569500	9.888851100	7.072167000
O	-5.535777900	12.452253300	3.466146700
O	-3.220379100	11.238930100	6.743743000
O	-7.049387800	7.424331200	5.003001000
Ti	-5.587623900	7.782386400	4.078042500
C	-8.361821200	10.820467400	4.412701800
O	-8.518000600	11.714079100	5.247727900
O	-8.811021800	9.834035800	3.935551500
H	-4.288820100	16.584529300	6.786948100
H	-7.056168100	15.272562300	4.507817100
H	-4.018225100	13.441314200	8.936579200
H	-3.129237100	14.682231300	5.204944100
H	-8.457679200	14.012658300	2.529301000
H	-3.398079100	10.962771200	9.905266200
H	-4.687498100	12.672340200	3.023844100

H	-2.665842000	11.453703200	5.971046100
H	-7.137631100	6.506661100	4.677700100
O	-6.993842100	10.861699200	1.439719000
O	-4.981733100	9.657382200	4.399317100
O	-2.943005100	8.427261200	7.328697100
O	-6.349805100	8.769934200	2.559492000
O	-4.265286100	7.546419100	5.452575100
O	-4.267067100	10.903130200	2.011558000
O	-2.245963000	9.757564200	4.981690100
O	-5.784783100	5.911670100	3.382999100
O	-3.926151100	7.345828100	2.653047000
H	-7.453541100	11.353864200	0.741615000
H	-2.395247000	8.310490200	8.120674100
H	-3.540197100	10.658276200	1.417752000
H	-1.506259000	9.551404200	4.389038100
H	-6.901595100	8.883176200	1.769806000
H	-3.796756100	7.050582100	6.142159100
H	-5.064077100	5.695593100	2.770793100
H	-4.135070100	6.429463100	2.413197000
H	-3.119171100	7.508166100	2.139890000

Appendix C

Supplementary Information for Chapter 4

C.1 Cartesian coordinates for bent-CO_2 clusters modeled using the b3lyp/def2-SV(P) model chemistry

1. Ti2Vo_010_CO2_1 (μ_1-η^2)

O	-0.6926411	1.1285100	-0.6563663
Ti	-0.5644799	-0.6376799	-1.3973064
Ti	0.2282476	1.0894135	1.0246119
O	-1.3309659	0.9746638	2.1470455
O	-0.1794550	3.1473178	1.4229377
O	1.8472332	1.9452679	0.4252714
O	-1.5162300	0.1450510	-2.7131150
O	1.1453240	-0.5703250	-2.3027570
O	-2.0621920	-1.5398620	-0.5620640
O	-0.3012540	-2.5290570	-1.9637540
H	2.6335230	1.9973090	-0.1892040
H	-2.1864120	0.5403860	2.4265350
H	0.8326040	3.3614540	1.3476520
H	-0.7798170	2.8740670	2.2226990
H	-1.2069110	1.5805740	-1.3435820
H	-1.9880070	0.1859440	-3.5596670
H	-2.8883950	-1.5960810	-0.0569600
H	1.9315420	-0.1391570	-2.6727000
H	0.5249470	-2.4728350	-2.4688570
H	-1.0874720	-2.9602210	-1.5938110
O	1.1440059	-0.4101378	1.8630220
C	0.7516548	-1.0163366	0.8041954
O	0.8806221	-2.1473210	0.4069550

2. Ti2Vo_010_CO2_2 (μ_2-η^3)

O	-0.6993131	1.1162157	-0.6624944
Ti	-0.5759755	-0.6339846	-1.4148437
Ti	0.2230720	1.1315118	1.0416652
O	-1.3213820	0.9885640	2.1981758
O	-0.1750499	3.1568749	1.4371481
O	1.8691142	1.9732222	0.4560643
O	-0.3012540	-2.5290570	-1.9637540
O	-1.5162300	0.1450510	-2.7131150

O	1.1453240	-0.5703250	-2.3027570
O	-2.0621920	-1.5398620	-0.5620640
H	2.6335230	1.9973090	-0.1892040
H	-2.1864120	0.5403860	2.4265350
H	0.8326040	3.3614540	1.3476520
H	-0.7798170	2.8740670	2.2226990
H	-1.2069110	1.5805740	-1.3435820
H	-1.9880070	0.1859440	-3.5596670
H	-2.8883950	-1.5960810	-0.0569600
H	1.9315420	-0.1391570	-2.6727000
H	0.5249470	-2.4728350	-2.4688570
H	-1.0874720	-2.9602210	-1.5938110
C	1.0956617	-0.6380707	1.5754756
O	1.7426977	-1.3688676	2.2685428
O	0.4879080	-0.8305012	0.4244947

3. Ti6Vo_001_CO2 (μ_2-η^3)

Ti	1.7896198	12.9837585	5.5411335
Ti	2.5765906	11.8999276	9.6687832
O	1.3669343	10.3769978	9.2437003
Ti	-0.5114230	9.5109885	9.4096752
O	-1.0139198	10.4775076	7.7722978
Ti	-1.3319797	10.4020336	5.9197850
O	0.6213675	11.3036384	5.6446252
O	0.9224882	13.8400852	4.1368233
O	3.5709399	13.5949255	5.6663641
O	4.0796801	12.9535051	9.5289109
O	2.4353471	11.7504119	11.4615148
O	-0.2270481	9.3155064	11.2735745
O	-1.9146282	8.3522553	9.3038217
O	-2.6523376	9.1712877	6.0974892
O	-1.8141812	11.1012182	4.2082188
O	2.9099766	11.3934841	4.8951049
O	3.6735447	10.5158074	8.8333482
Ti	2.5234658	8.8638883	8.7701368
O	0.6455760	8.1165793	8.7341406
O	-0.1265891	9.0235981	5.2623881
Ti	1.7093092	9.8985369	5.2071726
H	1.0410560	13.6316340	3.1852140
H	4.0721120	14.4276720	5.7218010
H	4.8542130	13.5072850	9.2994240
H	2.9984150	11.3281820	12.1389310
H	0.0588470	8.9583660	12.1718830
H	-2.5026450	7.5763440	9.3818890
H	-3.2847430	8.4967300	5.8042660
H	-1.8985150	11.2618190	3.2181660
O	1.5264180	10.0208290	3.1519130
O	2.8504650	8.3963300	4.4372310
O	2.3085160	9.1004450	6.7295320

O	3.6325640	7.4759420	8.0148480
O	3.0906180	8.1800560	10.3071540
H	3.7726600	11.7822790	5.1067080
H	4.5547600	10.8618930	8.6843270
H	3.1685320	8.0968040	11.2704290
H	0.1374710	7.3007680	8.7338410
H	3.9478120	7.0965140	8.8500450
H	-0.6446270	8.2211550	5.1562200
H	2.8832420	8.3832310	6.4193790
H	2.7725530	8.4795800	3.4739560
H	2.1011440	9.3036150	2.8417610
H	1.2111690	10.4002560	2.3167140
O	0.8148025	14.3048012	6.9183491
C	1.3554295	13.3545769	7.5230103
O	1.3799704	13.1799495	8.7957758

4. Ti2Vo_110_CO2c (μ_2-η^4)

Ti	-2.8141466	6.8187491	7.5296116
Ti	-1.1642843	5.2906300	9.3983069
O	0.0317273	3.8690371	9.6391874
O	-2.6892565	7.7355024	5.8468604
O	-4.2550450	5.8087370	7.6968970
O	-1.2480590	8.3862620	7.6968970
O	-2.5576450	6.8712840	9.6226350
O	-1.0955410	5.1655680	11.5483730
O	0.2140450	6.6805470	9.6226350
O	-2.7929420	4.1030210	9.6226350
O	-4.0197480	8.5770000	7.6968970
H	-4.3704390	4.9733590	8.1761940
H	-0.4048590	8.3725700	8.1761940
H	-1.1326650	9.2216410	7.2176000
H	-4.4305910	9.0562970	8.4333630
H	-4.1162710	8.6896060	6.7383020
H	-3.5767420	8.0601810	5.7711580
H	0.0752710	3.7996780	10.5812290
H	-2.9083350	3.2676420	10.1019320
H	1.0398610	6.6671410	10.0920480
H	-2.9684880	7.3505810	10.3591010
H	-1.5063840	5.6448650	12.2848390
H	-0.4642580	4.4291020	11.5483740
O	-1.9969802	5.4557597	6.1644389
C	-1.3336133	5.2654440	7.1809889
O	-0.3598996	4.6119329	7.5218971

5. Ti2Vo_110_CO2d (μ_2-η^3)

O	-0.0193800	3.9356380	9.6338686
Ti	-1.2394807	5.3456552	9.4591497
Ti	-2.7869355	6.7896939	7.5081205
O	-2.7693406	7.5424689	5.7530208

O	-2.5576450	6.8712840	9.6226350
O	-4.2550450	5.8087370	7.6968970
O	-1.2480590	8.3862620	7.6968970
O	-4.0197480	8.5770000	7.6968970
O	-1.0955410	5.1655680	11.5483730
O	0.2140450	6.6805470	9.6226350
O	-2.7929420	4.1030210	9.6226350
H	-0.4048590	8.3725700	8.1761940
H	-1.5063840	5.6448650	12.2848390
H	-4.4305910	9.0562970	8.4333630
H	-2.9684880	7.3505810	10.3591010
H	-4.3704390	4.9733590	8.1761940
H	-1.1326650	9.2216410	7.2176000
H	-2.9083350	3.2676420	10.1019320
H	-3.5767420	8.0601810	5.7711580
H	-4.1162710	8.6896060	6.7383020
H	0.0752710	3.7996780	10.5812290
H	-0.4642580	4.4291020	11.5483740
H	1.0398610	6.6671410	10.0920480
C	-1.8823845	5.2547541	6.4161336
O	-1.7413940	4.5371212	5.4838253
O	-1.1981207	5.3426234	7.5635110

VITA

Venkata Pradeep Indrakanti

EDUCATION

2003– 2009 **THE PENNSYLVANIA STATE UNIVERSITY (Penn State),** University Park, PA
Doctor of Philosophy in Energy and Geo-Environmental Engineering, expected May 2009, GPA : 4.0/4.0

1998– 2002 **NATIONAL INSTITUTE OF TECHNOLOGY (NIT),** Tiruchirapalli, India
Bachelor of Technology in Chemical Engineering GPA : 9.20/10

EXPERIENCE

2003-2009 Department of Energy and Mineral Engineering, Penn State, University Park, PA
Research & Teaching Assistant

- Developed a model for the initial steps of CO_2 conversion on TiO_2 surfaces using quantum chemical calculations in Gaussian 03 and Turbomole.
- Developed 7 financial scenarios, calculated internal rates of return and payback periods and discovered that a doubling of algal yields and/or a doubling of oil prices would be required to make algal biofuel production economically justifiable.
- Assisted in teaching an undergraduate course for 170 students on energy conservation and environmental protection.

2002-2003 ACC Ltd., Wadi Cement Works, India
Assistant Process Manager

- Measured the performances of the kiln, cooler and preheater sections of a 2.6 MTPA cement plant over a four month period, calculated mass and energy balances and identified bottlenecks for increasing production.
- Evaluated the technical feasibility of various energy-saving measures such as the use of waste heat from the cooler to dry pond fly ash. Recommended a plant retrofit based on this evaluation, resulting in 10% potential energy savings.

SELECTED AWARDS AND ACHIEVEMENTS

2008 GRC Poster Presenter Grantee, Gordon Research Conference on Green Chemistry
2008 ACS Thematic Program Travel Grant, American Chemical Society
2007 EMS Centennial Graduate Research Award, College of Earth and Mineral Sciences
2003 Graduate Fellowship Award, Penn State
2002 Best Outgoing Student of Chemical Engineering, NIT Tiruchirapalli

SELECTED PUBLICATIONS

- V.P. Indrakanti, J.D. Kubicki, H.H. Schobert, "Quantum chemical modeling of ground states of CO_2 chemisorbed on anatase (001), (010) and (101) TiO_2 surfaces", Energy & Fuels (2008), 22(4), 2611-2618.
- V.P. Indrakanti, J.D. Kubicki, H.H. Schobert, "Photoinduced activation of CO_2 on Ti-based heterogeneous catalysts: Current State, Chemical Physics-based Insights and Outlook", accepted for publication in Energy & Environmental Science, 2009.
- V.P. Indrakanti, J.D. Kubicki, H.H. Schobert, "Quantum mechanical modeling of CO_2 interactions with irradiated anatase TiO_2 surfaces: Implications for the photocatalytic reduction of CO_2", to be submitted to Energy & Fuels.